This is to certify that the

dissertation entitled

POPULATION MODULATION SPECTROSCOPY:
PRACTICAL AND THEORETICAL CONSIDERATIONS

presented by

Lynn Marie Chakel

has been accepted towards fulfillment
of the requirements for

Ph.D degree in Chemistry

George B. Stevens
Christie G. Enke
Major professor

Date December 1, 1986

POPULATION MODULATION SPECTROSCOPY: PRACTICAL AND THEORETICAL CONSIDERATIONS

By

Lynn Marie Chakel

A DISSERTATION

Submitted To

Michigan State University
In Partial Fulfillment of the Requirements
For the Degree of

DOCTOR OF PHILOSOPHY

Department of Chemistry

1986

ABSTRACT

POPULATION MODULATION SPECTROSCOPY: PRACTICAL AND THEORETICAL CONSIDERATIONS

By

Lynn Marie Chakel

The high incident irradiances available from lasers can often promote a large fraction of an absorbing population to an electronic excited state, with concomitant depopulation of the electronic ground state. If a pulsed laser is employed as the excitation source, the ground state population is modulated with the pulse. The practical and theoretical aspects of population modulation spectroscopy are explored for a model compound, rhodamine 6G, in solution. The goal of this research is to assess the potential for applying population modulation spectroscopy to the identification of chromophores which arise from the same electronic ground state in a multicomponent solution.

The spectroscopy of rhodamine 6G has been characterized on the nanosecond timescale by population modulation spectroscopy. The transmittance vs. incident irradiance behavior of rhodamine 6G was investigated. Modulation of the ground state population was effected by

pumping the S_0 --> S_1 transition, but not by pumping the S_0 --> S_4 transition. Population modulation was found to occur at the onset and peak of the pulse by pumping the S_0 --> S_1 transition of rhodamine 6G at 532 nm and probing the pumped system with temporally delayed beams at the same wavelength. Through the use of dye-laser-generated probe beams, ground state concentration modulation was observed across the entire S_0 --> S_1 absorption band. The potential for identifying transitions which arise from the same ground state was investigated via a dual wavelength pump/probe experiment. The transmission of a probe beam corresponding to a wavelength within the S_0 --> S_4 absorption band (355 nm) was monitored vs. delay time during and between the 532 nm pump beam pulses. The orthogonal orientation of the transition moments which give rise to the two transitions precluded modulation of the probe beam by the simultaneous presence of the pump beam.

The limitation encountered with rhodamine 6G demonstrates that population modulation spectroscopy is not a completely general technique for the identification of chromophores which arise from the same electronic ground state. However, for many molecules population modulation by pump laser radiation may well affect the intensity of probe wavelength absorptions originating in the molecular ground state.

To my Mother and Father, and to John

ACKNOWLEDGMENTS

I would like to express my deepest gratitude to Professor Christie G. Enke and Professor George E. Leroi for their invaluable guidance and insight throughout the years. My life, both professional and personal, is enriched by their inspiration and example.

Sincere appreciation is extended to Dr. Carl Myerholtz and Dr. Bruce Newcome for helping me to effect an elegant solution to the problem of data acquisition. If it were not for you, I would still be acquiring data! I would also like to thank Dr. Tom Atkinson for LASERD and help with KINFIT, as well as for sharing his "philosophy" with me.

I am also grateful for the opportunity to get to know many very special people during my stay at Michigan State. You helped to make life stimulating at work and at play! Your friendships have made a lasting impression on me. Milton Webber, what can I say?

I would also like to express my appreciation to my family for their love and for their encouragement in this and all that I attempt. John, I thank you for your love and for helping me to endure and finish a task that at times seemed impossible.

TABLE OF CONTENTS

LIST OF TABLES

LIST OF FIGURES

CHAPTER 1

INTRODUCTION

Lasers are employed in applications which range from rocery store checkout scanner and personal computer er to research in ultrafast molecular processes and fusion. The flexibility which now exists with ct to available wavelengths, powers and pulsewidths tates research in areas of chemistry which were usly intractable. In analytical chemistry, the laser come a valuable tool. Wright (1.1) has recently ed the use of lasers in analytical chemistry and a dited by Omenetto provides a useful overview (1.2).

he high incident irradiances available via the laser en promote a large fraction of an absorbing ion to excited electronic states. Concomitant with icient transfer of absorbers to excited states is letion of absorbers in the ground state. If a laser is used as the excitation source, the ion of absorbers in the ground electronic state is ely modulated with the laser pulse. Investigation ractical and theoretical aspects associated with

state population modulation for a model compound in
on is the subject of this dissertation.

turation of Electronic Transitions

odulation of the ground state population with a
laser beam at high incident irradiance can result
easurable decrease in the absorbance (increase in
ttance) of the beam which is used to modulate the
ion. In order to understand this observed effect,
r a simple two-level system with a ground and an
electronic state.

e net absorbance of a population of absorbers
molecules which absorb photons of particular
s) is dependent not only on the cross-section for
ion at a given wavelength, but also on the fraction
bers present in the ground electronic state at any
room temperature and before excitation, nearly
he absorbers are in the ground electronic state.
on flux of conventional light sources is very low
lowing irradiation by such a source, an excited
usually relaxes back to the ground state before
photon can be absorbed. Therefore, under
ion by conventional sources, the fraction of
present in the excited state at any time is
small and the absorbance is dependent only on

absorbers in the ground electronic state. The
enuation of an incident beam is, therefore, linearly
endent on the total number of absorbers; the Beer-
ert Law is obeyed in these instances.

If a laser rather than a conventional light source is
for excitation, the photon flux is large and the
tion of absorbers in the excited electronic state at
time can become substantial. In the two-level system,
excited absorber can emit a photon of the same
uency and phase as the excitation beam; this process
rmed stimulated emission. Stimulated emission adds
ns to the excitation beam, whereas the absorption
ss removes photons from the excitation beam. The net
bance of a population of absorbers, when excited by
irradiance sources, is then clearly dependent on the
rence between the fraction of absorbers in the ground
and the fraction of absorbers in the excited state.
tenuation of the incident beam then is no longer
ly related to the total population of absorbers.
he photon flux is very high, the fraction of
ers in the excited state approaches the fraction of
ers in the ground state, the rate of stimulated
on approaches the rate of absorption and the net
nce approaches zero (complete transparency). As the
tic limit is approached (50 % of the absorbers in

cited state), the transition of interest is said to
ch saturation.

lated Applications

ne ability to saturate electronic transitions was
ed in the 1960's to generate nanosecond laser
. It had been discovered that "giant pulses" could
uced when saturable dyes were employed as
ble, passive Q-switches for pulsed ruby (1.3-1.5)
glass lasers (1.6). For this application, a cell
ing the saturable dye which absorbs light at the
avelength is inserted into the laser cavity where
ions as an optical shutter. The dye introduces an
cation loss into the laser cavity by absorbing
from the laser beam; the dye essentially allows
ted state population of the lasing medium to
ts maximal value. The initially weak laser beam
a small fraction of the dye molecules into the
state. The decrease in the ground state population
ve reduces the absorption of the dye which
the irradiance of the laser beam. The increase
ser beam irradiance further reduces the
n of the dye until the absorbing transition is
, or "bleached". As the transition is saturated,
al shutter opens. This sudden reduction in cavity
lts in rapid depopulation of the inverted

ulation of the lasing medium. The result is the "giant se". Trains of pulses with picosecond pulsewidths were er generated using saturable dyes with relaxation times ter than that of the Q-switching dyes. This passive locking technology was applied to Nd:glass (1.7,1.8) dye lasers (1.9-1.11). The Q-switched lasers were equently employed to investigate the transmission of rable dyes as a function of incident intensity. These ies led to models and mathematical expressions which unted for the observed intensity-dependent smission behavior (1.12-1.20). Excited state lifetimes absorption cross-sections can be estimated from the tical expressions developed for the transmission ior of saturable absorbers. The models developed for aturable dyes have been applied to the data obtained experiments which utilized Q-switched lasers to cally bleach" transitions in compounds other than the nally investigated dyes. For example, a value of the -section for absorption from the excited singlet of chlorophyll *a* was determined from a laser- ity-dependent transmission experiment (1.21). In r application, investigators employed a transmission cident intensity experiment to estimate the lifetime S_1 state of β-carotene (1.22); its low scence quantum yield rendered previously published of the S_1 lifetime unreliable. As a prelude to ace Raman studies of electronically excited states,

ransmission (or luminescence) of a sample is often
ored as a function of incident intensity; this
es that near-saturation yields of the pumped
ronic state are achieved (1.23,1.24). Saturable
ption has also been applied to determination of the
intensity (132) and the shape and duration (1.26) of
econd pulses. The theory of saturable optical
ption has been the subject of numerous publications
1.9,1.27-1.32).

Ground state recovery times have been determined by
ating the ground state population. A monochromatic
beam serves to depopulate the ground electronic state
probe beam or continuum is then used to monitor the
n of the ground state absorbance as a function of
[Pulses of picosecond duration are generally used
ound state recovery time studies in order to achieve
il time resolution.] The recovery times of various
cking dyes have been determined in this manner
1.36). The singlet lifetimes of β-carotene and
d carotenoids (1.37) and of crystal violet have also
btained using this technique (1.38). [When a
ium source is used to probe the transmittance,
ent spectra of the pumped excited state are obtained
hich facilitates the elucidation of the the nature
electronic states reached after excitation
.40).]

A brief discussion of concentration-modulated
rption spectroscopy (COMAS) (1.41-1.43) is included
to its analytical relevance and possible future
ntial in relation to this research project. This
nique does not require that a transition is saturated,
only that the normal thermal equilibrium between the
nd and excited state populations is perturbed. A
locked dye laser generates a pump beam which is split
ovide a probe beam at the same wavelength. The pump
is subsequently modulated by an electro-optic
ator. As the pump and probe beams prepare and
rogate the sample, respectively, a gain is
ienced by the probe beam due to the decreased ground
concentration. High-frequency modulation of the pump
and phase-sensitive detection of the probe beam
s shot-noise-limited performance. This extends the
ivity of absorption measurements to the limits
ed in fluorescence excitation spectroscopy (1.41).
in experienced by the probe beam has been shown to
ntitatively related to the ground state
tration of the absorber (1.42) and to the lifetimes
excited electronic states (1.43). A similar
ue has been utilized by Lytle, *et al* (1.44,1.45)
an, *et al* (1.46) to obtain ground and excited state
ion spectra and stimulated fluorescence spectra; in
nstances the probe beam is scanned.

The applications which have been referenced here are se which are related to or utilize techniques similar those employed during the course of the research ject which is the subject of this dissertation.

Objectives

As alluded to previously, the objective of the arch described herein is to investigate the practical theoretical aspects associated with population lation spectroscopy. An additional objective is to lop and characterize a data acquisition system for the imental studies. The experimental objectives are as ws. Initially, the transmission vs. incident iance behavior of three compounds is investigated to re the factors which theory predicts influence the ty to saturate a given transition. [A single compound n chosen for the remainder of the studies.] The ability of commonly-used models to the acquired data en be assessed. Saturation of fluorescence ments are performed to verify, independently of the ission experiments, that population modulation is ing. In order to examine the onset, duration and on of the population modulation induced by the pump ingle wavelength pump/probe studies are employed. tinct types of dual wavelength pump/probe studies n made. The first dual wavelength experiment

lores whether the induced ground state population
ılation is observable at wavelengths within the
rption band of the pumped transition. The second
rmines whether the induced ground state population
lation is observable if the probe wavelength
esponds to a different electronic transition which
es from the same ground state. From the data obtained
these population modulation studies, an assessment of
analytical applicability of the technique can be made.

The ultimate goal of this research is to gain insight
the potential applicability of population modulation
roscopy to the problem of mixture analysis, because
y provide a method of identifying chromophores which
from the same electronic ground state of a given
ic molecule in a multicomponent solution. Currently,
se of visible absorption spectroscopy for the
ification of the components comprising a complex
e is hampered by the difficulty in deconvoluting the
ite spectrum which is obtained. Population
tion spectroscopy may provide a means to
oscopically "sort" suitable mixtures. The sorting
be achieved in the following manner. The ground
population of a given component could be selectively
ted by the choice of the pump beam wavelength. A
robe beam would then be used to scan the entire
spectrum. The probe beam absorption intensity

ıld be modulated in the presence of the pump beam at
lengths which correspond to other transitions which
e from the selectively pumped ground state. The
tral sorting would be achieved by monitoring the
rption variations as a function of probe beam
length for each excitation wavelength.

Organization of the Dissertation

The dissertation is divided into five chapters. This
er provides an overview of the phenomena of
ation and ground state population modulation, which
o be utilized during the course of the research.
cations which are related to this work are briefly
ssed and referenced. The objectives of the research
utlined.

The second chapter expands on the brief description
uration which was given in Chapter 1. Multilevel
tion models are presented which account for
mentally observed transmission vs. incident
ance behavior of some solutions. The incomplete
ing which is often observed is thus explained. The
ysical properties of organic molecules which
the introduction of the multilevel saturation
are discussed.

Chapter 3 describes in detail the experimental
paratus and procedures. An overview of the Nd:YAG/dye
ser system is provided for clarity. The optical set-ups
r the different studies are diagramed. In addition,
ocedures for optimizing the optics and the data
quisition system are detailed.

The results of the experimental work are presented
d discussed in Chapter 4. The chapter is divided into
ctions, each devoted to the discussion of a particular
e of experiment. The sections describe the following
dies: (1) population modulation for rhodamine 6G,
ta)3-hydroxypropylporphyrin and (etio)hemechloride in
ch a 532 nm excitation beam is used, (2) population
ulation studies for rhodamine 6G under 355 nm
itation, (3) saturation of fluorescence for rhodamine
(4) ground state recovery for rhodamine 6G, (5)
ulation modulation across the S_0 --> S_1 absorption band
hodamine 6G, and (6) dual wavelength pump/probe
ies. The dual wavelength pump/probe experiments employ
2 nm excitation beam to pump the S_0 --> S_1 transition
hodamine 6G and a 355 nm probe beam to interrogate the
le within the S_0 --> S_4 absorption band. The probe
interrogates the sample at various delay times
ive to the pump beam in the ground state recovery
es and the dual wavelength pump/probe studies.

The fifth chapter contains the conclusions which can
-awn from the experimental work. The analytical
cability of population modulation spectroscopy is
ssed.

Details of the data acquisition system designed and
nbled for this dissertation project are included in
e appendices. Appendix A is a reprint of a paper which
-ibes the architecture of the data acquisition system
ts performance. Appendix B consists of schematic
-ams of those circuit boards designed specifically for
system. The circuit board and commercial integrator
ctors are also documented. Appendix C includes
iptions and lists software which are unique to this
cation.

REFERENCES

Kompa, K. L.; Wanner, J.; *Laser Applications in Chemistry;* Plenum Press; New York, 1984

Omenetto, N. *Analytical Laser Spectroscopy;* John Wiley and Sons; New York, 1979.

Sorokin, P. P.; Luzzi, J. J.; Lankard, J. R.; Pettit, G. D. *IBM J. Res. Dev.* **1964**, *8*, 182.

Kafalas, P.; Masters, J. I.; Murray, E. M. E. *J. Appl. Phys.* **1964**, *35(8)*, 2349.

Roess, D.; Zeidle, G.; *Appl. Phys. Lett.* **1966**, *8(1)*, 10.

Skeen, C. H.; York, C. M. *Appl. Opt.* **1966**, *5(9)*, 1463.

DeMaria, A. J.; Stetser, D. A.; Heynau, H. *Appl. Phys. Lett.* **1966**, *8(7)*, 174.

Giuliano, C. R.; Hess, L. D. *IEEE J. Quantum Electron.* **1967**, *QE-3(8)*, 358.

von Gutfeld, R. J. *Appl. Phys. Lett.* **1971**, *18(11)*, 481.

Arthurs, E. G.; Bradley, D. J.; Roddie, A. G. *Appl. Phys. Lett.* **1972**, *20(3)*, 125.

Maeda, M.; Miyazoe, Y. *Jpn. J. Appl. Phys.* **1974**, *3*, 193.

Tires, P. F. *IEEE J. Quantum Electron.* **1966**, *QE-2(9)*, 524.

osonocky, W. F.; Harrison, S. E. *J. Appl. Phys.* **1966**, *37(13)*, 4789.

osonocky, W. F.; Harrison, S. E.; Stander, R. *J. hem. Phys.* **1965**, *43(3)*, 831.

offer, B. H.; McFarland, B. B. *Appl. Phys. Lett.* **966**, *8(7)*, 166.

iuliano, C. R.; Hess, L. D. *Appl. Phys. Lett.* **1966**, *(5)*, 196.

7 Degiorgio, V. *Appl. Phys. Lett.* **1967**, *10(6)*, 175.

8 Huff, L.; DeShazer, L. G. *Appl. Opt.* 1970, *9(1)*, 233.

9 Degiorgio, V.; Potenza, G. *Nuovo Cimento* **1966**, *41(2)*, 458.

0 Bowe, P. W. A.; Gibbs, W. E. K. *Nature* **1966**, *209*, 65.

Arsenault, R.; Denariez-Roberge, M. M. *Chem. Phys. Lett.* **1976**, *40(1)*, 84.

Haley, L. V.; Koningstein, J. A. *Chem. Phys.* **1973**, *77*, 1.

Dallinger, R. F.; Woodruff, W. H. *J. Am. Chem. Soc.* **1979**, *101*, 4391.

Asano, M.; Mongeau, D.; Nicollin, D.; Sasseville, R.; Koningstein, J. A. *Chem. Phys. Lett.* **1979**, *65(2)*, 293.

Penzkofer, A.; Von der Linde, D.; Laubereau, A. *Opt. Commun.* **1972**, *4(5)*, 377.

Wiedmann, J.; Penzkofer, A. *Opt. Commun.* **1979**, *30(1)*, 107.

Hercher, M. *Appl. Opt.* **1967**, *6(5)*, 947.

Spaeth, M. L.; Sooy, W. R. *J. Chem. Phys.* **1968**, *48(5)*, 2345.

Muller, A.; Pfluger, E. *Chem. Phys. Lett.* **1968**, *2(3)*, 155.

Eason, R. W.; Greenhow, R. C.; Matthew, J. A. D. *IEEE J. Quantum Electron.* **1981**, *QE-17(1)*, 95.

Olson, G. L.; Greve, K. S.; Busch, G. E. *J. Chem. Phys.* **1978**, *68(4)*, 1474.

Rudolph, W.; Weber, H. *Opt. Commun.* **1980**, *34(3)*, 491.

Busch, G. E.; Jones, R. P.; Rentzepis, P. M. *Chem. Phys. Lett.* **1973**, *18(2)*, 178.

Eason, R. W.; Greenhow, R. C.; Goodall, D. M.; Holzwarth, H. *Opt. Commun.* **1980**, *32(1)*, 113.

Scarlet, R. I.; Figueira, J. F.; Mahr, H. *Appl. Phys. Lett.* **1968**, *13(2)*, 71.

36 Fan, B.; Gustafson, T. K. *Opt. Commun.* **1975**, *15(1)*, 32.

37 Wasielewski, M. R.; Kispert; L. D. *Chem. Phys. Lett.* *1986*, *128(3)*, 238.

38 Magde, D.; Windsor, M. W. *Chem. Phys. Lett.* **1974**, *24(1)*, 144.

39 Greene, B. I.; Hochstrasser, R. M.; Weisman, R. B. *J. Chem. Phys.* **1979**, 70(3), 1247.

40 Hilinski, E. F.; Rentzepis, P. M. *Nature* **1983**, *302*, 481.

41 Langley, A. J.; Beaman, R. A.; Baran, J.; Davies, A. N.; Jones, W. J. *Opt. Lett.* **1985**, *10(7)*, 327.

42 Langley, A. J.; Beaman, R. A.; Davies, A. W.; Jones, W. J.; Baran, J. *Chem. Phys.* **1986**, *101*, 117.

43 Beaman, R. A.; Davies, A. N.; Langley, A. J.; Jones, W. J. *Chem. Phys.* **1986**, *101*, 127.

44 Lytle, F. E.; Parrish, R. M.; Barnes, W. T. *Appl. Spectrosc.* **1985**, *39(3)*, 444.

45 Barnes, W. T.; Lytle, F. E. *Appl. Phys. Lett.* **1979**, *34(8)*, 509.

Baran, J.; Langley, A. J.; Jones, W. J. *Chem. Phys.* **1984**, *87*, 305.

CHAPTER 2

MODELS FOR THE SATURATION OF MOLECULAR ELECTRONIC TRANSITIONS

Introduction

A discussion of the models for the saturation of ctronic transitions in organic molecules is presented this chapter. The two-level model described in Chapter expanded to three- and four-level saturation schemes h are often more applicable to molecular systems ,2.2). As a preface to the introduction of the ilevel saturation schemes, the photophysical erties of organic molecules that require the oduction of such schemes are discussed. In addition, a inction is made between the models that are applicable the molecular relaxation times are short (power ation) or long (energy saturation) with respect to ulsewidth of the exciting radiation. Equations for ransmittance vs. incident irradiance behavior are for each of the models. An approach involving rate ions is used for the development of the model. This, than a quantum mechanical approach, is valid e the dephasing times of the molecular systems of st are much shorter than the nanosecond pulsewidths

the exciting radiation employed in the experimental
udies (2.2-2.4). The material presented, although not an
haustive treatment of the phenomenon of saturation,
vides the background information which is necessary to
cuss the experimental work contained within this
sertation.

Photophysical Properties of Organic Molecules Related to the Mechanism of Optical Saturation

The saturation of electronic transitions is often
led as a two-level system which requires that the
nd and excited state populations equalize and that
ted species return to the ground state via stimulated
sion at the excitation wavelength (2.5-2.9). However,
relaxation mechanisms of many molecular systems,
ined with the excitation conditions, often necessitate
a multilevel model be employed (2.2,2.10-2.12). For
ms with complex relaxation mechanisms, optical
ation can in fact occur without stimulated emission
e excitation wavelength and with complete
ulation of the ground electronic state (2.1,2.13).
er phenomenon which is often observed is incomplete
ning of the saturated transition at high incident
ances; this is thought to occur as a result of
d state absorption at the incident wavelength
2.14-2.16). The necessity for the introduction of

multilevel saturation models becomes clearer when the
rgy of the transition, the rates of relaxation
cesses, and the overlap of absorption and emission
ds are considered. The discussion proceeds by
sidering the excitation conditions which must be met in
er for saturation to be modeled by the two-level
me. If the proper conditions are not met and if
ration does occur, a multilevel scheme is invoked to
unt for the saturation of the transition. Figure 2.1
Jablonski diagram for a generalized organic molecule
ing the electronic states, absorptive transitions and
relaxation rate constants which are pertinent to this
ussion.

Initially, the absorbed photon is assumed to be at an
y where the absorption and emission bands do not
ap. The transitions which are considered are in the
> S_n manifold and in the absorption band of an
> S_1 transition; the latter correspond to excitation
he upper vibrational levels of the S_1 manifold.
ing absorption, the primary relaxation pathway from
internal conversion to the ground vibrational level
and the rate constant for this process is 10^{10} -
ec^{-1} (2.1,2.17-2.19). Excitation from the electronic
state to the excited vibrational sublevels of S_1 is
ed by rapid relaxation within the S_1 manifold to the
vibrational sublevels, from which the majority of

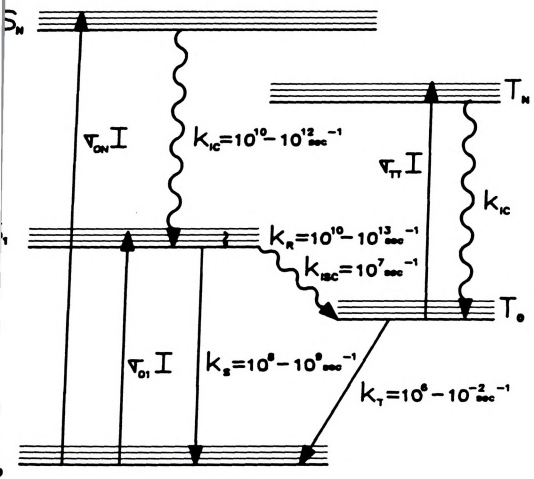

2.1 Jablonski diagram for a generalized organic molecule. The transition probabilities are $\sigma_{ij} I$. The rate constants for internal conversion (k_{IC}), intersystem crossing (k_{ISC}), radiative and nonradiative relaxation from the S_1 and T_1 manifolds (k_S and k_T), and relaxation within the S_1 manifold (k_R) are indicated along with the values.

adiative transitions occur. The relaxation within the S_1 anifold has a rate constant of 10^{12} sec^{-1} (2.12,2.19). In oth of these cases, stimulated emission at the excitation avelength can occur only if the stimulated transition te (σI sec^{-1}) is greater than or equal to the internal nversion rate. This means that saturation by stimulated ission and population equalization can occur only if the cident irradiance, I (cm^{-2}-sec^{-1}), is equal to or ceeds k_{IC}/σ. Given a typical absorption cross-section of ^{17} - 10^{-16} cm^2, k_{IC}/σ is approximately equal to 10^{26} - ^{9} cm^{-2}-sec^{-1}. An incident irradiance of this magnitude responds to power densities of 10^2 - 10^4 MW/cm^2 in the ible region of the spectrum.

If, however, excitation of S_o --> S_1 occurs at a elength where the absorption and emission bands do lap, the incident irradiance required for stimulated sion at the excitation wavelength need only exceed a mum value which is determined by k_s/σ cm^{-2}-sec^{-1}, e k_s is the rate constant which governs relaxation l radiative and nonradiative) from S_1. The value of k_s enerally 10^8 - 10^9 sec^{-1} (2.1,2.19). In contrast to wo cases discussed previously, incident power ties of only 10^5 - 10^6 W/cm^2 could, therefore, result turation of the transition by population ization.

Another process which must also be considered is
›sorption of photons from the excitation beam by
lecules which have been promoted to the S_1 and T_1
ates. Excited state absorption results in reduced
ansparency at high incident irradiances, and can in fact
sult in increased optical density if the cross-section
r absorption from the excited state is larger than the
›ss-section for absorption from the ground state
1,2.12).

The lowest-lying triplet state can become
nificantly populated during optical pumping, depending
the magnitude of the rate constant for intersystem
ssing. For example, it has been shown that saturation
›hthalocyanines results because the entire population
›bsorbers is removed to the triplet manifold (2.20).
intersystem crossing rate constants for most molecules
approximately 10^7 sec^{-1}, but they can be as large as
sec^{-1} for molecules containing a transition metal
). Intersystem crossing rates of 10^9 sec^{-1} make
let formation a process which is quite competitive
relaxation from S_1.

From the above discussion, it is clear that if
ation occurs at an energy higher than that at which
›bsorption and emission bands overlap, or if there is
erlap, saturation probably does not occur by
ation equalization. In these cases, optical

ransparency can result from removal of the ground state
opulation to an excited state which is longer-lived than
ne pumped state (2.1). Deexcitation then occurs via both
ontaneous radiative and nonradiative processes and/or
imulated emission at a longer wavelength than that of
e excitation beam (2.12). Power densities of 10^2 - 10^4
/cm^2 are required to induce stimulated emission if
citation occurs at an energy where the absorption and
ission bands do not overlap; this is in contrast to the
wer densities of 0.1 - 1.0 MW/cm^2 required to induce
mulated emission when the absorber is excited at an
rgy where the absorption and emission bands do overlap.
triplet state manifold and excited state absorption
play a significant role in the saturation mechanism.

Three-level System - "Power-Saturation"

A model for a three-level "power-saturated" system is
loped in the following manner. Power-saturation is
ned and a general three-level energy scheme is
ented. A steady-state solution is applied to the rate
tions which describe the time rate of change of the
lations of the energy levels considered. An expression
he steady-state non-thermal difference in the ground
xcited state populations results from the rate
ions. An expression for the overall lifetime also
ts. The "saturation irradiance" is defined and an

uation for transmittance as a function of incident radiance is then presented. The model development stems om the work of Hercher (2.14) and Hercher, *et al.* (2.5). ferenced additions from other publications and the sights of this author are also included.

A "power-saturated" system is one in which the lecular relaxation times are fast enough that one may ume that the populations of the various energy levels ch a steady-state even during the evolution of a osecond Q-switched laser pulse. A steady-state dition is usually achieved for absorbers with effective axation times of a few nanoseconds, providing the sewidth of the exciting radiation is 10-20 nsec or ger (2.14). The temporal intensity profile of the laser is then assumed to appear to the molecular system as ep function in time.

Figure 2.2 is an energy level scheme for a ralized three-level system. Absorption occurs between ground state (level 1) and another electronic state of er energy (level 3). The probability for stimulated ption (and stimulated emission) at the wavelength of ncident beam is W_{13} and is equal to (σI), the product e absorption cross-section (cm^2) and the incident n irradiance (photons-cm^{-2}-sec^{-1}). This generalized e allows level 3 to be considered as any of the wing: (1) an excited vibronic sublevel of S_1 with

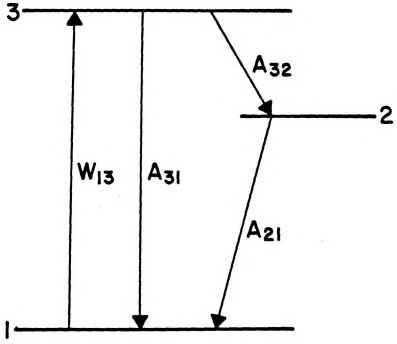

ure 2.2 Energy level diagram for a generalized three-level system. The transition probabilty is W_{13}. The rate constants for relaxation processes betweem levels are given by A_{ji}.

evel 2 as the lowest vibronic sublevel of S_1; (2) an xcited state S_n with level 2 as the lowest vibronic ublevel of S_1; or (3) the ground vibrational level of S_1 ith level 2 as the lowest level of T_1. A_{31} and A_{21} are he probabilities (sec^{-1}) for spontaneous transitions hich include both radiative and non-radiative relaxation rocesses to S_0 (level 1). A_{32}, then, can be considered as ny of the following rate constants (sec^{-1}) depending on he assignment of level 2: (1) the rate constant for ibrational relaxation within the vibrational manifold of ; (2) the rate constant for internal conversion between and S_1; or (3) the rate constant for intersystem ossing from S_1 to T_1.

The rates of change of the normalized populations of e energy levels shown in Figure 2.2 are given by the llowing rate equations:

$$dn_1/dt = -W_{13}(n_1 - n_3) + n_3A_{31} + n_2A_{21} \qquad (2\text{-}1)$$

$$dn_2/dt = n_3A_{32} - n_2A_{21} \qquad (2\text{-}2)$$

$$dn_3/dt = W_{13}(n_1 - n_3) - n_3(A_{32} + A_{31}) \qquad (2\text{-}3)$$

e

$$n_1 + n_2 + n_3 = 1. \qquad (2\text{-}4)$$

The normalized populations are N_i/N where Ni and N are the population densities (molecules/cm^3) in a particular level and the total population density, respectively.

Application of the steady-state solution (i.e.; setting the time derivatives of the populations equal to zero) to equations (2-1) through (2-4) results in a steady-state population difference between levels 1 and 3 of

$$n_1 - n_3 = (1 + W_{13}[(2 + A_{32}/A_{21})/(A_{31} + A_{32})])^{-1}. \quad (2-5)$$

f each A_{ji} in Eq. (2-5) is replaced with $1/\tau_{ji}$, where τ_{ji} is the associated lifetime and W_{13} is replaced with $\sigma_{13}I$, the steady-state population difference becomes

$$n_1 - n_3 = (1 + \sigma_{13}I\tau)^{-1} \quad (2-6)$$

here

$$\tau = (2\tau_{31}\tau_{32} + \tau_{31}\tau_{21})/(\tau_{32} + \tau_{31}) \quad (2-7)$$

d is defined as the effective lifetime. If the generacies of levels 1 and 3 are not equal Eq. (2-7) comes

$$\tau = \tau_{31}\tau_{32}(1 + g_1/g_3)/(\tau_{32} + \tau_{31}) \qquad (2\text{-}7a)$$

where g_1 and g_3 are the degeneracies of levels 1 and 3, respectively.

It can be seen from Eq. (2-6) that the steady-state population difference is inversely dependent on the product of the transition cross-section, the effective lifetime and the incident irradiance. Recall from Chapter 1 that linear absorption (governed by the Beer-Lambert law) occurs when the incident intensity is low and essentially all of the molecules remain in the ground electronic state (i.e., in thermal equilibrium). The steady-state population difference is therefore at a maximum in the case of linear absorption. Equation (2-6) shows that as the incident irradiance becomes comparable to the reciprocal of the product of the transition cross-section and the effective lifetime, $(\sigma\tau\ \text{cm}^2\text{-sec})^{-1}$, the population difference begins to decrease. The absorption is then nonlinear. At very high irradiances the population difference approaches zero and the transition becomes transparent to the incident irradiation. As discussed in section 2.1 of this chapter, the population difference can approach zero either by population equalization or by level 3 rapidly relaxing to level 2, a longer lived state than the pumped state, and level 1 then becoming completely depopulated.

2.2.1 The Saturation Irradiance

The "saturation irradiance", which is a constant for particular transition and molecular system, is commonly sed to define the range of the incident irradiance equired to saturate the transition. The saturation rradiance is defined for the general three-level system

$$Is = (\sigma_{13}\tau \text{ cm}^2\text{-sec})^{-1}. \qquad (2\text{-}8)$$

rcher (2.14) has also considered two special cases of e general three-level system and has given expressions r the saturation irradiance for each case. The first ecial case is the two-level system where $\tau_{32} \dashrightarrow \infty$ in (2-7) and the saturation irradiance becomes

$$Is = (2\sigma_{13}\tau_{31})^{-1}. \qquad (2\text{-}9)$$

saturation irradiance defined by Eq. (2-9) agrees with Is defined for two-level systems by other authors 4,2.21,2.22).

The second special case is the fast three-level em where $\tau_{32} \dashrightarrow 0$ in Eq. (2-7) and the saturation diance is given by

$$I_S = (\sigma_{13}\tau_{21})^{-1}. \qquad (2\text{-}10)$$

The significance of the saturation irradiance and the reason for defining such a term may be best understood by rewriting Eq. (2-6) as

$$(n_1 - n_3) = (1 + I/I_S)^{-1}. \qquad (2\text{-}11)$$

and considering the absorption coefficient.

The small-signal absorption coefficient is

$$\alpha_o = \sigma_{13}(N_1 - N_3) = \sigma_{13}N. \qquad (2\text{-}12)$$

In the case of low incident irradiance the population density of absorbers in the ground electronic state, N_1, is equal to the total population density of absorbers, N, since essentially all of the molecules remain in the ground state. It is now possible to define a steady-state absorption coefficient, $\alpha_S(I)$, which is applicable when the incident irradiance is high. In this case

$$\alpha_S = \alpha_o(n_1 - n_3) \qquad (2\text{-}13)$$

which upon substitution from equation (2-9) becomes

$$\alpha_s = \alpha_o (1 + I/I_s)^{-1}. \qquad (2\text{-}14)$$

The significance of I_s then becomes clear. The small-signal absorption coefficient (α_o) is reduced by a factor of two when the incident irradiance (I) is equal to the saturation irradiance (I_s) (2.14). This means that the normalized steady-state population difference, ($n_1 - n_3$), has decreased by a factor of two due to a reduction in the fraction of absorbers in the ground state and a corresponding increase in the fraction of absorbers in the excited (pumped) state.

The saturation irradiance can be used as a marker for significant ground state depopulation. From the inverse relationship of the saturation irradiance to the product of the transition cross-section and the absorber lifetime, it is obvious that absorbers with large cross-sections and long lifetimes are saturated with lower incident irradiances. It is worth noting, however, that the expression for the saturation irradiance, as it has been defined, is strictly applicable only when the lifetimes of the absorbers are short with respect to the laser pulse. Considered alone, the value of the saturation irradiance can thus be misleading for an absorber which has a low saturation irradiance due to a very long lifetime.

2.2.2 Transmittance vs. Incident Irradiance Behavior

An expression for the transmittance vs. incident radiance for the generalized three-level saturable sorber is easily obtained by considering the attenuation the incident beam by the absorber. The absorber is sumed to be "thick", meaning that the absorption of otons is a function of position within the cell (2.23). om the expression for the steady-state absorption fficient, Eq. (2-14), the attenuation of the incident m is given by

$$dI_{(x)}/dx = -I_{(x)}\ \alpha_o[1 + I_{(x)}/I_s]^{-1} \qquad (2\text{-}15)$$

re x is the distance within the absorbing medium. arating variables, integrating and imposing the ndary condition that the incident irradiance is I_o s

$$\alpha_o = \ln [I_o/I_{(x)}] + [I_o - I_{(x)}]\ /I_s. \qquad (2\text{-}16)$$

tion (2-16) can be rewritten in terms of the smittance obtained under low incident irradiance, $\exp(-\alpha_o x)$, giving

$$\ln(T_o/T) + I_o/I_s(1 - T) = 0, \qquad (2\text{-}17)$$

which was first derived by Keyes (2.22).

Equation (2-17) is plotted in Figure 2.3 for three different T_o values for a fixed, arbitrary value of I_s. The transmittance is seen to approach 1.0 (complete transparency) as I_o becomes large relative to I_s.

.3 Four-level System with Excited State Absorption - "Power-Saturation"

In numerous cases, the experimentally observed ransmittance vs. incident irradiance curves do not pproach 1.0, but asymptotically approach a value which is ess than one at high values of the irradiance. This enomenon is termed residual absorption and is thought to due to absorption of incident photons by species in the cited state(s).

Figure 2.4 is an energy level diagram for a four vel system. Levels 1 and 2 are assumed to be the only vels populated. Absorptive transitions take place tween levels 1 and 3 as well as levels 2 and 4. The nsition from level 2 can either represent an $S_1 \dashrightarrow S_n$ $T_1 \dashrightarrow T_n$ transition.

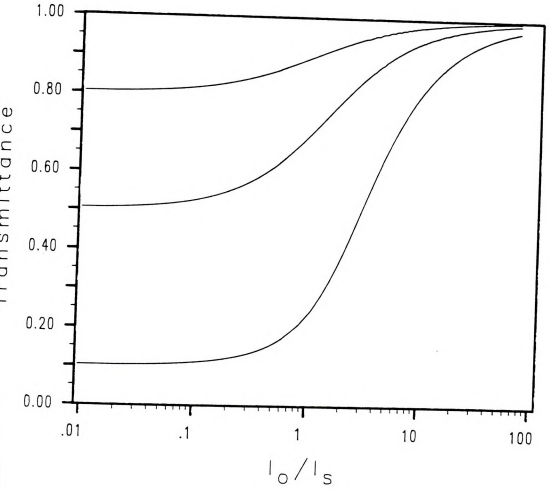

re 2.3 **Transmittance of a three-level absorber plotted vs. I_o/I_s. I_o and I_s are the incident and saturation irradiances, respectively. The three curves are for different intial transmittances.**

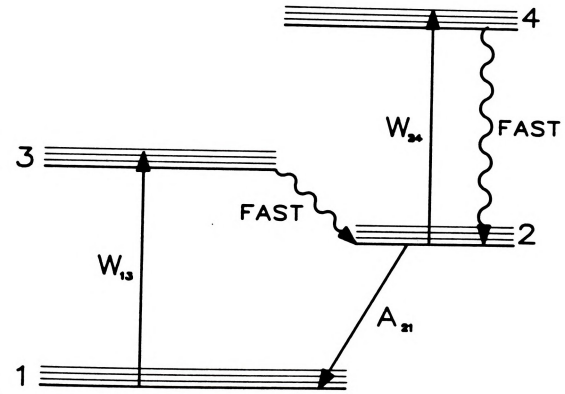

gure 2.4 Energy level scheme for a four-level absorber. Levels 1 and 2 are assumed to be the only levels populated. Level 4 is either an excited singlet or excited triplet manifold. W_{ij} is a stimulated transition probability ($\sigma_{ij}I$). A_{21} is the rate constant for relaxation (both radiative and nonradiative) from level 2.

2.3.1 Transmittance vs. Incident Irradiance Behavior

An expression for the transmission vs. incident irradiance behavior of this system is obtained in a manner similar to that for the three-level system. The net absorption coefficient is given by (2.14)

$$\alpha + \beta = \alpha_o n_1 + \beta_o (1-n_1) \qquad (2\text{-}18)$$

where

$$\alpha_o = \sigma_{13} N \qquad (2\text{-}19)$$

and

$$\beta_o = \sigma_{24} N. \qquad (2\text{-}20)$$

The total population is N and multiplying the net absorption coefficient by the fractional population (n_1 or n_1) gives the absorption coefficient for each state.

The attenuation of the incident irradiance by a thick saturable absorber is given by (2.14)

$$dI_{(x)}/dx = -I\,(\alpha + \beta) \qquad (2\text{-}21a)$$

$$dI_{(x)}/dx = -I\,[\alpha_o + \beta_o (I_{(x)}/I_s)]/[1 + I/I_s]. \qquad (2\text{-}21b)$$

ntegration yields the following expression for the
ransmittance vs. incident irradiance behavior of the
ystem (2.14):

$$\ln(T/T_o) = (A - 1)\ln[(A + (I_o/I_s))/(A + T(I_o/I_s))] \quad (2\text{-}22)$$

ere A is given by

$$A = \sigma_{13}/\sigma_{24}. \quad (2\text{-}23)$$

Equation (2-22) is plotted in Figure 2.5 for three
fferent T_o values with an arbitrarily chosen I_s value
d an A value of 5. The curves are seen to approach a
ximum transmittance below unity. When $I_o >> I_s$, the
nsmission, T, approaches a maximum given by

$$T_{max} = T_o^{-A}. \quad (2\text{-}24)$$

the coefficient for absorption from the excited state
larger than that from the ground state at the
itation wavelength, T_{max} will be less that T_o (i.e.,
absorber will be less transmissive at high incident
adiances) (2.1,2.12).

Hammond has considered the case in which both
ulated emission and excited state absorption occur

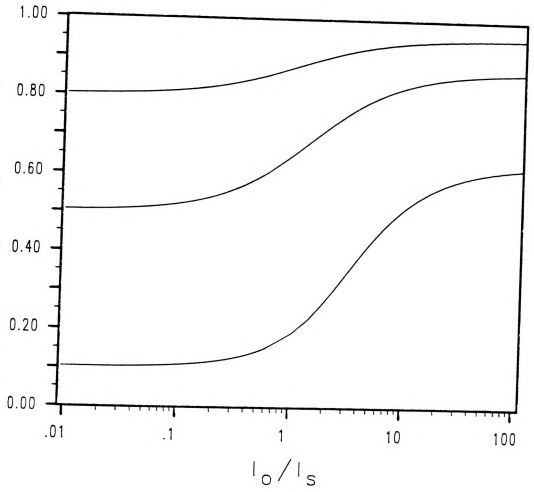

2.5 Transmittance of a four-level absorber plotted vs. I_o/I_s. I_o and I_s are the incident and saturation irradiances, respectively. The three curves are for three different initial transmittances. The asymptotic limit of the transmittance is below 1.0 indicating that absorption of photons occurs from an excited state.

5). Equation (2-22) also applies in this instance;
ver, A is then given by

$$A = (\sigma_{13} + \sigma_{31})/\sigma_{24}. \qquad (2\text{-}25)$$

the net effect of the stimulated emission is to raise
aximum transmittance value achieved over that which
hieved when excited state absorption is not
panied by stimulated emission.

nergy-Saturated Absorbers

The models for power-saturated absorbers are not
cable if the relaxation time of the system does not
t the assumption that a steady-state is attained.
ers whose relaxation times are long with respect to
lsewidth of the exciting radiation are termed
y-saturated" absorbers. The extent to which an
-saturated absorber is bleached depends not on the
nt irradiance (photons-cm^{-2}-sec^{-1}), but on the
density, which is the integrated irradiance
ns-cm^2). The energy density is given by (2.14)

$$(t) = \int I(t)dt. \qquad (2\text{-}26)$$

temporal profile of the laser pulse cannot be assumed
e a step-function and integration over the pulsewidth
equired. A general solution to the rate equations for
o-level system is, therefore, required since the
dy-state assumption is no longer valid. Frantz and
lk (2.24) have published the lengthy general solution
two-level system. Avizonis and Grotbeck (2.25)
equently integrated the equation resulting from the
al solution (2.15), giving Hercher's equation for the
y transmission of an optically thick energy-saturated
ber. The analytical expression for the energy
mission, T_J, is

$$T_J = J_s/J_o \ln[1 + T_o(\exp^{(J_o/J_s)} - 1)] \qquad (2\text{-}30)$$

T_J is given by

$$T_J = J/J_o \qquad (2\text{-}31)$$

and J_o are the transmitted and incident energy
ies, respectively. J_s is the saturation energy
(photons-cm^{-2}) and is $1/\sigma$ where σ is the
ion cross-section (2.4). Therefore, it is the
de of the transition cross-section which determines
rgy density required to achieve saturation for the
saturated absorber. Equation (2-31) is plotted in
2.6 for three values of T_o. The energy transmission

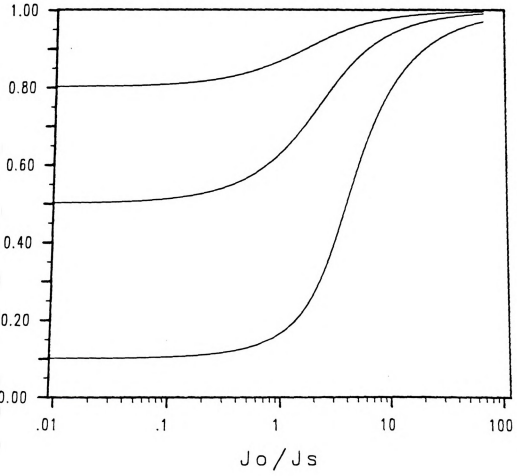

6. Transmittance of an energy-saturated absorber plotted vs. J_o/J_s where J_o and J_s are the incident and saturation energy densities, respectively. The three curves are for three different initial transmittances.

een to approach unity as J_o becomes much larger than
n analytical expression for the transmission was not
in the literature for an energy saturated absorber
excited state absorption. Equation (2-30) has been
by various authors to analyze the experimental
mission vs. incident energy density behavior for slow
gy-saturated) absorbers (2.4,2.26,2.27).

ummary

discussion of the photophysical properties which
saturation without stimulated emission and
tion equalization were discussed. Analytical
sions for the transmittance vs. incident irradiance
or have been presented for power-saturated systems
nd without excited state absorption. An analytical
sion was also presented for the energy transmission
vo-level energy-saturated absorber. Excited state
ion was seen to limit the maximum transmittance
ble for the power saturated absorber to a value
.0. It should be noted that power- or energy-
ion is not an inherent property of the absorber,
ults from the relationship between the lifetime of
orber of interest and the pulsewidth of the
radiation. There are no analytical expressions
transmittance vs. incident irradiance (or energy
behavior for absorbers with lifetimes

roximately equal to the pulsewidth of the exciting
m. In these instances, the transmittance behavior can
determined by solving a set of rate equations for the
ulation of the energy levels and the transmittance at
remental times during the pulse of a known or assumed
file.

REFERENCES

Giuliano, C. R.; Hess, L. D. *IEEE J. Quantum Electron.* **1967**, *QE-3(8)*, 358.

Stone, J.; Goodman, M. F. *Phys. Rev. A.* **1978**, *18(6)*, 2618.

Selden, A. C. *J. Phys. D.* **1970**, *3*, 1935.

Rudolph, W.; Weber, H. *Opt. Commun.* **1980**, *34(3)*, 491.

Hercher, M.; Chu, W.; Stockman, D. L. *IEEE J. Quantum Electron.* **1968**, *QE-4(11)*, 954.

Omenetto, N. *Analytical Laser Spectroscopy*; John Wiley and Sons; New York, 1979, p. 15.

Omenetto, N. *Analytical Laser Spectroscopy*; John Wiley and Sons; New York, 1979, p. 142.

Steinfeld, J. I. *Molecules and Radiation;* MIT Press; Massachusetts, 1985, p. 389.

Steinfeld, J. I., Ed. *Laser & Coherence Spectroscopy*; Plenum Press: New York, 1978, p. 14.

outillier, G. D.; Winefordner, J. D.; Omenetto, N. *ppl. Opt.* **1978**, *17(21)*, 3482.

uff, L.; DeShazer, L. G. *Appl. Opt.* **1970**, *9(1)*, 233

chafer, F. P. *Agnew. Chem. Internat. Edit.* **1970**, *(1)*, 9.

emtroder, W. *Laser Spectroscopy-Basic Concepts and nstrumentations*; Springer-Verlag: New York, 1981, 45.

rcher, M. *Appl. Opt.* **1967**, *6(5)*, 947.

mmond, P. R. *Appl. Opt.* **1979**, *18(4)*, 536.

ller, A.; Pfluger, E. *Chem. Phys. Lett.* **1968**, *2(3)*, 5.

wer, S. K.; El-Sayed, M. A. *Chem. Rev.* **1966**, *66*, 9.

rbold. P.; Gouterman, M. *Chem. Rev.* **1965**, *65*, 413.

paeth, M. L; Sooy, W. R. *J. Chem. Phys.* **1968**, *48(5)*, 345.

osonocky, W. F.; Harrison, S. E.; Stander R. *J. Chem. Phys.* **1965**, *43(3)*, 831.

menetto, N. *Analytical Laser Spectroscopy*; John iley and Sons; New York, 1979, p. 16.

eyes, R. W. *IBM J. Res. Dev.* **1963**, *7*, 334.

eeg, F. W.; Madison, L.; Fayer, M. D. *Chem. Phys.* **985**, *94*, 265.

rantz, L. M.; Nodvik, J. S. *J. Appl. Phys.* **1963**, *4(8)*, 2346.

vizonis, P. V.; Grotbeck, R. L. *J. Appl. Phys.* **1966**, *7(2)*, 687.

aenz de la Calzada, M.; Lam, H.; Denariez-Roberge, . M. *Can. J. Phys.* **1976**, *54*, 1449.

ason, R. W.; Greenhow, R. C.; Goodall, D. M.; olzwarth, J. F. *Opt. Commun.* **1980**, *32(1)*, 113.

CHAPTER 3

EXPERIMENTAL

Introduction

The apparatus and procedures for the experimental ies are discussed in this chapter. A brief description he Nd:YAG/dye laser system used for this work is ded in Section 3.1. Special procedures employed r limitations encountered with the laser system are ssed with the experimental details. Section 3.2 is an iew of the data acquisition system designed and bled as a part of this thesis research. Features of ata acquisition system that are directly related to cquisition of meaningful data are covered in Section [The reader is referred to Appendices A, B and C ore comprehensive information on the data acquisition .] Information on the photodiode detector circuit e sample preparation and handling is given in ns 3.3 and 3.4, respectively. Section 3.5 is a sion of the use of UV-Visible absorption spectra. ms of the optical set-ups and the procedures ic to each of the experimental studies are presented tions 3.6 - 3.10. Section 3.6.3 contains detailed ation on the alignment of the photodiode detectors.

experimental studies are categorized as follows:
lation modulation, saturation of fluorescence, ground
e recovery time, population modulation across the S_0 -
absorption band, and dual wavelength pump/probe
ies. The experimental studies are discussed in the
listed above.

Pulsed Nd:YAG/Dye Laser System

A pulsed Nd:YAG laser oscillator/amplifier (Model
A, Quanta-Ray, Inc., Mountain View, CA) plus
iary optics was used in this work; a block diagram is
in Figure 3.1. The fundamental output wavelength of
aser is 1.064 microns, and the full-width-at-half-
m (FWHM) pulse width is 8-9 ns. The pulse repetition
s variable between 2 and 22 Hz, although the pulse-
se stability of the laser is best when operated at
The resonator is diffraction-coupled and is an
le resonator (3.1, 3.2). In the current
uration, the beam profile is a "filled-donut", which
ended to approximate a Gaussian beam (3.3). For
ed operating procedures and specifications the
is referred to the literature provided by the
turer (3.4).

angle-tuned harmonic generator (Model HG 1,
Ray, Inc.) with Type II KD*P crystals, provides

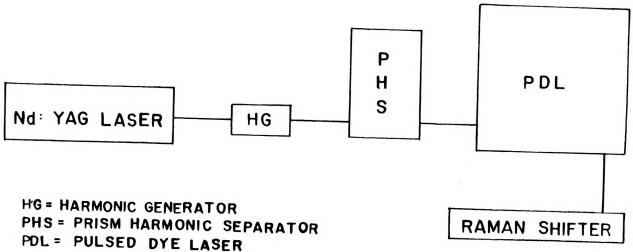

Figure 3.1 Block diagram of pulsed Nd:YAG/dye laser system.

beams at harmonic frequencies of the fundamental.
avelengths of the second, third and fourth harmonics
32 nm, 355 nm and 266 nm, respectively. The
widths for the 532 nm, 355 nm and 266 nm beam are 6-7
5-6 nsec, and 4-5 nsec, respectively. The harmonics
e generated in the following combinations: 532 nm
532 nm and 355 nm, or 532 nm and 266 nm. The
ıental is elliptically polarized and the harmonics
nearly polarized upon exiting the harmonic
tor. If two harmonics are generated, the
zation of one is orthogonal to that of the other.
ndamental and the generated harmonic(s) exit the
ic generator colinearly. Table 3.1 summarizes the
ngths, pulsewidths, energies, average powers and
›wers of the beams available from the laser system.

Quanta-Ray prism harmonic separator (PHS-1) serves
ially separate the different beams according to
gth. This unit consists of a Pellin-Broca prism and
s of turning prisms. Two beams can exit the PHS-1
neously through neighboring ports. If a third beam
ated and enters the PHS-1, it is dumped within the
a result of the optical configuration. The
tion of the emerging beam(s) can be rotated by
wave plates provided in the PHS-1. A beam exiting
l can be used to pump the dye laser (Model PDL-1,
ay, Inc.), or may pass directly through the PDL-1.

Table 3.1. Summary of the Nd:YAG Laser Beam Characteristics.

QUANTA-RAY
Nd: YAG LASER SYSTEM

WAVELENGTH(nm)	PULSE WIDTH(ns)	mj/PULSE	PEAK POWER(MW)	AVG. POWER(W)
1064	8-9	700	80	7
532*	6-7	225	32	2.25
355*	5-6	125	20	1.25
266*	4-5	60	12	0.6

WITH:
10 HZ REPETITION RATE
AMPLIFIER AND OSCILLATOR
*HG-1 HARMONIC GENERATOR AND TYPE II KD*P SHG CRYSTALS

two beams are required, both may pass directly through
dye laser, or one beam may be used to pump the dye
er while another beam passes through it.

The pulsed dye laser contains pre-amplifier and
ifier stages. Both end-on and side-on pumping of the
ifier can be utilized with this dye laser system. The
ce of pumping configuration depends on the dye used.
manufacturer has recommended that the amplifier be
-pumped when the blue dyes (i.e., stilbene 420 and the
arins) are used.

Several trigger outputs are available from the Nd:YAG
. These outputs are synchronized with laser-
ating events such as flashlamp firing and Q-
hing. The variable trigger output, which can be set
cur from 800 nsec prior to the pulse to 100 nsec
the pulse, was used to trigger the timing circuit
controls the data acquisition system. The relative
ard deviation of the timing of this trigger with
t to the laser pulse is
% of the nominal trigger setting.

erview of the Data Acquisition System

igure 3.2 provides a functional diagram of the data
ition system. The data acquisition system is gated,
ating and microprocessor-controlled. A detector (a

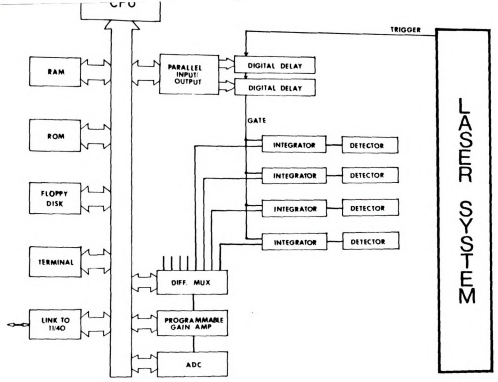

Figure 3.2 Functional diagram of data acquisition system. A detector and integrator are provided for each signal channel. Timing is controlled via the digital delay cards which are triggered by a laser generated pulse.

todiode or photomultiplier tube) and gated integrator
del 4130, Evans Associates, Berkeley, CA) are used for
of the signals monitored. Four signals can be
grated in the present configuration. Gating can occur
all channels coincidently or one (or two) of the
nels can be gated at different delay times. This
ichannel operation allows the signal of interest to be
alized with respect to a reference beam. For example,
ratio of the integrated intensity transmitted through
mple to the integrated incident intensity provides a
lized transmittance value. Normalization was a
sity due to the pulse-to-pulse intensity fluctuations
are inherent in the Nd:YAG laser. The data are
red and stored for every pulse on each channel, since
ging the integrated signals is often inappropriate
ne nonlinear response of the sample achieved in this
cation (3.5). The laser-generated trigger pulse was
occur 800 ns before the laser pulse in order to
time to initiate and complete the series of events
ed for the acquisition and storage of data. These
include gating and resetting the integrators and
ng the computer that data are ready for acquisition.
egrated signals are held and sequentially
exed, amplified and converted by the analog-to-
converter.

The acquired data can be immediately displayed on a terminal and/or stored on floppy disk. The ratio of signal and reference intensities, the averages of the al, reference and ratioed intensities, and the ciated relative standard deviations for a data set ically 150 pulses per set per channel) can also be diately displayed. The ability to immediately display data and standard deviations was an invaluable aid in set-up and fine-tuning of the various optical gurations used during the course of this work. [This will be addressed when the optimization and ment of the optical-set-ups is discussed.]

hotodiode Detector Circuit

The circuit for the PIN photodiode detectors (Part 082-4220, Hewlett-Packard Co., Palo Alto, CA) is in Figure 3.3. The photodiodes were reverse-biased V which results in a faster rise-time (< 1 nsec) hen no bias is applied. The power supply consisted 9 V batteries in series; this provided an ical and convenient source of clean power. The iodes protruded through a grommet which was fitted aperture in the grounded aluminum case which the circuit. Coaxial cables (50 ohm) transmitted todiode signals to the integrators.

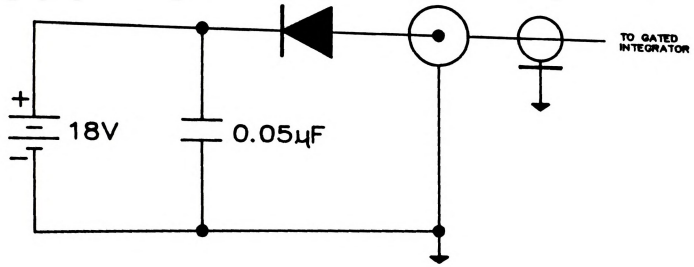

Figure 3.3 Photodiode detector circuit diagram. The circuit was housed in a grounded aluminum case with an aperture through which the photodiode protruded. The photodiode was reverse-biased at +18 V using two 9 V batteries in series.

Samples

Laser grade rhodamine 6G (R6G) (Eastman Kodak, hester, NY) was used as received. Reagent grade hanol (from Mallinckrodt, Inc., Paris, KY or MCB gents, Gibbstown, NJ) was initially distilled and used he solvent. No differences were observed in the UV- ble absorption spectra, or in the experimentally rmined laser transmission values, if the methanol was directly from the bottle. Therefore, distillation of solvent was discontinued. Experimental solutions with entrations of 1 x 10^{-5} M, 5 x 10^{-6} M, and 1 x 10^{-6} M prepared from a 1 x 10^{-4} M stock solution. New tions were prepared for each set of experiments and tions were stored in the dark when they were not in

The porphyrins, (etio)hemechloride and (octa)3- xypropylporphyrin, were used as received after esis and purification in the Michigan State rsity Chemistry Department. The (etio)hemechloride octa)3-hydroxypropylporphyrin were furnished courtesy fessors C. K. Chang and B.A. Averill, respectively. olic solutions of the porphyrins were investigated.

lowing sample solutions were used in order to ze thermal effects of the laser such as blooming and g, or photodecomposition. (The solvent, which

ovides normalized reference transmission values, was
mped through a matched cell and the set-up was identical
that described for the sample solutions.) A 1-liter
ree-necked flask contained 500 ml of the sample
lution; this flask served as the sample reservoir. The
lution volume was large in order to minimize any effects
e to evaporation or decomposition. The flask was fitted
h rubber septa. Holes were punched through two of the
ta and glass tubing was inserted. Silicone tubing was
ached to both ends of the sample cell and to the glass
ing on the sample reservoir. The sample cell was a
w-through quartz cuvette with two 1 cm pathlengths and
r optical surfaces. The tubing between the reservoir
the bottom of the sample cell was inserted in a
istaltic pump. In order to avoid bubbling within the
ette, the sample solution flowed in through the bottom
out through the top into the reservoir. The return
ng was fitted with a microfiber filter tube (Part No.
-DQ, Balston, Inc., Lexington, MA) in order to
mize particulate matter which would give rise to light
tering.

The flow rate was approximately 50 ml/min. The actual
e of this parameter was found to be non-critical by
ring the transmission of the sample at different flow
using a low power 532 nm laser beam. Averaged
lized transmission values for 150 pulses obtained at

w rates between 5 and 100 ml/min agreed within the 1-
relative standard deviations. However, slightly lower
ısmission values were observed if the solution was
ic. The slightly lower transmission values can most
ly be attributed to both thermal blooming and heating
he solution.

Both air-saturated and deoxygenated solutions were
. Solutions were deoxygenated by bubbling methanol-
ated N_2 through the solutions for 45 minutes prior to
iments. Methanol-saturated N_2 was used to minimize
vaporation. During experiments, solutions were kept
a slight positive pressure to maintain the degassed
tion.

V-Visible Absorption Spectra

UV-Visible spectra were taken with a Cary 17D
rophotometer (Varian, Palo Alto, CA). Spectra taken
to the experiments provided reference transmission
which were compared to the transmission values that
xperimentally obtained when the laser at low power
cident on the sample. Spectra (or absorbance
ements at the wavelengths of interest) taken after
et of experiments provided a check for sample
osition, evaporation and contamination from the
rough tubing.

A spectral check for sample photodecomposition was rformed in the following manner. Quartz cuvettes ntaining the sample solutions were placed in the paths the second and third harmonic laser beams. The cuvettes ed had 1 cm pathlengths and were irradiated for 30 nutes. The average energy per pulse was approximately 30 at 532 nm and 20 mJ at 355 nm. Comparison of the ectra taken prior and subsequent to irradiation showed evidence of photodecomposition at either wavelength e., no spectral changes were observed).

A check for was also made leaching and sample tamination from the silicone tubing used in the istaltic pump. Spectra were taken of methanol in which ces of the silicone tubing (from Cole-Parmer, Chicago, used in the peristaltic pump had been immersed for an ended period of time (approximately 48 hours). Tubing erioration and/or leaching was evidenced in the orption spectra by increasing absorption across the 300 o 190 nm spectral region. Sample contamination was ented by using new tubing for each set of experiments. silicone tubing was used because it afforded the best romise between pliability and acceptable chemical stance to methanol.

The spectrophotometer was also used to determine the bances at the wavelengths of interest of the Schott neutral density filters which were used as beam

:nuators. These absorbance values were used to
:ulate the attenuation achieved when they were placed
laser beam. [A list of the attenuation provided by
filter is stored with the filters.]

Population Modulation Studies

The transmittance vs. incident irradiance behavior of sample solutions was investigated. An increase (or ease) in the transmission with increasing irradiance cates that population modulation has been induced in sample solution. The experimental set-up for the lation modulation studies is shown in Figure 3.4.

3.6.1 Excitation with the 532 nm Beam

The 532 nm laser beam was used to pump the S_0 --> S_1 itions of rhodamine 6G, (octa)3-xypropylporphyrin, and (etio)hemechloride. For mine 6G both deoxygenated and air-equilibrated ions were investigated.

The incident laser beam was split, thus providing a nce beam for monitoring the incident intensity. The der of the beam passed through a 7 mm aperture (the width of the quartz cuvettes) and then through the or solvent cell. The transmitted beam was also

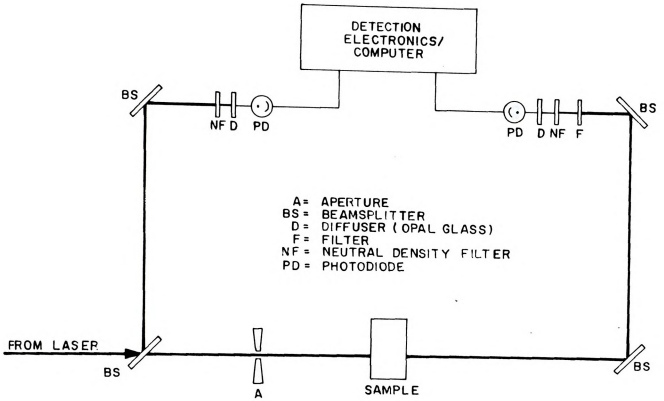

Figure 3.4 Diagram of the optical set-up for population modulation studies. The incident laser beam is split to provide a reference beam for monitoring incident intensity.

plit in order to attenuate the intensity reaching the notodiode detector. [The beamsplitters were microscope lides mounted in lens holders on magnetic bases.] The ormalized transmission of a sample solution is:

$$[\ (I/I_o)_{sample}\ /\ (I/I_o)_{solvent}\ ]\ x\ N$$

ere I_o and I are the incident and transmitted tensities, respectively, and N is the factor required to rrect for the intensity attenuation by the neutral nsity filters.

An aluminum holder, mounted on a magnetic base, was nstructed for the matched sample and solvent cells. The lls fit into the holder very precisely. The sample lder was designed to slide between two reproducible itions; one position places the sample cell in the path the laser beam, the other places the solvent cell ference cell) in the beam path. Position roducibility was evidenced by the agreement of the raged transmission values obtained after repeated ositioning of the cell holder between the sample and vent positions. Each replicate data set of 150 alized transmission measurements typically showed dard deviations of 1 %. [Note: the cell holder was ially aligned in the beam path by flowing solvent ugh both cells and adjusting the holder position such

that the ratio of the normalized transmission was the same for both of the cells.]

A 532 nm spike filter was placed in front of the photodiode which detected the transmitted beam intensity. This filter ensured that fluorescence emitted in the same direction as the incident beam was not detected in addition to the transmitted light. The magnitude of any stray light which may have impinged on the detectors was essentially infinitesimal in comparison to the intensity of the incident laser beam. Strategically placed black baffles further reduced the possibility of detecting stray light.

Transmission data were collected for 150 sequential laser pulses at each of ten nominal average laser powers between 0.50 mW and 600 mW. The laser power was set by a control on the laser panel, and a volume-absorbing disc calorimeter (Model 38-0101, Scientech, Inc., Boulder, CO) was used for the power measurements. [The power meter measures the average power per pulse or the total energy for a series of pulses.]

3.6.2 Excitation with the 355 nm Beam

Population modulation studies were performed using the 355 nm laser beam to pump the S_0 --> S_4 transition of rhodamine 6G. The experimental conditions were as

described for the studies at 532 nm. Short-pass filters (Corning 7-54 from Esco Products, Inc.) were placed in front of the neutral density filters in order to absorb the scattered 532 nm light that exits the prism harmonic separator in the same direction as the 355 nm beam. The short-pass filters were placed in front of the neutral density filters to minimize the possibility that fluorescence from the filters themselves might reach the detectors.

3.6.3 Photodiode Alignment and Linearity Check

Exact alignment of the photodiodes was found to be extremely critical due to the small active area of the photodiodes and the "hot spot" in the profile of the laser beam. The majority of the beam intensity is located in an area not larger than 1 mm in diameter. Since the active area of the photodiodes is 0.5 mm it is imperative that the hot spot be incident upon it.

Initial alignment was found to be best effected in the following manner. The photodiode output, terminated with a 50 ohm terminator, was monitored with an oscilloscope. The variable trigger from the laser was used as an external trigger to the scope. The photodiode was then positioned in the beam at the point where the maximum signal was observed on the oscilloscope. This procedure

was extremely tedious; however, it was necessary in order to assure proper spatial positioning.

The importance of exact alignment is illustrated by the following experiment. The experimental set-up for photodiode alignment was as shown in Figure 3.4, but without the sample cell in the path of the laser beam. One of the photodiodes was aligned as described above and the other was randomly positioned in the beam. Ideally, the ratio of the two digitized signals should be constant from one pulse to the next. In this case, the standard deviations of the ratios for 150-pulse data sets varied from 10% to 40%. The randomly positioned photodiode was then correctly aligned and the standard deviations of the ratios for data sets of the same size were typically 1%. These results show that the intensity fluctuations in one region of the laser beam are not linearly related to the intensity fluctuations in another region of the beam.

The intensity of the light incident on the photodiodes was attenuated such that the magnitude of the photodiode signal observed on the oscilloscope was between 5 mV and 150 mV. This was done in order not to damage the photodiodes by exceeding the limits of their heat dissipation capabilities. The beam is initially attenuated with Schott glass neutral density filters (Esco Products, Inc., Oak Ridge, NJ) and then diffused and further attenuated with opal glass. [Neutral density filters with

dielectric coatings cannot be used to attenuate the pulses from this laser except at extremely low incident powers due to the inadequate heat dissipation properties of such coatings; they are easily burned and destroyed.] The opal glass was placed against the grommet which held the photodiode in the aluminum housing. The neutral density filter(s) were placed in front of the opal glass.

Linearity of the photodiode response was insured by attenuating the laser beam before it reached the photodiode. To check the linearity of photodiode response after the opal glass and neutral density filters were in place, another neutral density filter was placed first in the path of the reference beam channel and then in the path of the transmitted beam channel. The changes in the ratioed value of the two channels was compared to the change that would be expected from the calibrated attenuation of the neutral density filters. The absolute percent error in the change in the averaged ratios was 1.4 % using a neutral density filter that transmitted 71.4 % of the incident beam and 0.4 % using a neutral density filter that transmitted 50.8 % of the incident beam. The manner in which the photodiode detectors were aligned and the laser beam was attenuated thus results in a linear response of the data acquisition system.

3.6.4 Integrator Balancing and Gate Positioning

The temporal position of the laser pulse with respect to the pulse used to trigger the data acquisition system is a function of the laser power setting. This requires that the position of the integrator gate be optimized each time the laser power is changed. If the gate is not positioned properly, the entire pulse may not be integrated and extremely large fluctuations will be observed in the digitized data. The gate position is optimized when the digitized data values for each channel are maximized; a corresponding decrease in the standard deviation of a data set for the channel of interest is observed.

The noise which is integrated when the laser beam is not incident on the photodiode is dependent on the laser power setting and integrator gate position. The magnitude of the noise generated increases with increasing laser power and varies in time. At a given laser power setting for a fixed period of time, however, this extra noise is essentially constant in integrated magnitude. This noise (baseline offset) was balanced out by applying a current of equal magnitude and opposite polarity to the summing junctions of the integrators; this option is provided on the integrator modules [see Appendix B].

3.7 Saturation of Fluorescence Studies

The normalized fluorescence intensity and transmission of rhodamine 6G solutions were simultaneously monitored as a function of the incident pumping power at 532 nm. Fluorescence measurements were made at 560 nm, the emission maximum of R6G in methanol (3.6). Air-saturated and deoxygenated solutions were investigated at several concentrations. Saturation of fluorescence is evidenced by a nonlinear increase in the fluorescence intensity as the incident pump beam intensity is increased. The optical set-up for these experiments is shown in Figure 3.5. Transmission measurements, optimization of the system electronics, and photodiode alignment were accomplished as discussed in Section 3.6.3.

The fluorescence was monitored at 90° to the incident 532 nm beam. Two lenses focused the fluorescent light into the monochromator (Model EU-700/E, Heath, Benton Harbor, MI). The slitwidth and resulting bandwidth were 100 microns and 2 Angstroms, respectively (3.7). Scattered light at the pump wavelength was discriminated against by a 532 nm notch filter at the entrance slit of the monochromator. The sample cell holder and optics were enclosed in a black box which had openings for the incident 532 nm beam and the fluorescent light only.

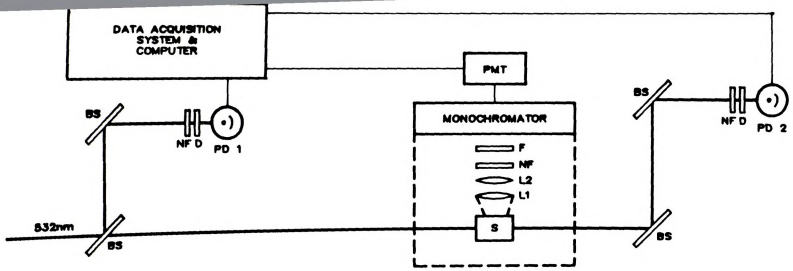

Figure 3.5 Optical set-up for saturation of fluoresence experiments. The dotted line represents the position of the black box placed over the cell holder, lenses and filters.

The fluorescence signal at 560 nm was detected using a thermoelectrically-cooled photomultiplier tube (Model R928, Hamamatsu Corp. Middlesex, NJ) with -680 V applied to the cathode. The applied voltage was not changed as the laser power was increased. To avoid a nonlinear response of the photomultiplier tube to the large fluorescence signal from the high incident laser powers, a calibrated Schott glass neutral density filter was placed at the entrance slit of the monochromator prior to acquiring data at the higher laser powers. Attenuation of the fluorescence signal in this manner ensured that the photomultiplier tube response was not saturated. The linearity of the PMT response was checked by using a neutral density filter to attenuate the fluorescence and observing that the decrease seen in the averaged ratio of the fluorescence signal to the incident 532 nm intensity matched that expected from the transmission of the neutral density filter.

The sample cell was aligned to ensure that the spatial maximum of the fluorescent light, resulting from the inhomogeneity of the laser beam, entered and exited the monochromator. This was accomplished by placing a high intensity tungsten lamp at the exit slit of the monochromator. The monochromator was then set to pass a wavelength which is very easily seen, such as 650 nm, and the sample cell was then positioned so that its center was

at the point in front of the entrance slit at which the 650 nm light refocuses. The lenses were then crudely positioned and the photomultiplier tube put in place. The PMT output at 560 nm was monitored by an oscilloscope and the lenses were adjusted laterally and horizontally until the fluorescence signal from the sample was maximized.

3.8 Ground State Recovery Studies

The ground state recovery studies were single-wavelength pump/probe experiments. A 532 nm probe beam monitored the transmission of a 1 x 10^{-5} M rhodamine 6G solution at several delay times relative to a 532 nm pump beam. Experiments were performed at two average pump beam powers, 50 mW and 100 mW. Information regarding the onset, duration and detection of the population modulation induced by the pump beam was sought. The transmissions of the pump and probe beams were measured as previously described. The optical set-up is illustrated in Figure 3.6.

Two 532 nm beams were split off from the pump beam; one beam served as the reference beam, as in previously-described experiments, and the other was employed as the low-energy probe beam. Two right angle prisms and a glass 2" retroreflector (Melles Griot, Irvine, CA) were used as an optical delay line for the probe beam. The pump and

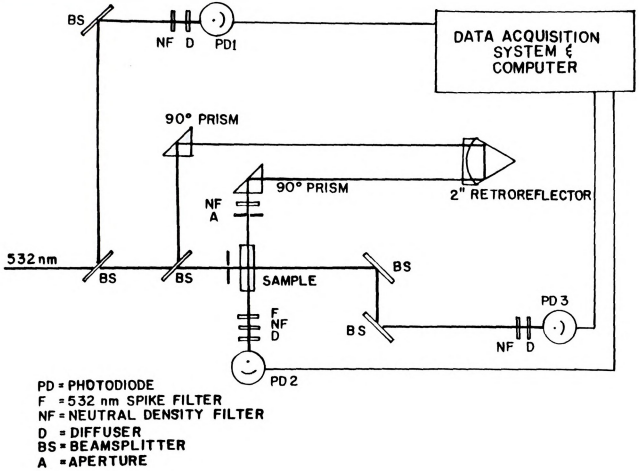

Figure 3.6 Optical diagram for ground state recovery studies. The reference signal was monitored by PD1. The probe and pump beam transmittances were monitored by PD2 and PD3, respectively.

probe beams passed through the cell along perpendicular axes. The transmission of the probe beam was measured at delay times ranging from 1.02 nsec to 14.99 nsec. A delay time of 1.02 nsec was the shortest delay possible due to the physical constraints of the optical set-up. A 532 nm spike filter was placed in the path of the probe beam to ensure that fluorescence emitted in the direction of the probe beam did not reach the photodiode detector.

The probe beam was attenuated by a neutral density filter, and its size was defined by an aperture. The probe and pump beam diameters were 6 mm and 7 mm, respectively. The pump beam diameter was 7 mm because the cell holder only allowed a 7 mm clear aperture. The diameter of the probe beam was made smaller than that of the pump beam in order to ensure that the volume sampled by the probe beam was also being pumped. Apertures, closed to 1 mm diameters, were used to align the optical paths so that the "hot spots" of both beams overlapped in the center of the cell. The experimental geometry required that the sample and solvent cells were alternately placed in the cell holder in order to measure the transmission of both the pump and probe beams simultaneously. In other words, the solvent cell was removed when measuring the transmissions of the pump and probe beam through the sample cell, and vice versa.

3.9 Population Modulation across the S_0 --> S_1 Absorption Band

The S_0 --> S_1 transition of rhodamine 6G was pumped at 532 nm and the transmission of the solution was simultaneously probed at selected wavelengths within the absorption band (see Figure 4.1 for the absorption spectrum). Information regarding whether the transmission of the probe beam at each wavelength was affected during pumping was sought. Transmission measurements were made as in the experiments described previously. Figure 3.7 illustrates the optical set-up for these studies.

The pump and probe beams were split, providing references for the incident intensities at both wavelengths. In order to obtain normalized transmission values at the pump and probe wavelengths, it is necessary that the incident dye laser beam and pump beam intensities are measured. Four signal channels were thus required in this application. The pump and probe beams pass through the cell at an angle of 90°. A right angle prism turns the probe beam and directs it through the sample cell. As described in Section 3.8, in order to simultaneously monitor the transmission of both the pump and probe beams through a single cuvette, the sample and solvent cells were alternately placed in the cell holder . In this set of experiments, measurements of residual signals at PD4 were also made when the probe beam was blocked. Any

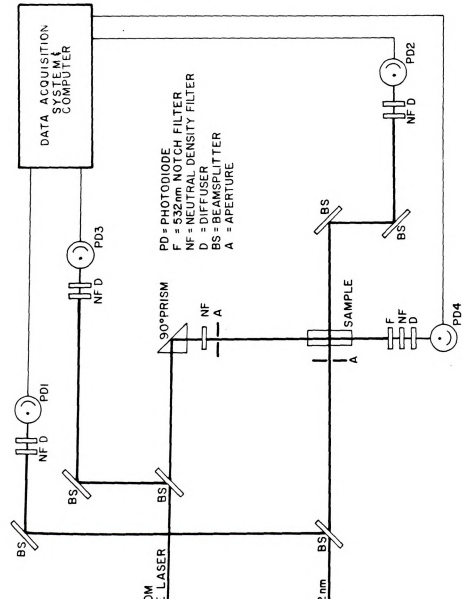

Figure 3.7 Diagram of the optical set-up for studies of population modulation across the $S_0 \rightarrow S_1$ absorption band of rhodamine 6G. The 532 nm beam was the pump beam and the dye laser provided the probe beam.

background fluorescence which may have reached that detector following excitation of the sample with the pump beam was measured and subtracted from the transmitted probe intensity. Spike filters were not available and a monochromator was not employed.

The probe beams were generated by the Quanta-Ray pulsed dye laser (PDL-1). Coumarin 500 (Exciton Chemical Co, Inc., Dayton, OH) was pumped with the 355 nm beam of the Nd:YAG laser. Probe beams at 500 nm, 520 nm, 527 nm, 532 nm and 540 nm were used. The delay time of the probe beam, relative to the pump beam, was fixed at 2.5 ns. The 2.5 nsec delay was longer than desired, but was the shortest available within the physical constraints of the optical set-up.

The concentrations of Coumarin 500 used in the dye laser oscillator and amplifier were 400 mg/ml and 95 mg/ml, respectively. The amplifier and pre-amplifier were employed; the amplifier was side-pumped, as recommended by the manufacturer. The peak in the tuning curve of Coumarin 500 occurred at 520 nm under these experimental conditions and the intensity dropped off rapidly below 500 nm and above 540 nm. Details regarding the operation and alignment of the dye laser can be found in the operation manual supplied by Quanta-Ray, Inc. (3.8).

3.10 Dual Wavelength Pump/Probe Experiments

Colinear 532 nm and 355 nm beams were used to simultaneously pump the S_0 --> S_1 transition and probe the S_0 --> S_4 transition of rhodamine 6G. The transmission of the probe beam was investigated as a function of delay time with respect to the pump pulse. The normalized transmission of the probe beam was compared in the presence and absence of the pump beam at each probe delay time. The intent of this experiment was to determine whether the population modulation induced by the 532 nm pump affected the transmission of the 355 nm beam. The optical set-up for these experiments is shown in Figure 3.8.

Since normalized transmission values were desired for both the pump and probe beams, the incident and transmitted intensities were monitored at both 532 nm and 355 nm. Signal detection and processing were accomplished as previously described. Short-pass filters (Corning 7-54, from Esco Products, Inc.) prevented detection of the scattered 532 nm light by the photodiodes monitoring the 355 nm beam. A 532 nm spike filter ensured that fluorescence was not detected with the transmitted 532 nm beam.

The probe beam was delayed in time by diverting it through an optical delay line (not shown in Figure 3.8)

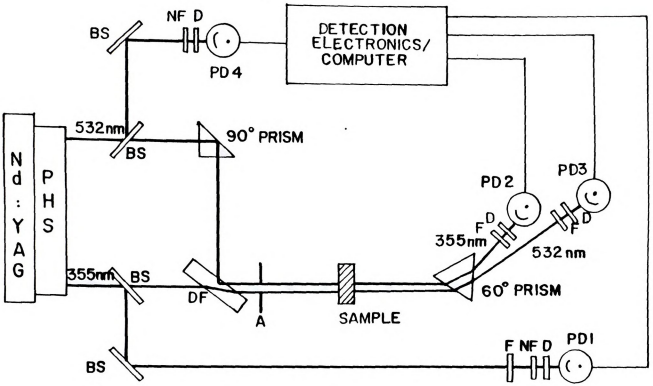

Figure 3.8 Optical set-up for dual wavelength pump/probe studies. The pump beam was the 532 nm beam and the 355 nm beam was the probe beam. The 355 nm and 532 nm reference beams were monitored by PD1 and PD4, respectively. The 355 nm and 532 nm transmitted beams were monitored by PD2 and PD3.

prior to transmission through the dichroic filter which was used to orient the 355 nm and 532 nm beams colinearly. A colinear orientation of the pump and probe beams assured that the 355 nm beam probed only the sample volume which was pumped. The beams were spatially separated by a 60° prism prior to detection.

Alignment of the two beams was accomplished in the following manner. The beamsplitter and dichroic filter were positioned in the 355 nm beam. The dichroic filter transmitted the 355 nm beam and reflected the 532 nm beam. Next, a photodiode was aligned to detect the 355 nm beam at a distance of approximately 3 ft. from the dichroic filter. Two irises, closed to a diameter of 1 mm, were positioned in the 355 nm beam, one in front of the photodiode and the other as close to the dichroic filter as possible. The irises were positioned such that the photodiode signal monitored on the oscilloscope was maximized. The irises were then opened and the 532 nm beam was crudely (i.e., visually) aligned with the 355 nm beam. The 355 nm beam was then blocked. After closing the irises as far as possible, the right angle turning prism was adjusted such that the "hot spot" of the 532 nm beam passed through the aperture of the iris closest to the dichroic filter. When this was accomplished, the position of the dichroic filter was tweaked (rotated) until the "hot spot" in the 532 nm beam was incident on the active

area of the photodiode. Evidence of the "hot spot" of the 532 nm beam being incident on the photodiode active area was the maximized signal observed on the oscilloscope. The sample cell holder and 60° prism were then put in place and aligned. The last step in the set-up of the optics for this study was to position the photodiodes which monitored the spatially separated 355 nm and 532 nm beams.

3.11 Summary

During the course of this experimental work, it was immediately apparent the desired signals (e.g., transmitted or fluorescent intensities) had to be normalized to a reference beam. This was required by the severe pulse-to-pulse fluctuations in beam power. The pulse-to-pulse stability of the harmonic beams improved if the laser was allowed to "warm up" prior to attempting to acquire data. The "warm up" period most likely allows the KD*P crystals to reach thermal equilibrium.

Other salient, and perhaps less obvious, points which became apparent are worthy of mention. The spatial inhomogeneity of the laser beam gives rise to extremely nonlinear fluctuations in intensity from one part of the beam to the next. This made alignment of the photodiodes extremely difficult. The ratios obtained for two monitored beams of the same wavelength and with no sample in the

path were not constant (normalized) unless the photodiode alignment was perfect. The integrator offset which results from laser generated "noise" was found to increase with laser power and also to vary in time relative to the variable trigger pulse used to trigger the data acquisition system. Thus balancing the integrator offset each time the laser power was changed and repositioning the gate such that the entire pulse was again integrated was crucial to the acquisition of meaningful data.

REFERENCES

3.1 Byer, R.L.; Herbst, R.L. *Laser Focus*, July 1978, 48.

3.2 Siegman, A.E. *Appl. Opt.* **1974**, *13*, 353.

3.3 DCR-2 product brochure, Quanta-Ray, Inc., Mountain View, CA, 1983.

3.4 DCR-1A User's Manual, Quanta-Ray, Inc., Mountain View, CA, 1978.

3.5 Jones, L.M.; Leroi, G.E.; Myerholtz, C.A.; Enke, C.G. *Rev. Sci. Instrum.* **1984**, *55(2)*, 204.

3.6 Exciton Laser Dye Catalogue, Exciton Chemical Co., Inc., Dayton, Ohio, 1979, 9.

3.7 Heath Model EU-700/E Operator's Manual, Heath Co., Benton Harbor, MI.

3.8 PDL-1 User's Manual, Quanta-Ray, Inc., Mountain View, CA, 1978.

CHAPTER 4

RESULTS AND DISCUSSION

4.0 Introduction

The results of the experimental work done in order to gain insight into the practical and theoretical aspects of population modulation spectroscopy are presented and discussed in this chapter. The experimental objectives of this work were as follows: (1) to explore parameters which affect the ability to induce ground state population modulation using a laser to pump a given transition; (2) to obtain information regarding the timeframe over which modulation of the ground state population is measurable; (3) to determine if the induced population modulation can be monitored by a weak probe beam at other wavelengths within the absorption band of the pumped transition; and (4) to determine if the ground state population modulation induced by pumping a given transition is observable by monitoring probe wavelengths which correspond to another allowed transition from the ground state. The reader is referred to Chapter 3 for details regarding the optical arrangements and experimental procedures.

4.1 Population Modulation Studies

The ability to effect laser-induced ground state population modulation of pumped transitions was investigated. In this set of experiments, sample transmittance was monitored as the intensity of the incident pump pulse was varied. The three compounds studied were: rhodamine 6G, (etio)hemechloride, and (octa)3-hydroxypropylporphyrin. The three compounds which were chosen for study allowed the effects of the absorption cross-section and the excited state lifetime to be investigated. For rhodamine 6G, solutions in equilibrium with air and solutions which had been deoxygenated were both investigated. Refer to Figure 3.4 for the optical set-up for the population modulation studies.

4.1.1 Rhodamine 6G - 532 nm Excitation

The absorption spectrum for a 1×10^{-5} *M* solution of rhodamine 6G in methanol and the molecular structure of rhodamine 6G are shown in Figure 4.1. Figure 4.2 is an energy level diagram for rhodamine 6G; the values of the cross-sections and rates indicated on Figure 4.2 are given in Table 4.1.

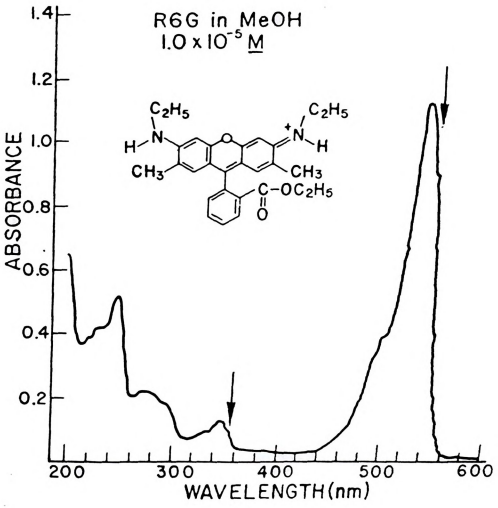

Figure 4.1 Absorption spectrum and structure of rhodamine 6G. Wavelengths of the second and third harmonics (532 nm and 355 nm, respectively) of the Nd:YAG laser are indicated by arrows.

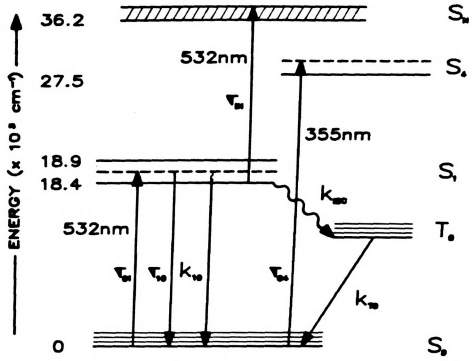

Figure 4.2 Energy level diagram for rhodamine 6G. Energy levels reached by laser frequencies shown by dashed lines (wavelength in nm). Stimulated absorption and emission cross-sections given by σ_{ij}. The rate constants (k_{ij}) include radiative and nonradiatve relaxation. The intersystem crossing rate is k_{isc}.

Table 4.1 Absorption Cross-sections and Relaxation Rates for Rhodamine 6G [1]

Parameter	Value	Reference
σ_{01}	2.0×10^{-16} cm^2	(4.8,4.12)
σ_{10}	0.372×10^{-16} cm^2	(4.12)
σ_{1M}	0.34×10^{-16} cm^2	(4.12)
σ_{04}	0.40×10^{-16} cm^2 [2]	
k_{10}	2.0×10^{8} sec^{-1}	(4.11,4.12)
k_{T0}	7.1×10^{6} sec^{-1} [3] 5.0×10^{5} sec^{-1} [4]	(4.9) (4.9)
k_{ISC}	1.6×10^{7} sec^{-1}	(4.9)

1. See Figure 4.2 for explanation of parameters.
2. Cross-section from absorption spectrum.
3. Rhodamine 6G solution air-equilibrated.
4. Rhodamine 6G solution deoxygenated.

The 532 nm pump beam used in this set of experiments corresponds to a wavelength near the 527 nm maximum of the $S_0 \dashrightarrow S_1$ transition. Figure 4.3 is a plot of absorbance at 532 nm versus concentration for the three experimental concentrations of rhodamine 6G (1×10^{-5} M, 5×10^{-6} M and 1×10^{-6} M). The plot is linear, indicating that the Beer-Lambert Law is obeyed within this concentration range. The absorbance values from this plot were converted to transmittances and are the "baseline transmittance" values to which the low irradiance laser beam transmittance measurements were compared. This comparison served as an initial check that the optical alignment was correct and the data acquisition system was functioning properly.

The data obtained from the ground state population modulation studies are shown in Figure 4.4. Normalized pump beam transmittances are plotted as a function of the incident photon irradiance (photons-cm^{-2}-sec^{-1}) for the three concentrations of rhodamine 6G investigated. The data for 150 sequential pulses at each of the incident powers set on the laser control panel are shown. The pulse-to-pulse fluctuations in laser power are apparent by the spread in values along the x-axis for each cluster of 150 data points. These pulse-to-pulse fluctuations in laser power, coupled with the fact that in these experiments the transmission of the sample is itself a function of power, make it necessary to ratio the

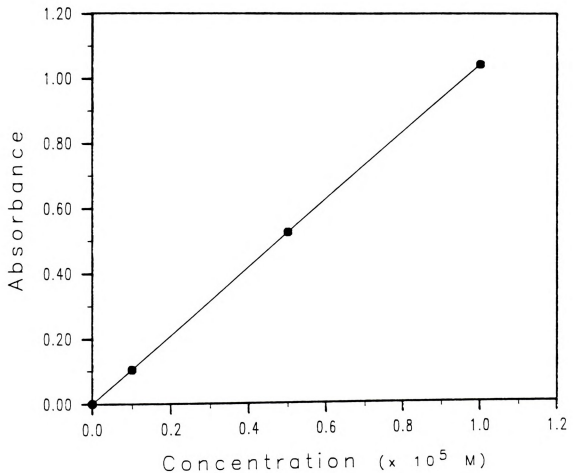

Figure 4.3 Beer-Lambert Law plot for experimental concentrations of rhodamine 6G. Absorbance measurements were made at 532 nm.

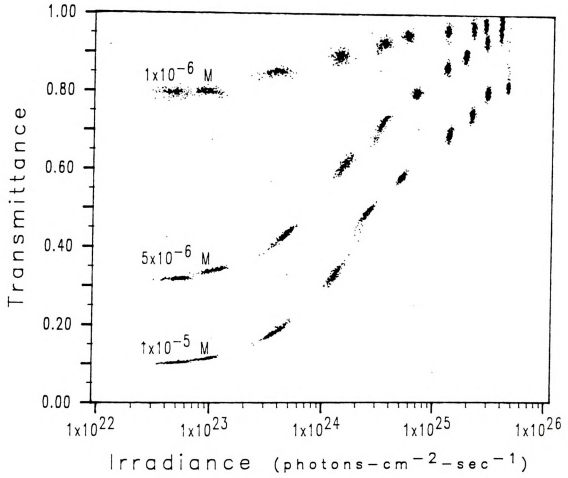

Figure 4.4 Normalized transmittance vs. incident photon irradiance - methanolic rhodamine 6G solutions pumped at 532 nm.

transmitted pulse intensities to the incident pulse intensities. This was done for both sample and solvent. Since the transmission of the solvent is not a function of power, an average of the 150 transmittance values obtained for the solvent was used to calculate the normalized transmittance of the sample for each pulse. The result is a normalized transmittance value which is relatively independent of the pulse-to-pulse fluctuations in incident laser power. The normalized transmittance is expressed by $(I_{R6G}/I_o)/(I_{solvent}/I_o)_{avg}$. The normalized transmittance measurements were observed to decrease in precision as the transmittance increased. This imprecision is due to the difficulty associated with measuring a small difference between two large numbers.

The x-axis was determined in the following manner. The average incident power per pulse was measured with a power/energy meter and divided by the 10 Hz pulse repetition rate to gives the average incident energy per pulse. The energy per pulse divided by Planck's constant and the frequency of the incident beam give the average number of photons per pulse. Division of photons per pulse by the 0.385 cm^2 area of the incident beam and the 7 nsec pulsewidth gives photons-cm^{-2}-sec^{-1}. In order to obtain photon irradiance values for the individual pulses, a scale factor was applied to each of the values obtained from the analog-to-digital conversion of the channel used

to monitor the incident pulses. The scale factor was calculated by assigning the lowest nominal incident energy measured by the power meter to the average raw value of the analog-to-digital converter at the incident energy and determining what factor was required to make the conversion to photons-cm^{-2}-sec^{-1}. The clusters of 150 data points correspond to average incident energies per pulse of 0.05 mJ, 0.15mJ, 0.65 mJ, 2.1 mJ, 5.0 mJ, 10.0 mJ, 20 mJ, 30 mJ, 45 mJ and 60 mJ. These average energies correspond to a photon irradiance range from 5×10^{22} to 6×10^{25} photons-cm^{-2}-sec^{-1}.

The average percent transmittance values of the incident pump beam obtained at the lowest average incident energy, 0.05 mJ, are 10.3 %, 31.8 % and 78.0 % for the 1×10^{-5} M, 5×10^{-6} M, and 1×10^{-6} M rhodamine 6G solutions, respectively. Percent transmittance values of 9.1 % , 29.9 %, and 76.0 % were obtained from the absorption spectra. The slope observed in the sets of data points at the lowest incident pump irradiances indicate that some ground state depopulation was occurring. Further evidence of this is the increase in transmittance seen when the data are sorted by increasing incident irradiance. This ground state depopulation accounts for the fact that the transmittance values obtained by monitoring the laser pulse were higher than the transmittances determined from the absorption spectra.

Transmittance is seen to increase with increasing incident energy and to asymptotically approach a different maximum value for each of the three concentrations. The maximum average percent transmittance achieved in each case is seen from the plot to be less than 100 %. As discussed in Chapter 2, absorption of pump beam photons from both singlet and triplet excited states has been cited in the literature to account for this phenomenon [termed residual absorption] in various dyes (4.1-4.6).

Absorption of 532 nm photons from S_1 has been reported for rhodamine 6G (4.7,4.8). The S_1 population of ethanolic solutions of rhodamine 6G in equilibrium with air has been calculated from a set of rate equations to be approximately 90 % of the total population at an incident irradiance of 5×10^{25} photons-cm^{-2}-sec^{-1} (4.8). The T_1 state population was calculated by the same investigators to be 2-3 % of the S_1 population. Since the absorption cross-sections for absorption from T_1 to T_n and from S_1 to S_n can often be of the same magnitude as the absorption cross-sections for S_o --> S_1 transitions (4.2), it is reasonable to question whether it is absorption from both S_1 and T_1 which occurs in rhodamine 6G and which then results in the transmission values below 100 %.

4.1.2. Deoxygenated Rhodamine 6G - 532 nm Excitation

In order to further investigate the origin of the observed residual absorption, solutions of rhodamine 6G were deoxygenated with methanol-saturated N_2 and ground state population modulation studies were again performed. Oxygen is a well known triplet quencher (4.3,4.9) and is present in concentrations of approximately 10^{-3} M in alcoholic solutions in equilibrium with air (4.10,4.11). The quenching of triplets by oxygen is termed impurity quenching and the decay of triplet state molecules in air-equilibrated solutions is generally dominated by the rate constant for impurity quenching. The rationale behind this set of experiments was that the increase in the triplet state lifetime resulting from deoxygenating the solutions should result in an increase in the steady-state triplet concentration relative to that in the air-equilibrated solutions. The increase in triplet concentration would then be expected to result in increased absorption from molecules in the lowest triplet state if this process does indeed occur. An increase in the residual absorption (decreased maximum transmission) was expected for the deoxygenated solutions relative to the residual absorption observed in the air-equilibrated solutions.

The results of the population modulation studies for the three experimental concentrations of deoxygenated

rhodamine 6G solutions are shown in Figure 4.5. As seen previously for the rhodamine 6G solutions in equilibrium with air, the ground state population is modulated and the transmittance vs. incident irradiance data approach transmission maxima which are below unity. Also apparent is the break in continuity in the curve defined by the data for the 1×10^{-5} M solution. An undetermined systematic error is thought to be the cause of this discontinuity.

Comparison of the transmission vs. incident irradiance curves for the deoxygenated (Figure 4.5) and the air-equilibrated (Figure 4.4) solutions shows that the transmission values at the higher incident irradiances for the 1×10^{-5} M and 5×10^{-6} M deoxygenated solutions are lower by approximately 10 % than the corresponding values for the same two concentrations of air-equilibrated solutions. The transmission vs. incident irradiance curves for the 1×10^{-6} M deoxygenated and air equilibrated solutions are lower by only a few percent. However, the differences in maximum transmission values for each concentration are reduced if Figures 4.4 and 4.5 are overlayed and the data at the lowest incident irradiance are aligned to correct for the differences in the true concentrations of the solutions. (The deoxygenated solutions are more concentrated than the air-equilibrated solutions due to the solvent evaporation which occurred

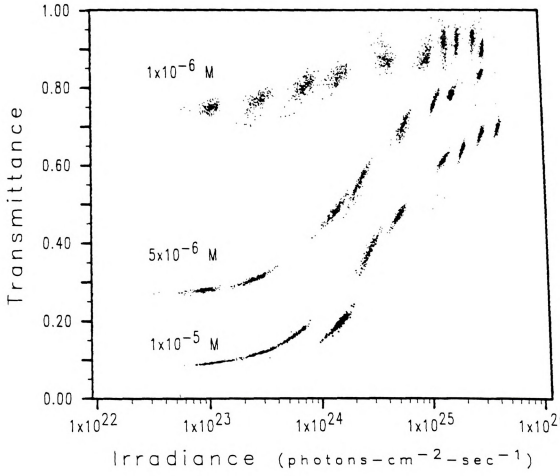

Figure 4.5 Normalized transmittance vs. incident photon irradiance - deoxygenated methanolic rhodamine 6G solutions pumped at 532 nm.

when sparging with N_2.) Closer inspection of Figures 4.4 and 4.5 when they are overlayed reveals that no significant differences are observed in the transmission vs. incident irradiance data for the oxygenated and deoxygenated solutions if the incident irradiance axis for the deoxygenated solutions is shifted toward lower values by 20 %. Given the difficulty in measuring the incident power more precisely than $\pm$ 5 - 10 % and in determining the global scale factors by which the data are multiplied to give incident irradiance, it is entirely possible, and perhaps even expected, that the incident irradiance axes for the two data sets could be offset by 20 %. An error of 10 % in opposite directions for the deoxygenated and and air equilibrated solutions would result in the offset which is observed. (The process for determining the incident irradiance from the raw data was discussed in Section 4.1.1 of this chapter.)

The experimentally observed result that the deoxygenated and air-equilibrated solutions show no significant differences in the transmission vs. incident irradiance is, in fact, expected. Subsequent investigation into the literature for rhodamine 6G intersystem crossing rates and triplet state lifetimes in air-equilibrated and deoxygenated alcoholic solutions confirms the experimental results.

The intersystem crossing rate is cited in the literature as 2×10^{7} sec^{-1} (4.9). The intersystem crossing rate is an order of magnitude slower than the 2×10^{8} sec^{-1} (4.11,4.12) relaxation rate from $S_1 \dashrightarrow S_0$, making intersystem crossing a less competitive deactivation pathway for S_1. The high fluorescence quantum yield, cited to be 0.88 or 0.95 (4.9,4.12) is evidence of the favored deactivation to S_0 directly from S_1. The low triplet yield [1 - 10 % (4.9,4.13)] in air-equilibrated alcoholic rhodamine 6G solutions is the result of the slow intersystem crossing rate.

The triplet state lifetime is cited as 2×10^{-6} sec in deoxygenated alcoholic solutions (4.9) and as 50 nsec (4.10), 140 nsec (4.9), and 250 nsec (4.14) for air-equilibrated solutions. The longer T_1 lifetime in the deoxygenated solutions is a result of a reduction in impurity quenching by O_2. Clearly, any increase in the already low triplet state concentration which would result from deoxygenating the solutions would not be significant on the 7 nsec timescale of the ground state depopulation studies. The triplet state concentration of rhodamine 6G can be considered essentially constant in these experiments due to both the slow intersystem crossing rate and the long triplet state lifetime. Therefore, any difference in the transmission vs. incident irradiance behavior of the deoxygenated and the air-equilibrated

solutions is not expected to be as significant as we first supposed.

The results of these studies do not indicate whether the residual absorption is due in part to absorption from the lowest triplet state. Published triplet-triplet absorption spectra do not show a cross-section at 532 nm (4.9,4.10,4.15). However, the methods employed to obtain the spectra may preclude measuring the triplet-triplet absorption cross-section in the region of strong singlet absorption.

4.1.3 Curvefit Analysis of 532 nm Excitation Data for Rhodamine 6G

Transmission vs. incident photon irradiance data for all of the rhodamine 6G solutions discussed above were fit to the three model equations presented in Chapter 2. This was done in order to (1) validate the assumption that excited state absorption accounts for the fact that the maximum percent transmission achieved in these experiments is less than 100 % and (2) gain insight into whether the ground state depopulation of rhodamine 6G solutions is better modeled by "power saturation" or "energy saturation" when pumped with a 7 nsec FWHM pulse.

KINFIT, a general curve-fitting program which implements least-squares procedures for fitting both

linear and nonlinear equations (4.16) was used to fit data to the model equations. Since the maximum number of data points accepted by KINFIT is 300, the average values of the transmission and incident irradiance obtained at each nominal incident irradiance were used rather than the 1500 discrete data points acquired for each solution. The use of average values is justified in this case because the experimental curve is defined adequately by these points for the purposes of the general discussion which follows.

Weighting was used because the data acquired at each nominal incident irradiance are assumed to have errors which can be described by independent normal distributions. The use of weighting results in maximum likelihood estimates for the adjustable parameters contained in the model equations. KINFIT calculates the weights for the dependent and independent variables from the variances associated with each data point which have been supplied to the program. The variances for the average incident irradiance values (the independent variable) were calculated using a relative standard deviation of 0.1% for each of the incident irradiance values because the error associated with determining these values was assumed not to be a function of the magnitude of the incident irradiance. The relative standard deviations of the transmission values were determined from inspection of the experimental transmission vs. incident

irradiance curves. Relative standard deviations of 1.0, 2.0 and 3.0 % were used for transmission values which were from 0.0 to 50.0 %, 50.0 to 80.0 %, and 80.0 to 100.0 %, respectively, because the error associated with the transmission measurements was shown to be a function of the fraction of the beam which was transmitted.

As will be seen subsequently, in two of the three model equations, direct calculation of the dependent variable from a knowledge of the independent variable and all of the parameters is not possible. For these two cases a subroutine, ROOTB, was included in order to find the root of the model equation (4.17). This subroutine started with the experimental average T values and iterated within KINFIT until a new value of T was found for which the equation could be satisfied by adjustment of the parameters.

The first model which was fit was that for the saturable absorber which undergoes power saturation and in which species in excited states also absorb incident photons. Recall that this model assumes that the system exhibits a steady-state response to the incident light pulse due to fast relaxation times. The equation which describes the transmission vs. incident irradiance behavior of a saturable absorber of this type is given by (4.1)

$$T - T_o\ [A + (I_o/I_s)]^{A-1}/\ [A + T(I_o/I_s)] = 0 \qquad (4\text{-}1)$$

where T is the steady-state transmission, I_o is the incident irradiance, and T_o is the transmission of the solution measured by a spectrophotometer (i.e., under irradiation by a low-irradiance light source which does not modulate the ground state population). I_s is the "saturation irradiance" which was defined in Chapter 2; the incident irradiance at which the steady-state absorption coefficient has been reduced by a factor of two from the absorption coefficient of the system when essentially all of the absorbers are in the ground electronic state. The ratio of the ground state absorption cross-section to the effective excited state absorption cross-section for an absorber which undergoes excited state absorption but not stimulated emission is defined as A (4.1,4.18). For an absorber which undergoes both stimulated emission and excited state absorption, A is the ratio of the sum of the cross-sections for ground state absorption and stimulated emission to the effective excited state absorption cross-section (4.18). I_s and A were treated as adjustable parameters. T_o was treated first as a constant at its measured value and subsequently as an adjustable parameter. The dependent and independent variables are T and I_o, respectively.

KINFIT, the curvefitting program, requires initial estimates of the adjustable parameters that are to be determined. These estimates were made from inspection of the experimental curves in the case of I_S and by using a ratio for A from cross-sections which are cited in the literature (4.12). The estimates for T_o were the transmissions of the solutions measured by the spectrophotometer.

The model equation employing the parameters determined by KINFIT is superimposed on the plot of the acquired data in Figures 4.6a and 4.6b. The curves and data plotted are for the three experimental concentrations of rhodamine 6G solutions in equilibrium with air. The curves shown in Figure 4.6a resulted when the model equation was fit with A and I_S as the adjustable parameters and with T_o as a constant. The curves shown in Figure 4.6b resulted when T_o was treated as an adjustable parameter rather than as a constant. It is apparent from visual comparison of the curves as well as from comparison of the residuals (i.e., the difference between the fit and experimental values) for each data point that a slightly better fit is obtained when T_o is treated as a parameter; this was also the case for the deoxygenated solutions. The curves which resulted from fitting the data for the deoxygenated solutions with T_o treated as a parameter are shown in Figure 4.7. Prior to discussing the resulting

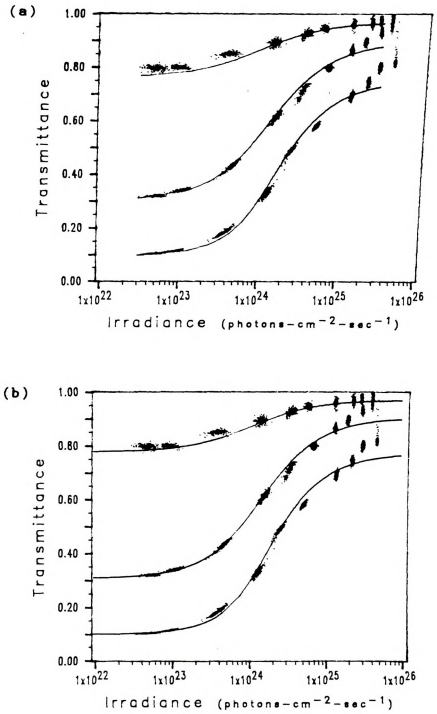

Figure 4.6 Curves from fit of experimental data for rhodamine 6G solutions in equilibrium with air to a model for a power-saturated absorber with excited-state absorption - (a) T_o treated as a constant and (b) T_o treated as a parameter.

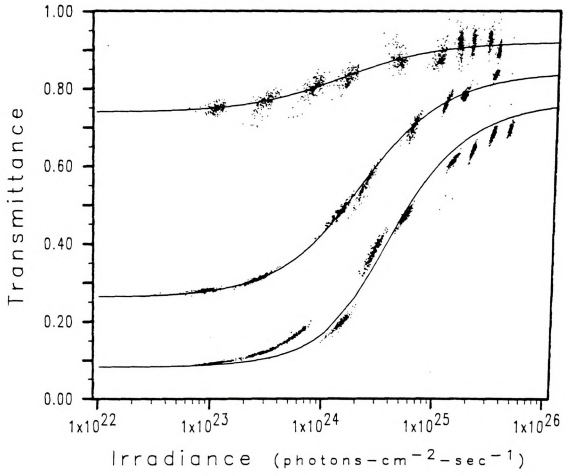

Figure 4.7 Curves from fit of data for deoxygenated rhodamine 6G solutions to a model for a power-saturated absorber with excited state absorption - T_0 treated as a parameter.

parameters and details of the fit for this model, the curves which resulted from fitting the other two model equations will be presented.

The second model considered is that for "power saturation" without excited-state absorption. The transmission vs. incident irradiance behavior of this model is given by (4.1)

$$\ln(T_o/T) + (I_o/I_s)(1 - T) = 0 \qquad (4\text{-}2)$$

where T and I_o are again the dependent and independent variables, respectively. I_s and T_o were treated as the adjustable parameters. The initial estimates made for the parameters were the same as in the first model.

The curve resulting from the fit of this model is shown by the solid lines in Figures 4.8a and 4.8b for a 5×10^{-6} M rhodamine 6G solution in equilibrium with air and for a 5×10^{-6} M deoxygenated rhodamine 6G solution. Immediately apparent is the fact that the fit curves approach 100 % transmission at high incident intensities. This is in sharp contrast to the curves of the previous model as well as the data which approach a transmission limit below 100 %. Upon inspection of the plotted curves and residuals for this second model it is also apparent

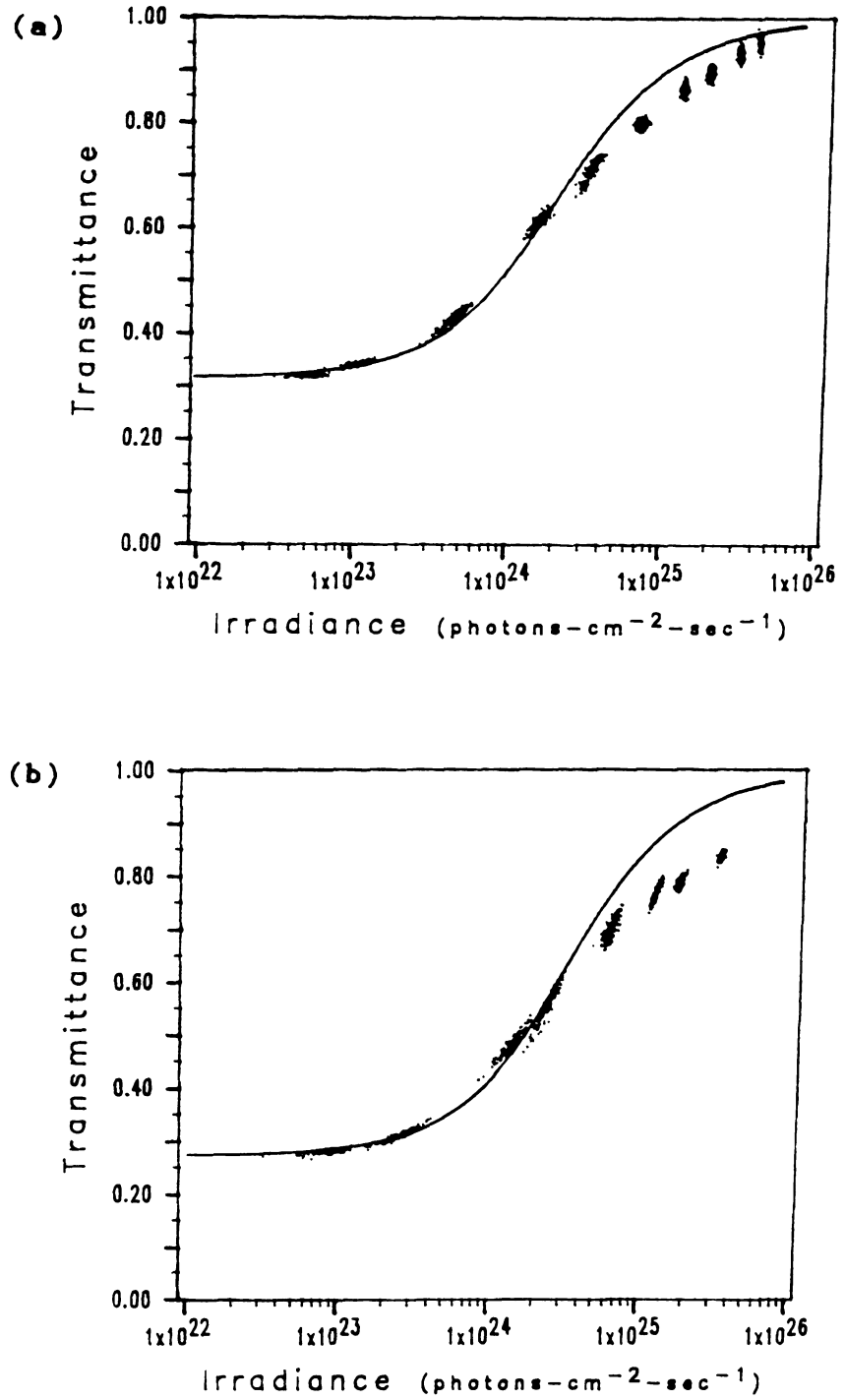

Figure 4.8 Curves from fit of experimental data to a model for a power-saturated absorber without excited-state absorption - (a) 5 x 10^{-6} M rhodamine 6G in equilibrium with air and (b) a deoxygenated 5 x 10^{-6} M rhodamine 6G solution.

that the fit at the low incident intensities is also not as good as in the case of the first model. Similar results were obtained for the 1 x 10^{-5} M and 1 x 10^{-6} M solutions.

The third model fit was that for the case in which the saturable absorber is "energy-saturated" rather than "power-saturated". Recall from Chapter 2 that this means that the extent to which the dye is bleached depends on the integrated energy density (i.e.; on photons-cm^{-2} rather than on photons-cm^{-2}-sec^{-1}) and requires that the lifetime of the terminal excited state is long compared to the duration of the saturating light pulse (4.3). Ground state depopulation occurs by a steady reduction of the ground state as excited molecules accumulate in the terminal excited state. The transmission behavior of saturable absorbers with these properties is given by (4.1)

$$[T - (J_s/J_o)] \ln [1 + T_o(e^{J_o/J_s} - 1)] = 0 \qquad (4\text{-}3)$$

where T is the transmitted energy density divided by the incident energy density, J_s is the energy density required to reduce the absorption coefficient by a factor of (1/e) and J_o is the incident energy density. The independent and dependent variables are J_o and T, respectively. The adjustable parameters are T_o and J_s.

The curves resulting from fitting the third model to the data are presented in Figures 4.9a and 4.9b for the 5×10^{-6} M rhodamine 6G solution in equilibrium with air and for the 5×10^{-6} M deoxygenated solution, respectively. As in the case of the second model, the transmission curves are seen to approach 100 % transmission at high incident energy densities whereas the data approach a transmission limit below 100 %. In addition, the residuals at the low irradiance end of the curve are observed to be larger than the residuals for the curves generated from either of the two previously considered models. Similar results were obtained for the 1×10^{-5} M and 1×10^{-6} M solutions.

At this point it is appropriate to note that a model for an "energy-saturated" absorber which exhibits excited-state absorption was not available for a curvefit analysis. However, since the model for "power-saturation" without excited state absorption fits the data at the low incident irradiance end better than the model for "energy-saturation" without excited state absorption, it seems reasonable to to assume that the model for "power-saturation" with excited-state absorption would still fit the data better than would a model for an "energy-

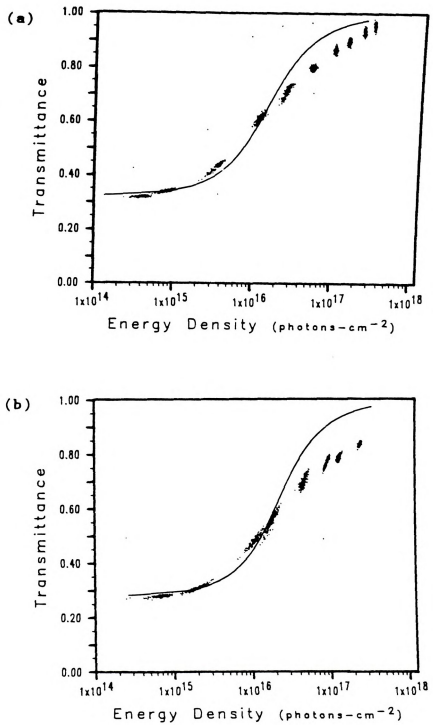

Figure 4.9 Curves from fit of experimental data to a model for an energy-saturated absorber without excited-state absorption - (a) 5 x 10^{-6} M rhodamine 6G in equilibrium with air and (b) a deoxygenated 5 x 10^{-6} M rhodamine 6G solution.

saturated" absorber which undergoes excited state absorption.

The parameters which resulted from fitting the three models are presented in Tables 4.2, 4.3 and 4.4 for all of the experimental rhodamine 6G solutions. The multiple correlation coefficient is shown in parentheses below the parameter with which it is associated. Multiple correlation coefficients are a measure of the goodness-of-fit where a value of one indicates complete mathematical correlation of the parameters and a perfect fit (4.19). Inspection of the multiple correlation coefficients for each of the three models verifies that the model for a "power-saturated" absorber with excited-state absorption is indeed the best fit. The fact that the multiple correlation coefficients are significantly less than one even for the best fitting model is not surprising, considering the poor fit at the higher incident intensities. Although the model for the power-saturated absorber with excited state absorption is not quantitatively accurate for rhodamine 6G, the parameters derivable from it merit further discussion.

From Table 4.2, a comparison of the fit values of T_o with the values of of T_o which were measured with the spectrophotometer shows that the fit values were slightly larger with only one exception. This trend is most

Table 4.2 Results of Curvefit Analysis of Experimental Data to Power-saturation Model with Excited-state Absorption

Rhodamine 6G Concentration (in moles/l)	Transmittance (%) True	Transmittance (%)[1] from Fit	I_s from Fit [1] ($\times 10^{24}$ photons-cm^{-2}-sec^{-1})	A from Fit [1]	A Calculated [2]
in equilibrium with air:					
1×10^{-5}	0.091	0.097 + .003 (0.68)	0.550 + .050 (0.86)	9.1 + 1.4 (0.78)	10.9
5×10^{-6}	0.299	0.305 + .004 (0.73)	0.730 + .070 (0.84)	12.0 + 2.5 (0.69)	14.5
1×10^{-6}	0.760	0.775 + .004 (0.55)	0.970 + .110 (0.84)	8.6 + 0.6 (0.80)	9.3
deoxygenated:					
1×10^{-5}	0.054	0.081 + .007 (0.81)	1.500 + .300 (0.90)	9.6 + 3.3 (0.81)	7.8
5×10^{-6}	0.270	0.260 + .002 (0.78)	1.400 + .030 (0.88)	7.9 + 0.3 (0.78)	7.4
1×10^{-6}	0.711	0.738 + .007 (0.84)	1.300 + .080 (0.89)	3.7 + 0.2 (0.74)	4.1

1. Multiple correlation coefficients shown in parentheses below values determined by fit.

2. A_{calc} is from $T_{max} = T_0^{1/A}$ calculated using the maximum average experimental transmission values and the baseline transmittance.

Table 4.3 Results of Curvefit Analysis of Experimental Data to Power-saturation Model

Rhodamine 6G Concentration (in moles/l)	Transmittance (%) True	Transmittance (%)[1] from Fit	Is from Fit [1] ($\times 10^{24}$ photons-cm^{-2}-sec^{-1})
in equilibrium with air:			
1×10^{-5}	0.091	0.101 ± .068 (0.58)	0.830 ± .068 (0.58)
5×10^{-6}	0.299	0.312 ± .070 (0.61)	1.020 ± 1.25 (0.61)
1×10^{-6}	0.760	0.783 ± .070 (0.51)	1.810 ± 3.04 (0.51)
deoxygenated:			
1×10^{-5}	0.054	0.086 ± .011 (0.77)	2.000 ± .330 (0.77)
5×10^{-6}	0.270	0.270 ± .013 (0.70)	2.080 ± .310 (0.70)
1×10^{-6}	0.711	0.762 ± .012 (0.62)	5.570 ± 1.640 (0.62)

1. Multiple correlation coefficients shown in parentheses below values determined by fit.

Table 4.4 Results of Curvefit Analysis of Experimental Data to Energy-saturation Model

Rhodamine 6G Concentration (in moles/l)	Transmittance (%) True	Transmittance (%)[1] from Fit	I_s from Fit [1] ($\times 10^{24}$ photons-cm^{-2}-sec^{-1})
in equilibrium with air:			
1×10^{-5}	0.091	0.106 ± .009 (0.53)	0.584 ± .083 (0.53)
5×10^{-6}	0.299	0.320 ± .010 (0.56)	0.704 ± .119 (0.56)
1×10^{-6}	0.760	0.788 ± .009 (0.49)	1.040 ± .330 (0.49)
deoxygenated:			
1×10^{-5}	0.054	0.084 ± .012 (0.74)	1.280 ± .200 (0.74)
5×10^{-6}	0.270	0.277 ± .017 (0.65)	1.360 ± .250 (0.65)
1×10^{-6}	0.711	0.769 ± .013 (0.53)	4.360 ± 1.370 (0.53)

1. Multiple correlation coefficients shown in parentheses below values determined by fit.

probably the result of the curvefitting program optimizing the fit rather than consistent errors made when measuring the T_0 values with the spectrophotometer. The fact that the experimental transmission values are generally higher than the fit curve at the high incident irradiance end would be expected to affect the low end in this manner.

It must be pointed out that the values of A and T_0 determined for the most concentrated deoxygenated solution have large standard deviations associated with them. This is explained if one refers back to Figure 4.5 and observes the apparent break in the continuity of the curve determined by the clusters of data acquired at the lower incident intensities. A systematic error is thought to be the cause of the observed discontinuity in this data set (as noted in Section 4.1.2 of this chapter). The transmission data acquired at the three lowest nominal incident intensities seem to be higher than they should be in order to be contiguous with the rest of the transmission vs. incident irradiance curve for this solution. Such higher transmission values would be expected to raise the fit values for A and T_0, as is indeed seen.

The parameter A for rhodamine 6G pumped at 532 nm is the ratio of the sum of the cross-sections for absorption and stimulated emission to the cross-section for excited state absorption ($A = \sigma_{01} + \sigma_{10}/\sigma_{1N}$). The stimulated

emission cross-section must be included here because the overlap of the absorption and emission bands at 532 nm allow stimulated emission at the excitation wavelength (4.2). In fact, time resolved stimulated emission has been observed at 528 nm, the absorption maximum for rhodamine 6G in ethanol (4.20). If excitation is at higher energy than the region in which the absorption and emission bands overlap, stimulated emission at the excitation wavelength cannot occur (4.3,4.21); the cross-section for stimulated emission is highest at the wavelength of the emission maximum (4.9,4.22).

A value of 7.0 for the parameter A is expected using values from the literature of 2.0×10^{-16} cm^2 for the absorption cross-section (4.8,4.12), 0.372×10^{-16} cm^2 for the stimulated emission cross-section (4.12), and 0.34×10^{-16} cm^2 for the absorption cross-section from S_1. The average value of A for all of the solutions is 8.5 ± 2.7. An average value for A is used for comparison to the value of A expected using cross-sections from the literature because the standard deviations of the determined values do not clearly indicate that there is a difference between the values of A which were determined for the air-equilibrated and for the deoxygenated solutions. A single value of A should result for all three concentrations for the solutions in equilibrium with air and a single (but possibly different) value of A should

result for the deoxygentated solutions (4.1). From the discussion of the lifetime of the lowest triplet state in air-equilibrated and deoxygenated solutions (Section 4.1.2 of this chapter), a difference in the values of A for the two sets of solutions was not expected.

The values of I_S determined by KINFIT should be independent of concentration since the primary relaxation processes in solution result from solute-solvent interactions and not solute-solute interactions (4.23). This is roughly the case, although the I_S values for the deoxygenated solutions differ from each other less than for the solutions in equilibrium with air. The values of I_S for the air-equilibrated solutions are apparently lower than the values of I_S for the deoxygenated solutions. The difference in I_S values between the two sets of solutions is attributed to the difficulty in determining an absolute value for the incident photon irradiance (discussed in Section 4.1.2 of this chapter) and is therefore not considered significant.

The expression for I_S and the average values determined for this parameter can be used to calculate an effective lifetime of S_1. An average effective lifetime of 7.0 nsec for the solutions in equilibrium with air and of 4.4 nsec for the deoxygenated solutions results if a reported value of 2.0×10^{-16} cm^2 for the transition cross-section (4.12) is used for the calculation. The

lifetime which results by averaging the I_S values for all of the solutions is 5.7 $\pm$ 1.9 nsec. The effective lifetime of S_1 has been reported in literature to be 4.2 to 6.0 nsec (4.12,4.13,4.22,4.24-4.26). The average effective lifetime estimated from the I_S values from all of the experimental solutions is close to the cited values, given the overall quality of the fit. The difference in the average lifetimes which are estimated from the I_S values for the two sets of solutions is not thought to be significant and is attributed to the aforementioned uncertainty associated with determining the scale factor for incident irradiance.

It is concluded that this curvefit analysis has provided qualitative information regarding the transmission vs. incident irradiance behavior of rhodamine 6G. It was seen that excited-state absorption must be included when modeling the transmission vs. incident irradiance behavior of rhodamine 6G. It was also shown that a power-saturated model is a better approximation for rhodamine 6G than is an energy-saturated model.

The values of the parameters (A and I_S) which were determined by fitting the experimental data to the model for a power-saturated absorber with excited-state absorption lead one to conclude that rhodamine 6G is not quantitatively described by this model. This conclusion is particularly apt when considering the values of A because,

as discussed previously, the absolute values of I are a function of the scale factors which are applied to the raw data to give the incident photon irradiance.

Since rhodamine 6G has a effective lifetime which is approximately the same as the pulsewidth of the laser used in these experiments, steady-state populations are probably never fully realized under the present experimental conditions. Recall that the assumption of steady-state populations in the energy levels considered was key to the models for "power-saturation". The transmission vs. incident irradiance behavior of rhodamine 6G observed in these experiments is undoubtedly described most accurately by a set of rate equations which are solved for the populations of the various states and for the transmission as a function of time during the pulse. This approach would be necessary if a quantitative fit were required. In fact, a rigorous determination of the transmission vs. irradiance behavior of rhodamine 6G in these experiments would most likely require that a different set of rate equations be written for each incremental volume within the sample cell in order to account for non-uniform absorption from the front to the rear of the sample cell. A rigorous analysis of the type just described would be required in order to determine whether the poor fit at the high incident irradiances is the result of the model used to analyze the data or

whether undetermined systematic errors are the cause of the poor fit at the high end.

The transmission behavior of rhodamine 6G when irradiated with high intensity lasers could indeed be described by a power-saturation model if a laser were used that had pulsewidths which are longer (by a factor of 5 or 10) than those used here. On the other hand, rhodamine 6G would act as an energy-saturated absorber under irradiation by substantially shorter (psec) pulsewidths than used in these studies. In fact, the latter case has been cited in the literature (4.27). Thus, it is important to note that power- or energy-saturation is not an inherent property of the absorber, but is a function of the excitation conditions.

4.1.4 Rhodamine 6G - 355 nm Excitation

The S_0 --> S_4 (4.28) transition of rhodamine 6G was pumped at 355 nm with the third harmonic of the Nd:YAG laser. The objective of this study was to explore whether it was possible to modulate the ground state population by pumping a transition at higher energy and with a smaller cross-section for absorption than the S_0 --> S_1 transition. A 3×10^{-5} M solution of rhodamine 6G was used for this study. The reader is referred to Figure 4.1 for

features of the absorption spectrum at 355 nm and to Figure 3.5 for the optical set-up for this experiment.

Figure 4.10 shows transmittance of the 355 nm pump beam plotted as a function of the incident pump beam irradiance. The data were acquired and manipulated as described in the previous section of this chapter. The fact that the transmission does not increase with increasing pump beam irradiance shows that the ground state population is not measurably modulated by pumping the S_0 --> S_4 transition. In order to understand why ground state depopulation was not observed when the S_0 --> S_4 transition was pumped, the expression for the saturation irradiance (I_S) and the energy level model from which it was derived are discussed. An excitation/deexcitation scheme which is consistent with the experimental observations is then proposed.

Recall from Chapter 2 that I_S is the incident irradiance at which the absorption cross-section has been reduced to one-half of the value obtained if absorption measurements are made when the ground state is the only state which is populated. I_S is inversely proportional to the product of the absorption cross-section for the transition of interest and the lifetime of the terminal

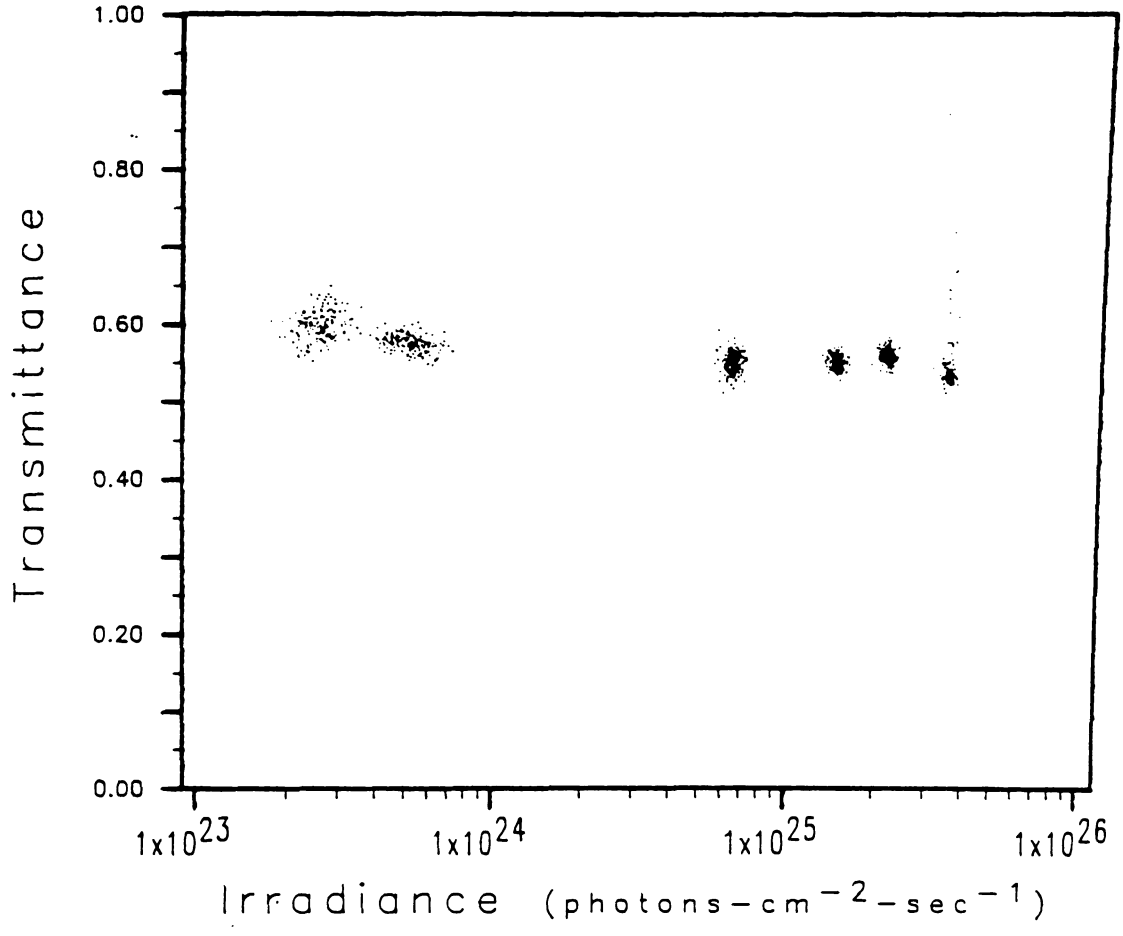

Figure 4.10 Transmittance vs. incident photon irradiance - 3 x 10^{-5} M rhodamine 6G pumped at 355 nm.

excited state. The terminal excited state is assumed, as is the usual case, to be S_1 after the excited molecule undergoes internal conversion from S_4. I_S was calculated using values of 4×10^{-17} cm^2 (4.13) as the absorption cross-section of rhodamine 6G at 355 nm and 4.5×10^{-9} seconds (4.13) as the lifetime of S_1, giving an expected value of approximately 4.5×10^{24} photons-cm^{-2}-sec^{-1}. This value of I_S falls within the range of accessible experimental intensities and on this basis ground state depopulation was expected to be observed. Apparently, the model from which the expression for I_S was derived does not describe the processes occurring in rhodamine 6G which result from pumping at 355 nm.

The general energy level scheme used in Chapter 2 to describe the behavior of a saturable absorber and the expectations which result from it are now examined. It is generally accepted that excitation to a state at higher energy than that of the first excited singlet state predominantly results in fast internal conversion to S_1, from which subsequent relaxation to the ground state occurs (4.29,4.30). In the case of strongly fluorescent species, such as rhodamine 6G, the subsequent relaxation to the ground state is primarily radiative. Evidence of this relaxation pathway in rhodamine 6G solutions pumped (or merely excited) at 355 nm is the fluorescence which is observed. It would have been possible to observe ground

state depopulation at 355 nm if fluorescence from S_1 is indeed the primary deexcitation pathway for rhodamine 6G when it is pumped at 355 nm. S_1 would become substantially populated and a bottleneck for repopulation of S_0 would occur in the lowest vibrational level of the S_1. Ground state absorption at 355 nm would return only after relaxation of this fluorescent state. Absorption of a second photon at 355 nm from the S_1 state would also result in observation of ground state depopulation if the resulting excited state relaxed back to S_1 because of the aforementioned bottleneck. (Recall that saturation was observed when rhodamine 6G was pumped at 532 nm.) It must be concluded that although internal conversion to S_1 and fluorescent decay to S_0 do occur when rhodamine 6G is pumped with a laser beam at 355 nm, other processes come into play which prevent depopulation of the ground state.

An energy level diagram which can account for the experimental results via the excitation and deexcitation processes is presented in Figure 4.11. The energy level diagram includes absorption of a 355 nm photon from S_1 to form a highly excited species (probably a reversible photoproduct) which undergoes rapid decay to S_0. Internal conversion from S_n to S_1 is also included since fluorescence is observed from S_1. Blue fluorescence from S_n has been observed, but the low quantum yields reported for this phenomenon [10^{-4} (4.7)] justify the assumption

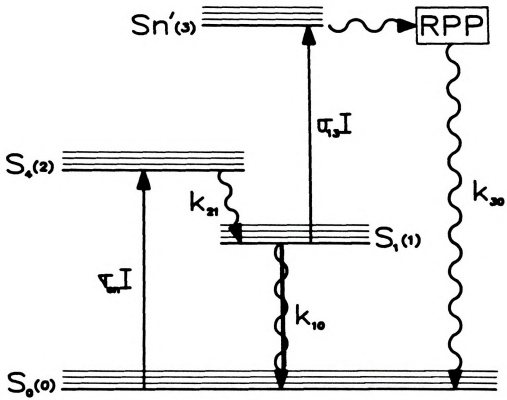

Figure 4.11 Energy level diagram for rhodamine 6G showing the excitation/deexcitation processes which are considered when pumping occurs at 355 nm.

that it can be ignored since the addition of so few fluorescent photons to the transmitted laser beam simply would not be detected in these experiments. The rate equations which describe this model are as follows:

$$d[n_0]/dt = -\sigma_{02} I[n_0] + k_{10}[n_1] + k_{30}[n_3] \qquad (4\text{-}4)$$

$$d[n_1]/dt = k_{21}[n_2] - k_{10}[n_1] - \sigma_{13} I[n_1] \qquad (4\text{-}5)$$

$$d[n_2]/dt = \sigma_{02} I[n_0] - k_{21}[n_2] \qquad (4\text{-}6)$$

$$d[n_3]/dt = \sigma_{13} I[n_1] - k_{30}[n_3] \qquad (4\text{-}7)$$

and if a steady-state is assumed, the ratio of the populations of S_0 and S_1 is found to reduce to

$$[n_0]/[n_1] = (k_{10} + \sigma_{13} I)/(\sigma_{02} I). \qquad (4\text{-}8)$$

From equation (4-8), it can be seen that at high incident irradiances the ratio of the S_0 and S_1 populations is a function only of the ratio of cross-sections for absorption from S_1 and S_0. Absorption of a photon from S_1 results in rapid repopulation of the ground

state rather than relaxation back to S_1 which would instead result in a bottleneck for ground state repopulation. Since fluorescence was visually observed, a fraction of the molecules in the first excited singlet state do not absorb a second 355 nm photon but radiatively relax to S_1. If absorption of a second 355 nm photon followed by decay directly to S_o is favored over fluorescence, ground state depopulation will not occur.

Shevandin and Aristov have also proposed the relaxation scheme shown in Figure 4.11 in order to explain the results of fluorescence experiments which monitored the 590 nm fluorescence intensity of rhodamine 6G solutions pumped at 353 nm, 530 nm and with both wavelengths simultaneously (4.13). Their investigations showed that the fluorescence intensity was lower when alcoholic rhodamine 6G solutions were pumped with a laser at 353 nm than when pumped at 530 nm. An intermediate intensity level was observed if beams at both wavelengths pumped the solution simultaneously. The intermediate level of fluorescence observed when the solutions were pumped with both 353 nm and 530 nm beams shows that the relaxation pathways to the ground state do indeed differ depending on whether the second photon absorbed is a 353 nm photon or a 530 nm photon. The dependence of fluorescence intensity on the excitation wavelength (excitation energy) has also been observed for beta-

naphtylamine (4.31), phenol (4.32) and various other substances (4.33,4.50). Excitation to states (or species) which undergo radiationless deactivation to the ground state rather than relaxing back to S_1 was cited as an explanation in these cases also.

Shevandin and Aristov have estimated via a calculation that the lifetime of the reversible photoproduct formed after rhodamine 6G absorbs two photons at 353 nm is 50 - 80 psec (4.13) and they speculate that the reversible photoproduct is the half-oxidized form of the dye (4.34). These investigators have also stated that the mean lifetime of molecules in the S_1 state is considerably shortened due to the induced radiationless deactivation of S_1 that occurs upon absorption of a photon at 353 nm from S_1. They calculated a rate constant for the induced radiationless deactivation by taking the product of the incident irradiance at 353 nm (10^{26} photons-cm^{-2}-sec^{-1}) and a value of the absorption cross-section for the $S_1 \dashrightarrow S_n$ transition (4.2×10^{-17} cm^2), and multiplying by their previously calculated quantum yield for the radiationless deactivation of S_1 (0.9-1.0). From this rate constant for induced radiationless deactivation of S_1, they have determined that the mean lifetime of molecules in the S_1 state is 220 psec when rhodamine 6G is pumped at 355 nm. This is in contrast to the 4.5 nsec mean lifetime of a molecule in the S_1 state when the pumping is at 532

nm, and deexcitation arises primarily from radiative relaxation to the ground state (4.13). The decrease in the mean lifetime of S_1 results in a decrease in the fluorescence quantum yield by a factor of 21.4 (4.13).

It can be concluded from the ground state depopulation studies at 355 nm and the corroborating results of other investigators at 353 nm that the inability to modulate the ground state population using a 355 nm pump beam is due to fast nonradiative deactivation of a reversible photoproduct (i.e., half-oxidized rhodamine 6G) which is formed by the absorption of a 355 nm photon from S_1. The deexcitation scheme proposed accounts for fluorescent decay from S_1 being a predominant relaxation pathway at low incident intensities as well as for the fact that ground state depopulation can not be achieved at high incident intensities.

4.1.5 (octa)3-hydroxypropylporphyrin and (etio)hemechloride - 532 nm Excitation

In order to further investigate the inverse relationship of the product of the lifetime and the absorption cross-section on the ability to effect ground state depopulation, two porphyrins were chosen for preliminary studies. The lifetime of one of the porphyrins is much shorter and the lifetime of the other is on the same order of magnitude as that of rhodamine 6G. The

absorption cross-sections for both of the porphyrins at the excitation wavelength (532 nm) are lower than the absorption cross-section of rhodamine 6G at 532 nm; they are approximately the same as the absorption cross-section for rhodamine 6G at 355 nm. The porphyrins studied were (octa)3-hydroxypropylporphyrin (hereafter termed OPP) and (etio)hemechloride. The molecular structures of OPP and (etio)hemechloride and their absorption spectra for methanolic solutions are shown in Figures 4.12 and 4.13, respectively.

Free-base porphyrins, such as OPP, are classified as fluorescent and have fluorescence quantum yields between 0.2 and 10^{-3} with radiative lifetimes of approximately 120 nsec (4.35). Given this information, the effective lifetimes of the free-base porphyrins are expected to fall, in general, between 120 psec and 24 nsec. The lifetimes were determined in the following manner. The rate constants for non-radiative relaxation were first calculated using the values cited for the fluorescence quantum yields and the inverse of the cited radiative lifetime. The lifetime is then obtained from the inverse

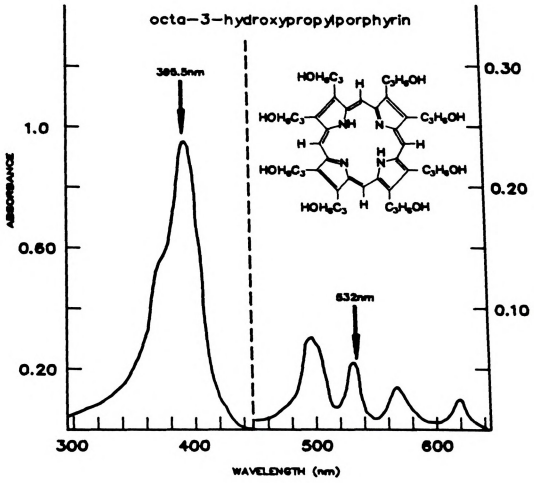

Figure 4.12 Absorption spectrum and structure of (octa)-3-hydroxypropylporphyrin - 5 x 10^{-6} M. Arrow indicated pump wavelength (532 nm).

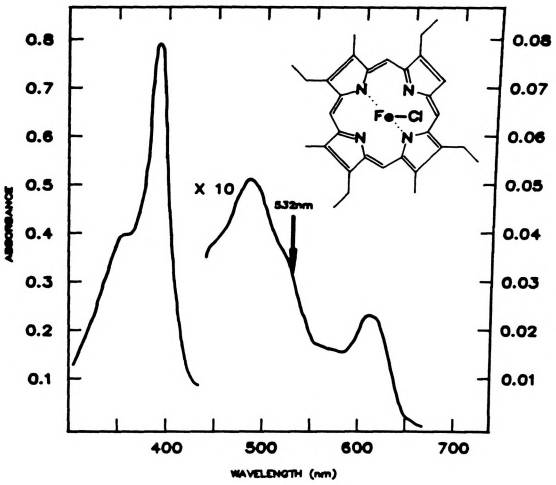

Figure 4.13 Absorption spectrum and structure of (etio)hemechloride - 1 x 10^{-5} M. Arrow indicated pump wavelength (532 nm).

of the sum of the rate constants for radiative and non-radiative relaxation.

The magnitudes of the of the fluorescence quantum yields for the free-base porphyrins indicate that radiative relaxation is not the dominant deexcitation pathway from S_1. (This is in contrast to rhodamine 6G which has a fluorescence quantum yield of 0.92-0.95 (4.9).) Intersystem crossing from S_1 to T_1 followed by nonradiative relaxation to S_0 is apparently a major decay process for the free-base porphyrins (4.36). However, the relative importance of intersystem crossing and internal conversion to S_0 in the deexcitation of S_1 is a subject still under much debate (4.37).

From the range of lifetimes for free-base porphyrins and the cross-section for absorption, it is possible to calculate a range of values of I_S for OPP. The absorption cross-section for OPP at 532 nm was calculated from the absorption spectrum to be approximately 2.4×10^{-17} cm^2. I_S is expected to fall in the range of 1.7×10^{24} and 4.2×10^{26} photons-cm^{-2}-sec^{-1}. It was expected that it may be possible to observe ground state depopulation within the range of experimental intensities in spite of the smaller absorption cross-section.

Figure 4.14 shows average transmission plotted as a function of the incident irradiance of the pump beam for

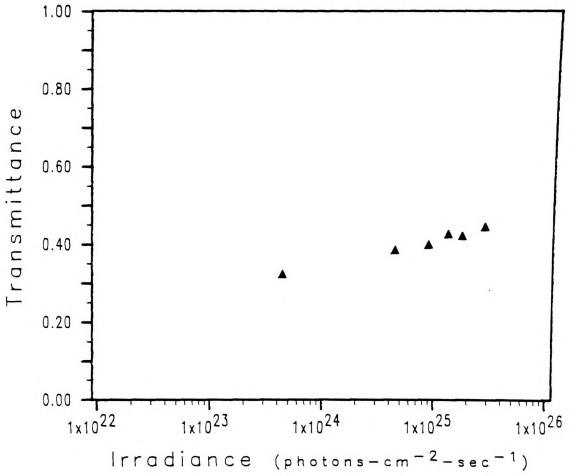

Figure 4.14 Transmittance vs. incident photon irradiance - 6 x 10^{-5} M (octa)-3-hydroxpropylporphyrin pumped at 532 nm.

6×10^{-5} M methanolic solution of OPP. The percent transmission of the solution measured on a spectrophotometer was 22.6 %. Here, the plotted transmission values represent the averaged normalized transmission for five pulses. The increase in transmission indicates that the ground state of OPP was modulated with the 532 nm pump beam. From these measurements, it can be said that the lifetime of OPP is indeed in the nanosecond range and the magnitude of the absorption coefficient does not prevent depopulation of the ground state. However, OPP was not studied in great detail, and from the data obtained it is not possible to determine the shape of the transmission vs. irradiance curve and whether or not the transmission approaches 100 %. It is interesting to note that ground state depopulation has been observed and studied quite extensively for another class of porphyrins, the free-base and metallo phthalocyanines. Residual absorption and, therefore, excited state absorption has been observed for some of these phthalocyanines (4.2,4.4,4.38).

The iron porphyrins, such as (etio)hemechloride, have been characterized as **radiationless**. Radiationless has been defined to mean that the total emission yield (i.e., quantum yield of fluorescence plus phosphorescence) is $10^{-4} - 10^{-6}$ with excited state lifetimes of from 6 psec to 60 fsec (4.39,4.40). Radiationless actually means that the

emission yield is near the limit of detection (4.40). The absorption cross-section for (etio)hemechloride was determined from the absorption spectrum to be approximately 1.7 x 10^{-17} cm^2 and it was used along with the range of lifetimes to calculate the value of I_S to be between 9.8 x 10^{27} and 9.8 x 10^{29}. Thus ground state depopulation was not expected within the range of experimental intensities.

Figure 4.15 shows the average normalized transmission for five pulses for a 1 x 10^{-4} M (etio)hemechloride solution vs. incident irradiance. The baseline transmission was 34.9%. Not surprisingly, the transmission is seen to remain constant due the short lifetime of this iron porphyrin.

4.1.6 Summary

These population modulation studies have demonstrated the inverse relationship between the irradiance required to induce modulation of the ground state population and the product of the effective lifetime and the absorption cross-section. Depopulation is most readily achieved for absorbers with large absorption cross-sections at the pump wavelength and long excited state lifetimes. For rhodamine 6G, it was seen that excited-state absorption is required to explain the transmission behavior of this absorber when

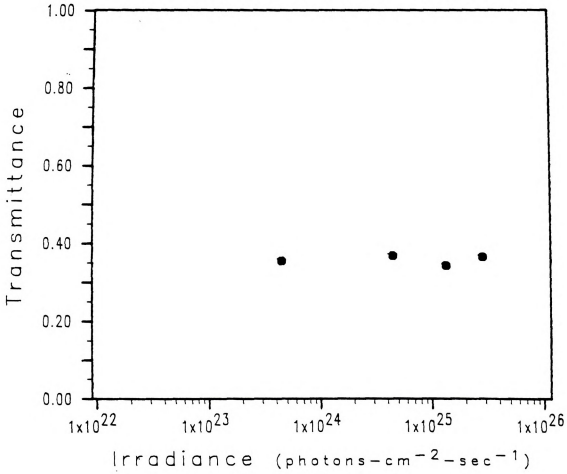

Figure 4.15 Transmittance vs. incident photon irradiance - 1 x 10^{-4} M (etio)hemechloride pumped at 532 nm.

irradiated by high intensity laser pulses. The studies that employed a 355 nm beam have shown that the effective time for repopulation of the ground state of rhodamine 6G in is a function of the excitation wavelength (energy) when high incident intensities are employed.

4.2 Saturation of Fluorescence Studies - Rhodamine 6G

The ground state depopulation induced in rhodamine 6G by pumping the S_0 --> S_1 transition at 532 nm was confirmed by simultaneously monitoring fluorescence from the excited singlet state. Fluorescence was monitored at 560 nm, the fluorescence maximum of rhodamine 6G in methanol (4.41), as a function of the incident irradiance of the pump beam. Fluorescence data were obtained for an air-equilibrated solution and for three concentrations of deoxygenated solutions. Refer to Figure 3.5 for the optical set-up.

Figures 4.16 and 4.17 are log-log plots of average fluorescence signal for 150 pulses vs. incident pump beam irradiance for the 1×10^{-6} M solution in equilibrium with air and the deoxygenated solutions, respectively. The fluorescence is plotted in relative units which correspond to the digital values obtained from the channel on the data acquisition system which monitored the fluorescence signal from the photomultiplier tube. The data are

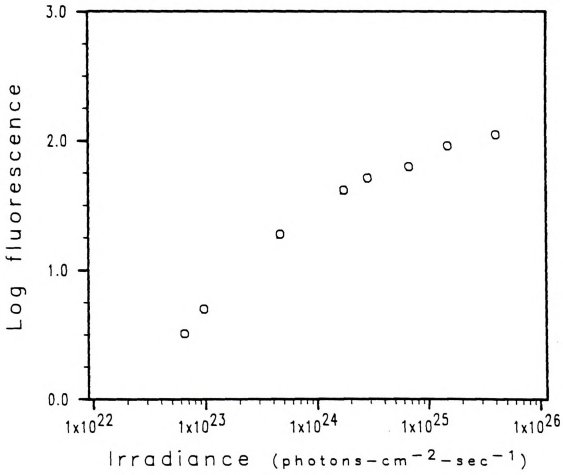

Figure 4.16 Log relative fluorescence intensity (560 nm) vs. incident photon irradiance - 1 x 10^{-6} M rhodamine 6G in methanol pumped at 532 nm.

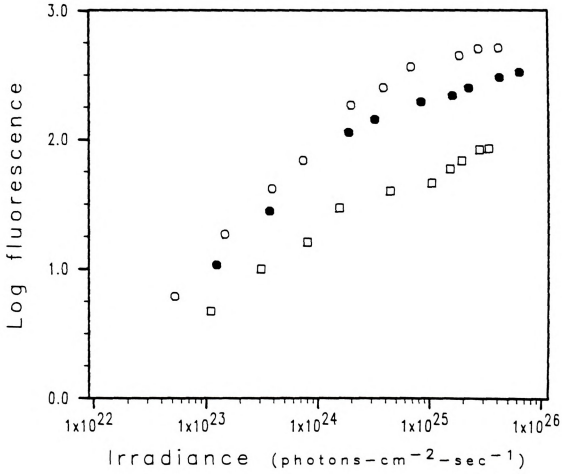

Figure 4.17 Log relative fluorescence intensity (560 nm) vs. incident photon irradiance - deoxygenated methanolic rhodamine 6G solutions pumped at 532 nm - (□) 1 x 10^{-5} M, (●) 5 x 10^{-6} M, (○) 1 x 10^{-6} M.

corrected for the attenuation by neutral density filters (see Chapter 3). The fluorescence signals are seen to increase with incident pump beam irradiance as the ground state population is excited to S_1. The increase in fluorescence is seen to be slow relative to the increase in incident photons at the higher incident intensities as the population of the excited state approaches a maximum. In rigorous studies of this type, the irradiance at which the curve bends is precisely determined and is compared to the theoretical saturation irradiance (4.42,4.43).

The saturation of fluorescence study has shown, independently of the transmission measurements, that the ground state was indeed depopulated. The curve for the air-equilibrated solution bends at approximately 1.1 x 10^{24} photons$cm^{-2}sec^{-1}$. The curves for the deoxygenated solutions bend in the range of 1.2 x 10^{24} to 1.4 x 10^{24} photons-cm^{-2}-sec^{-1}. The I_S values determined from this set of experiments are considered to be the same for the air-equilibrated and deoxygenated solutions. For the deoxygenated solutions, the values of I_S determined from the saturation of fluorescence studies agree with the values of I_S which were determined from curvefit analysis of the transmission data (see Table 4.2). This agreement is expected because the transmission and fluorescence data were acquired simultaneously. For the air-equilibrated solution, the value of I_S from the fluorescence experiment

is higher than the values of I_S shown in Table 4.2 which were determined from the transmission experiments. This discrepancy is a measure of the imprecision with which the incident irradiance is determined since the fluorescence data and transmission data for the air-equilibrated solutions were not acquired simultaneously. The previously drawn conclusion that the transmission vs. incident irradiance curves for the deoxygenated and air-equilibrated solutions are not different is, therefore, further supported by the I_S values determined from the fluorescence data.

4.3. Ground State Recovery Studies - Rhodamine 6G

Information regarding the onset, duration and detection of the population modulation induced by pumping a solution of rhodamine 6G with a 7 nsec (FWHM) 532 nm pulse was obtained by probing the pumped system with temporally delayed beams at the same wavelength and pulsewidth as the pump beam. (See Figure 3.6 for the optical set-up.) The weak probe beam, which was split off from the pump beam and directed through the sample cell at 90° relative to the pump beam, was delayed via an optical delay line. The transmittance of the sample was measured by the probe beam in the presence of the pump beam and was compared to the sample transmittance measured in the absence of the pump beam at each of the probe delay times.

In order to determine the effect of the temporal intensity profile of the pump beam on the extent of the induced population modulation, average incident pump beam energies of 5mJ and 10 mJ (irradiances of 5×10^{24} and 1×10^{25} photons-cm^{-2}-sec^{-1}) were used. This also provided verification that differences in the extent of population modulation induced by pump beams of different intensities could be distinguished by monitoring the probe beam.

The data obtained from a 1×10^{-5} M solution of rhodamine 6G are presented in Table 4.5 as average probe transmittance values for 150 pulses and are plotted in Figure 4.18. The true percent transmittance measured with a spectrophotometer was 9.1 % for this solution, whereas the average percent transmittance values obtained by monitoring the probe laser beam only were found (Table 4.5) to be between 9.0 % and 11.8 %. In order to determine the cause of this discrepancy, the transmittance values were sorted by incident irradiance and examined. The individual transmittance data did not show the increase with increasing incident irradiance that would be expected if the irradiance of the probe beam was sufficiently high to cause modulation of the ground state population. Therefore, the somewhat high average transmittance values were not due to depopulation of the ground state by the probe beam. The experimental set-up and the measurement

Table 4.5 Ground State Recovery Studies - Transmittance Data for Rhodamine 6G at Two Incident Pump Beam Intensities[1,2,3]

Probe Delay Time / Incident Intensity (photons-cm^{-2}-sec^{-1}) x 10^{-24}	Transmittance (%) Probe Only	Transmittance (%) Probe With Pump	Transmittance (%) Pump Beam
1.0 nsec			
5	9.0 ± 0.3	19.6 ± 0.5	41.5 ± 1.7
10	9.0 ± 0.2	21.5 ± 0.5	56.0 ± 1.2
2.0 nsec			
5	10.2 ± 0.4	17.8 ± 0.7	50.3 ± 1.3
10	10.1 ± 0.4	19.6 ± 0.7	61.5 ± 1.3
4.0 nsec			
5	10.7 ± 0.4	17.2 ± 0.7	52.6 ± 2.0
10	9.9 ± 0.2	17.8 ± 0.5	63.8 ± 1.8
6.2 nsec			
5	10.6 ± 0.3	16.3 ± 0.5	53.4 ± 2.2
10	11.4 ± 0.4	16.6 ± 0.7	63.5 ± 1.2
8.1 nsec			
5	11.4 ± 0.4	15.8 ± 0.5	48.4 ± 2.4
10	10.5 ± 0.2	15.4 ± 0.5	64.6 ± 1.2
12.5 nsec			
5	11.8 ± 0.3	13.4 ± 0.3	47.9 ± 2.2
10	10.3 ± 0.2	13.0 ± 0.3	61.3 ± 1.4
15.0 nsec			
5	10.6 ± 0.5	11.8 ± 0.5	52.2 ± 1.6
10	10.8 ± 0.4	12.6 ± 0.4	61.2 ± 1.9

1. Data acquired for 1 x 10^{-5} M rhodamine 6G in methanol.
2. Pump and probe beams are at 532 nm and at 90°.
3. Transmittance values are the normalized averages for 150 pulses.

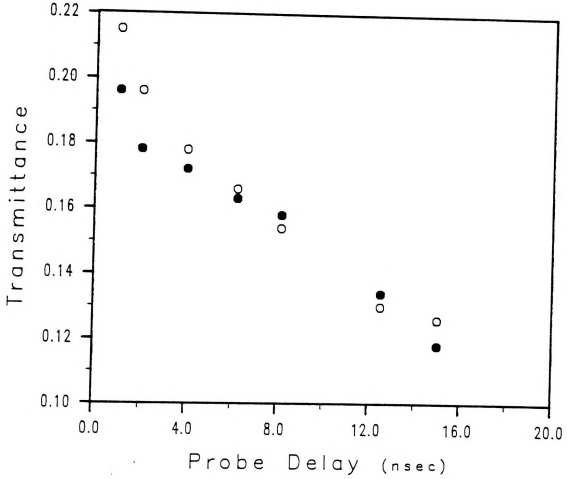

Figure 4.18 Transmittance (%) of 532 nm probe beam vs. probe delay time for a 1 x 10^{-5} M methanolic rhodamine 6G solution pumped at 532 nm: (●) 5x10^{24} and (○) 1x10^{25} photons-cm^{-2}-sec^{-1}.

process most probably contributed to the observed discrepancies. The experimental set-up was such that the sample and solvent cells had to be placed in the cell holder alternately. In addition, the solvent cell was turned in order to monitor the transmittance of the 90° probe beam since it had only two optical surfaces, whereas the sample cell had four. Removing and replacing the sample and solvent cells could very well have resulted in average probe beam transmittance values differing from one another and from the sample transmittance which was measured with the spectrophotometer.

It should also be noted that the absolute probe beam transmittance values obtained in the presence of the pump beam are lower than the transmittance values obtained by monitoring the pump pulse itself. The lower probe beam transmittance resulted because, with the 90° geometry probe beam, photons are absorbed by a portion of the sample volume that is not irradiated by the pump pulse. Moreover, many laser excited molecules have already relaxed back to the ground state as a result of the delay time of the probe beam. A colinear and temporally coincident probe beam should have a transmittance value identical to that of the pump beam. A colinear configuration of the pump and probe beams was not used because it would not have been possible to optically separate two colinear beams of the same wavelength.

The percent relative standard deviations seen in the ratioed probe beam transmittance values for both sample and solvent were 2 - 5 %. This occurred despite careful reoptimization of the elements in the optical delay line for each of the probe beam delay times. These deviations were minimized before the cell holder and cells were placed in the path of the probe beam and they are of the same magnitude for probe beam transmissions measured for both sample and solvent. By contrast, the relative standard deviations are approximately 1 % when the pump beam transmission is monitored through the solvent. The spread in the probe beam ratios is attributed to the increased number of optical elements in the probe beam path. Alignment of the photodiodes became less precise as the number of degrees of freedom increased. As discussed in Chapter 3, less than optimal photodiode alignment results in an increase in the standard deviations of ratioed measurements due to nonlinear fluctuations in the intensity across the beam profile. However, a distinction should be made regarding the cause of the standard deviations of the pump and probe beams. The standard deviations for the average pump beam transmittance values are due to the fact that the ratios for pump beam transmittances are indeed a function of the incident irradiance; therefore, they increase as the intensities of the incident pump pulses increase. The average standard deviation for the pump beam thus results from a sample-

related phenomenon and not from the imprecision of the optical alignment, which is the cause of the probe beam deviation.

The average pump beam transmittances for the two nominal incident irradiances at the 1.0 nsec probe delay are significantly lower than the average pump beam transmittances at each of the longer probe delay times. If one refers to Figure 4.4, the average pump beam transmittances shown in Table 4.5 at the 1.0 nsec delay time occur at 3.6×10^{24} and 7.5×10^{24} photons-cm^{-2}-sec^{-1} rather than at the nominal irradiances of 5.0×10^{24} and 10×10^{24} photons-cm^{-2}-sec^{-1}. If the experimental measurements were indeed obtained at irradiances which were lower than nominal incident irradiances, the probe beam transmittances reported at the 1.0 nsec delay in the presence of the pump beam are lower than would be expected had the incident irradiances been their nominal values. The trends apparent from this study are unaffected.

From Table 4.5 it is readily apparent that the transmittance of the probe beam increases in the presence of the pump beam for all the experimental probe delays at both incident intensities. For the shorter probe delay times, a difference is observed between the data acquired at the two incident irradiances. These effects are explained by considering both the pump beam pulse shape

and the relaxation time of the first excited singlet state.

As discussed in Chapter 3, the rise time of the 7 nsec (FWHM) laser pulse is approximately 1 nsec and the intensity drops off more slowly on the trailing edge of the pulse. This results in the ground state being depopulated to a greater extent on the rising edge and at the peak of the pump pulse. As the incident intensity falls off, the ground state population is modulated to a lesser extent and thus the probe beam transmittance decreases as the delay time increases. This is further verified if the data acquired at pump beam intensities of 5×10^{24} and 1×10^{25} photons-cm^{-2}-sec^{-1} are compared and examined in more detail.

From Figure 4.18 it is clear that for probe delay times of 1.0 and 2.0 nsecs, the probe beam transmittances are clearly higher when the solution is pumped at the higher incident irradiance. As the probe beam delay increases the difference in transmittance observed between the probe beams at the higher and lower incident irradiances begins to decrease and the transmittances agree within experimental error beyond a probe delay time of approximately 4 nsec. This observation verifies the expectation that population modulation occurs to the greatest extent at the onset and peak of the pump pulse and that the incident irradiance in the tails of the pump

pulses is not sufficient to cause significant ground state depopulation. If this were not the case, one would expect that the probe beam transmittances would differ for different incident pump irradiances even at the tailing end of the pump pulse. In order to draw this conclusion, however, the intensity profile of the pump beam must be assumed to remain constant as the incident irradiance of the pulse increases. A fast storage oscilloscope could be used to monitor the intensity profile of the pump beam as a function of the pulse energy.

Relaxation of the first excited singlet state also contributes to the decrease seen in probe beam transmittance with increasing delay time. The lifetime of S_1 of rhodamine 6G has been reported to be 4.5 to 6.0 nsec (4.12,4.13,4.24-4.26), and therefore, one would expect that some ground state repopulation contributes to the observed decrease in the probe beam transmittance at the longer probe delay times. Note that the probe beam transmittance at a 15 nsec delay time is still slightly higher than the value obtained in the absence of the pump beam. This observation is attributed primarily to incomplete relaxation of the absorbers in the first excited singlet state back to the ground state and also to the possibility of a metastable excited state population (i.e., a triplet state population). This explanation is required because the intensity profile of the laser pulse,

monitored by a photodiode and oscilloscope, is essentially at baseline value 15 nsec after the onset of the pulse. Deconvolution of the temporal intensity profile of the incident pulse would be required in order to verify the existence of such a metastable state and to obtain more quantitative information regarding the lifetime of rhodamine 6G from an experiment of this type.

4.4 Population Modulation Across the S_0 --> S_1 Absorption Band - Rhodamine 6G

The objective of this set of experiments was to determine if the ground state population modulation induced by the pump beam at 532 nm is observable across the entire S_0 --> S_1 absorption band. Probe beams were generated at selected wavelengths by a pulsed dye laser and used to interrogate a solution of rhodamine 6G at 90° relative to the pump beam. The probe beams were delayed 2.5 nsec from the pump beam and had pulsewidths of 5 - 6 nsecs (FWHM). The 2.5 nsec delay was used because it was the minimum delay attainable due to the geometrical set-up of the dye laser and optical bench. Ideally the probe beam would have been temporally coincident with the pump beam in order to probe the solution prior to the relaxation of excited molecules; maximum changes in probe beam transmittance could thus have been observable with minimum

ground state absorption. (See Figure 3.7 for optical set-up.)

The data presented in Table 4.6 for a 1 x 10^{-5} M rhodamine 6G solution show clearly that an increase in the average percent transmission values of the probe beams is observed in the presence of the pump beam at all the experimental wavelengths. Therefore, the population modulation induced by the pump beam is observable across the entire S_0 --> S_1 absorption band. The percent transmission values of the probe beams measured in the absence of the pump beam differ from the true spectrophotometer transmission values in a manner similar to the values obtained for the previous set of experiments. These discrepancies are once again attributed to the errors induced in the measurement by removing, replacing and turning the sample and solvent cells during the course of the experiment. The percent relative standard deviations for the probe beam transmission values in the absence of and during pumping are approximately 7 - 10 %. These deviations were minimized during the set-up of the numerous optical elements and represent, as discussed previously, less than optimal alignment of the transmitted probe beams with the photodiode detectors. The average percent transmission of the 532 nm pump beam is

Table 4.6 Probe Beam Transmittance at Selected Wavelengths within the $S_0 \rightarrow S_1$ Absorption Band of Rhodamine 6G[1]

Probe Beam Wavelength	Spectrophotometer Transmittance (%)	Transmittance (%) Probe Only[2,3]	Transmittance (%) Probe With Pump[2,4]
500 nm	42.7	45.6 ± 4.4	65.7 ± 5.4
520 nm	13.8	12.1 ± 0.8	23.4 ± 1.6
527 nm	8.1	9.6 ± 0.9	22.5 ± 2.2
532 nm	9.1	8.4 ± 0.6	19.6 ± 1.3
540 nm	24.2	27.7 ± 2.4	56.6 ± 4.1

1. 1×10^{-5} .M rhodamine 6G in methanol.
2. Transmittance values are the normalized averages for 150 pulses.
3. Probe beam is at 90° to the pump beam.
4. Pump beam is at 532 nm and pump beam transmittance is 40%.

40.0 $\pm$ 3.5 %; the transmission of the unpumped solution measured on a spectrophotometer was 9.1 %. For this experimental configuration, an increase in the sample transmittance by roughly a factor of four is reflected in increases in the transmittance of the perpendicular probe beam by factors of 1.4 to 2.3. As noted earlier, the difference is due to absorption of the probe beam by unpumped sample volume. The probe beam transmittances from Table 4.5 have been converted to absorbance values and are shown superimposed on the absorption spectrum of the solution in Figure 4.19. The modulation of the ground state population across the entire absorption band is clearly seen in this manner.

From the ground state recovery experiments, it was seen that as the probe beam delay time increases, the transmittance measured by the probe beam decreases. It is reasonable, then, to conclude that that the transmittance values acquired in this set of experiments at a delay time of 2.5 nsec are indeed lower than those which would result from monitoring probe beams with no delay relative to the pumping pulse. Furthermore, the transmittance values obtained here would be expected to increase with the irradiance of the pump beam and approach a maximum value. Aristov and Shevandin have shown that the absorption of probe beams generated by a dye laser approaches zero across the entire $S_0 \dashrightarrow S_1$ absorption band when a

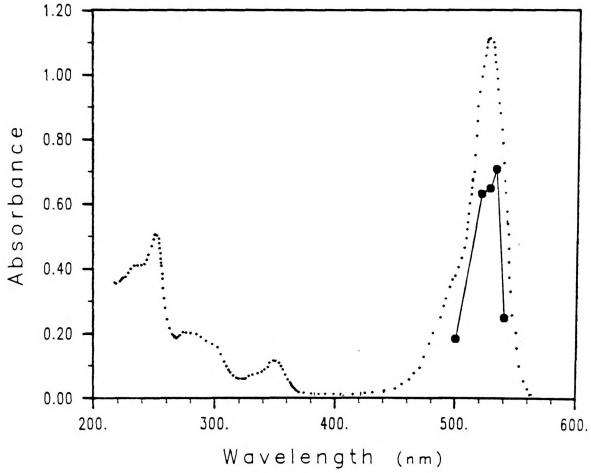

Figure 4.19 Absorbance spectrum of a 1 x 10^{-5} M methanolic rhodamine 6G solution (....). Absorbance of probe beam vs. wavelength during pumping at 532 nm as shown by the (●).

2.5×10^{-5} M solution of rhodamine 6G in ethanol is pumped at 530 nm and simultaneously and colinearly probed across the band (4.8,4.48). The absorption that did occur across the absorption band was essentially flat and did not reflect the shape of the unperturbed absorption band. The irradiance of the 25 - 30 nsec pump beam used in those experiments was 5×10^{25} photons-cm^{-2}-sec^{-1}, whereas the irradiance of the pump beam used here was 4×10^{24} photons-cm^{-2}-sec^{-1}. At the incident pump irradiance used by the Russian investigators, the excited state population was at a maximum, as discussed in the section on ground state population modulation studies. The fact that the transmittance observed as a function of wavelength did not resemble the shape of the absorption spectrum from the ground state further supports the hypothesis that the residual absorption observed in the population modulation studies is due to excited state absorption and not to absorption from absorbers remaining in the ground state.

The uniform increase in transmission (decrease in absorption coefficient) observed at all the probe wavelengths may initially lead one to conclude that the absorption band is homogeneously broadened and that holeburning is not occurring. In fact, the timescale of these experiments is such that it is not possible to determine whether or not holeburning occurs. It is indeed possible that a narrow spectral hole was initially burned

in the absorption band at the frequency of the pump wavelength. The thermal relaxation time of the pumped state, however, is on the order of 10^{-13} seconds and as this relaxation occurred, the hole would have diffused and resulted in an absorption coefficient which was reduced uniformly across the absorption band (4.1). Since relaxation occurs on a timescale much shorter than the pulsewidth of the pump and probe beams it would not have been possible to observe this phenomenon if it had occurred.

4.5 Dual Wavelength Pump/Probe Studies - Rhodamine 6G

The potential for identifying transitions which arise from the same ground state via population modulation was investigated. A 1×10^{-5} M solution of rhodamine 6G was probed at 355 nm as the ground state population was modulated by a colinear pump beam at 532 nm. An increase in probe beam transmission was expected due to the decreased ground state population which could absorb photons at 355 nm. The solution was also interrogated at probe delay times from 0 - 5 nanoseconds to ascertain whether the probe beam contained information regarding the rate of relaxation of the excited state back to the ground state. (The appropriate optical diagram is given in Figure 3.8)

The data acquired are shown in Table 4.7. Probe beam transmissions are shown as a function of the delay time between the pump and probe beams. The incident irradiances of the probe and pump beams were 1×10^{22} and 5×10^{24} photons-cm^{-2}-sec^{-1}, respectively. As shown in previous experiments, the probe beam irradiance was not sufficient to induce ground state depopulation. The irradiance of the pump beam was such that the transmittance of the solution was increased from 9.1 % to an average of 45.0 $\pm$ 1.8 %; this corresponds to a ground state population that is approximately one-third of the unperturbed ground state population. The population modulation induced at 532 nm did not result in a modulation of the transmitted 355 nm probe beam irradiance at any of the experimental delay times. In fact, the average transmission values of the probe beam were seen to decrease slightly (approximately 4 %) in the presence of the pump beam from the average transmissions measured without the pump beam at each delay time. This is attributed to heating of the solution by the pump beam and the resultant thermal lensing effect. Slight divergence of the probe beam by a thermal lens could cause the irradiance impinging on the active area of the transmittance photodiode detector to be less than if no divergence occurred, resulting in a lower transmission

Table 4.7 355 nm Probe Beam Transmittance for Dual Wavelength Pump-Probe Studies[1,2,3]

Probe Delay Time (nsec)	Transmittance (%) Probe Only[4]	Transmittance (%) Probe With Pump[4]
0	84.5 ± 1.2	80.5 ± 1.1
1.5	82.5 ± 2.9	78.0 ± 2.5
3.0	85.1 ± 3.4	80.3 ± 3.3
4.0	85.2 ± 1.7	81.7 ± 1.7
4.6	85.4 ± 2.4	81.7 ± 2.2

1. 1×10^{-5} M rhodamine 6G in methanol.
2. 355 nm probe beam at 1×10^{22} photons-cm^{-2}-sec^{-1}.
3. 532 nm pump beam at 5×10^{24} photons-cm^{-2}-sec^{-1}.
4. Transmittance values are the normalized averages for 150 pulses.

measurement. Although thermal lensing is known to occur in non-absorbing solvents (4.44), the transmittance of the 355 nm probe beam through the solvent was not measurably affected by the presence of the 532 nm pump beam in this case. This explanation for the lower probe beam transmittance is thus supported. As indicated by the relative standard deviations in Table 4.7, these transmittance decreases in any case are not significantly larger than the combined uncertainties of the two transmittance measurements. Therefore, the results of this experiment have shown that the transmittance of the probe beam was unaffected by the ground state population modulation induced by pumping the S_0 --> S_1 transition at 532 nm.

Why was modulation of the probe beam transmittance not observed? Three potential explanations will be considered: (1) insufficient data system sensitivity, (2) population of an excited state which absorbs at 355 nm as does the ground state, and (3) uncoupled or independent chromophores.

Insufficient data system sensitivity is considered first. From the observed transmission of the pump beam, the ground state population was determined to be approximately one-third of the population of the unpumped solution. With a temporally coincident and perfectly aligned probe beam, the transmission of this beam would be

expected to increase from the average "probe only" value of 84.5 % to an average "probe with pump" value of 94.5 %. An increase in transmission of this magnitude would have been readily observed with the data acquisition system. In fact, modulation of the ground state population to a value that is two-thirds the equilibrium value should have been distinguishable by the system; this would correspond to "probe only" and "probe with pump" transmission values of 84.5 % and 89.5%, respectively. It is concluded that the probe beam transmission changes which would have occurred due to the observed modulation of the ground state population were well within the performance capabilities of the data acquisition system.

Although in principle the molecular orbitals describing the electronic energies of a molecule encompass the entire nuclear framework, in practice many molecular orbitals are essentially localized on a single atom (e.g., core electrons, lone-pairs) or specific functional groups, or conjugated in a certain sub-system. If these localized electrons are geometrically isolated from one another, their electronic excitations will be effectively uncoupled; one can then say that the electronic chromophores do not communicate. Rhodamine 6G is a fairly complex organic molecule and if the chromophore being probed at 355 nm is not coupled to the chromophore being pumped at 532 nm, absorption at the probe wavelength may

be unaffected by excitation of the S_0 --> S_1 transition at 532 nm. The molecular structure of rhodamine 6G is shown in Figure 4.20. If one of the transitions in the pump-probe experiments would involve the oxygen-bridged pyronine ring and the other the out-of-plane substituted phenyl (benzoin) ring then the results given in Table 4.7 might be expected. However, it has been established (4.9,4.28,4.45-4.47) that both the S_0 --> S_1 and S_0 --> S_4 transitions in rhodamine 6G involve the pi-electrons of the pyronine ring. [For example the UV-visible electronic absorption spectrum of pyronine itself - where the position across from the O-atom on the center ring is unsubstituted - is almost identical to those of the rhodamine series formed by altering the alkyl groups shown in Figure 4.20 (4.48). Thus the absorptions in rhodamine 6G at 532 nm and 355 nm involve the same electronic chromophore.

The remaining possibility is that rhodamine 6G in its excited electronic state (S_1) following absorption of pump radiation at 532 nm absorbs light at 355 nm, and that the cross-section for this excited state absorption differs little from its value at 355 nm for rhodamine 6G ground-state absorption. In the usual perception of excited state absorption, this possibility would appear highly fortuitous. If the transition from the ground state at 355

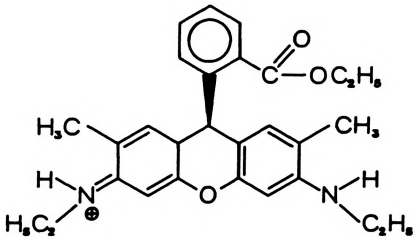

Figure 4.20 Structure of rhodamine 6G. The pyronine ring is the chromophore. The transition moment for the So → S_1 transition is along the long axis. The transition moment for the So → S_4 transition is oriented through the bridging carbon and oxygen of the pyronine ring.

nm corresponds to S_0 --> S_4, is it likely that there is an excited state, S_n, which lies at an equivalent energy above S_1 such that S_1 --> S_n absorption will occur at 355 nm? If so, by what coincidence would its absorption cross-section be similar to that for S_0 --> S_4? In the special circumstance that the two transitions of the same chromophore, S_0 --> S_1 and S_0 --> S_4, are independent, the answer to the first question is affirmative, and to the second is not coincidental, but expected. For example, if the polarizations of the two transitions are orthogonal, the excitation of one has essentially no effect on the energetics or probability of the other. [In this respect, the problem is similar to the independent frequencies and extinction coefficients of orthogonal harmonic oscillations in vibrational spectroscopy (4.49)]. In fact, just this situation applies to the S_0 --> S_1 and S_0 --> S_4 transitions of the rhodamines. The orientation of the transition moment of the S_0 --> S_1 absorption band is along the long axis of the chromophoric fragment and passes through the nitrogens of the auxochrome groups, whereas the transition moment of the S_0 --> S_4 absorption band is oriented along the short axis and passes through the bridging carbon and oxygen (4.9,4.28,4.45,4.46). The orthogonality of the transition moments accounts for the excitation at 532 nm not affecting the "chromophore" which gives rise to the S_0 --> S_4 transition. Verification of this has been obtained by experimental polarization

measurements (4.28,4.48), by theoretical calculations (4.47), and by measurement of the absorption spectrum from the excited state (4.48). Thus, for the rhodamine 6G model compound utilized in the pump/probe experiments, excitation of the molecule at 532 nm has little effect on the independent transition at 355 nm. More explicitly, excitation from S_0 to S_1 excites electrons in the "long-axis MO" leaving the electrons in the "short axis MO" (those excited by the S_0 --> S_4 transition) unexcited. The excited state absorption at 355 nm differs little from the ground state absorption at his wavelength, which accounts for the observed results. Modulation of the ground state population by the pump radiation is not observable at the probe wavelength because both ground and excited states show equivalent absorption there.

Regarding the transmittance measurements made as a function of probe beam delay time, one would expect to see the transmittance of the probe beam change in the presence of the pump beam as a function of the delay time only if the cross-sections for absorption from the ground and excited states differed measurably. As discussed previously, a change in probe beam transmittance would result both from relaxation back to the ground state and from the fact that the induced population modulation is greatest at the onset and peak of the pump pulse. This provides experimental confirmation that the S_1 excited

state absorbs photons at 355 nm to the same extent as the ground state.

4.6 Conclusions

This experimental work has explored ground state population modulation and associated phenomena. The excited state lifetimes were shown to be the primary property which determines whether or not it is possible to modulate the ground state population. However, it is ultimately the product of the absorption cross-section and the excited state lifetime which dictates whether population modulation can be achieved within the constraints of the experimental incident intensities. It was not possible to depopulate the ground state of rhodamine 6G by pumping at 355 nm. It was concluded that the effective lifetime of the system was shortened compared to excitation into the S_1 state by 532 nm radiation due to radiationless deactivation pathways which become accessible when rhodamine 6G is excited at 355 nm with high incident irradiances.

Information regarding the onset and relaxation of the population modulation was obtained from ground state recovery studies which were single-wavelength pump-probe experiments at 532 nm. The transmission increases observed for the probe beam were a function of the delay time from

the pump pulse, and it was apparent that the ground state was depopulated to the greatest extent at the onset and peak of the pulse. Since the decay of the excited state was convoluted with the intensity profile of the pump beam, it was not possible to determine if the increased probe beam transmission observed at a probe delay time of 15 nsec was due entirely to excited singlet species or whether there was a contribution from species in the triplet manifold.

Pump-probe studies at wavelengths within the S_0 --> S_1 absorption band have shown that the population modulation is observable across the entire absorption band. The increase in the probe beam transmission at a delay time of 2.5 nsec was readily observed despite the absorption of photons from the probe beam by unexcited sample volume, and some repopulation of the ground state.

Dual-wavelength pump-probe studies have shown that the ground state population modulation which results from pumping rhodamine 6G at 532 nm is not observable at 355 nm, a wavelength which corresponds to another allowed transition from the ground state. The excitation of the S_0 --> S_1 transition is not reflected in concomitant modulation of S_0 --> S_4 absorption. The excited state absorption at 355 nm in rhodamine 6G is indistinguishable from ground state absorption at this wavelength because the pump and probe transitions are independent.

REFERENCES

4.1 Hercher, M. *Appl. Opt.* **1967**, *6(5)*, 947.

4.2 Giuliano, C. R.; Hess, L. D. *IEEE J. Quantum Electron.* **1967**, *QE-3(8)*, 358.

4.3 Hercher, M.; Chu, W.; Stockman, D. L. *IEEE J. Quantum Electron.* **1968**, *QE-4(11)*, 954.

4.4 Gires, P. F., Comband, F. *J. Phys. (Paris)* **1965**, *26*, 325.

4.5 Gires, P. F. *J. Phys. (Paris)* **1969**, *30*, 203.

4.6 Selden, A. C. *Br. J. Appl. Phys.* **1967**, *18*, 743.

4.7 Aristov, A. V.; Shevandin, V. S. *Opt. Spectrosc. (USSR)* **1978**, *44*, 279.

4.8 Aristov, A. V.; Shevandin. V. S. *Opt. Spectrosc. (USSR)* **1977**, *43*, 131.

4.9 Schafer, F. P., Ed. *Topics in Applied Physics (Volume 1, Dye Lasers)*; Springer-Verlaz: New York, 1974.

4.10 Dempster, D. N.; Morrow, T.; Quinn, M. F. *J. Photochemistry* **1973**, *2*, 343.

4.11 Korobov, V. E.; Chibisov, A. K. *J. Photochemistry* **1978**, *9*, 411.

4.12 Shilov, V. B.; Neporent, B. S. *Opt. Spectrosc. (USSR)* **1971**, *31*, 58.

4.13 Shevandin, V. S.; Aristov, A. V. *Opt. Spectrosc. (USSR)* **1980**, *33*, 48.

4.14 Webb, J. P.; McColgin, W. C.; Peterson, O. G.; Stockman, D. L.; Eberly, J. H. *J. Chem. Phys.* **1970**, *53(11)*, 4227.

4.15 Korobov, V. E.; Shubin, V. V.; Chibisov, A. K. *Chem. Phys. Lett.* **1977**, *45(3)*, 498.

4.16 Dye, J. L.; Nicely, V. A. *J. Chem. Ed.* **1971**, *48*, 443.

4.17 Manning, M. R. MRMLIB (ROOTB); Decus Program Library, 1973.

4.18 Hammond, P. R. *Appl. Opt.* **1979**, *18(4)*, 536.

4.19 Meyer, S. L. *Data Analysis for Scientists and Engineers*; John Wiley and Sons: New York, 1979 p. 143.

4.20 Topp, M. R.; Rentzepis, P. M.; Jones, R. P. *Chem. Phys. Lett.* **1971**, *9(1)*, 1.

4.21 Schafer, F. P. *Agnew. Chem. Internat. Edit.* **1970**, *9(1)*, 9.

4.22 Falkenstein, W.; Penzkofer, A.; Kaiser, W. *Opt. Commun.* **1978**, *27(1)*, 151.

4.23 Steinfeld, J. I. *Molecules and Radiation*; MIT Press: Massachusetts, 1985.

4.24 Snegov, M. I.; Reznikova, I. I.; Cherkasov, A. S. *Opt. Spectrosc. (USSR)* **1974**, *36*, 55.

4.25 Aristov, A. V.; Maslyukov, Yu. S. *Opt. Spectrosc. (USSR)*, **1973**, *35*, 660.

4.26 Orner, G. C.; Topp, M. R. *Chem. Phys. Lett.* **1975**, *36*, 295.

4.27 Penzkofer, A.; Falkenstein, W.; Kaiser, W. *Chem. Phys. Lett.* **1976**, *44(1)*, 82.

4.28 Penzkofer, A.; Wiedmann, J. *Opt. Commun.* **1980**, *35(1)*, 81.

4.29 Lower, S. K.; El-Sayed, M. A. *Chem. Rev.* **1966**, *66*, 199.

4.30 Seybold, P.; Gouterman, M. *Chem. Rev.* **1965**, *65*, 413.

4.31 Bogdanov, V. L.; Klochkov, V. P.; Makushenko, A. M. *Opt. Spectrosc. USSR*, **1976**, *41*, 341.

4.32 Kohler, G.; Gettoff, N. *Chem. Phys. Lett.* **1974**, *26(4)*, 525.

4.33 Bogdanov, V. L. *Opt. Spectrosc. (USSR)*, **1984**, *56*, 270.

4.34 Aristov, A. V.; Shevandin, V. S. *Opt. Spectrosc. (USSR)*, **1981**, *50*, 320.

4.35 Dolphin, D., Ed., *The Porphyrins, Volume III;* Academic Press: New York, 1978, p. 27.

4.36 Dolphin, D. Ed., *The Porphyrins, Volume III*; Academic Press: New York, 1978, p. 35.

4.37 Dolphin, D., Ed. *The Porphyrins, Volume III*; Academic Press: New York, 1978, p. 25.

4.38 Gires, P. F. *IEEE J. Quantum Electron.* **1966**, *QE-2(9)*, 624.

4.39 Dolphin, D., Ed., *The Porphyrins, Volume III*; Academic Press: New York, 1978, p. 48.

4.40 Dolphin, D., Ed. *The Porphyrins, Volume III*; Academic Press: New York, 1979, p. 40.

4.41 Exciton Laser Dye Catalogue, Exciton Chemical Co., Inc., Dayton, Ohio, 1979, 9.

4.42 Blackburn, M. B.; Mermet, J. M.; Bautillier, G. D.; Winefordner, J. D. *Appl. Opt.* **1979**, *18(11)*, 1804.

4.43 VanDijk, C. A.; Omnetto, N.; Winefordner, J. D. *Appl. Spectrosc.* **1981**, *35(4)*, 389.

4.44 Phillips, C. M.; Crouch, S. R.; Leroi, G. E. *Anal. Chem.* **1986**, *58*, 1710.

4.45 Jakobi, H.; Kuhn, H. Z. *Elektro. Chem. Ber. Bunsenges Phys. Chem.* **1962**, *66*, 46.

4.46 Yamashita, M.; Ikeda, H.; Kashiwagi, H. *J. Chem. Phys.* **1975**, *63(3)*, 1127.

4.47 Aristov, A. V.; Maslov, V. G.; Semenov, S. G.; Shevandin, V. S. *Opt. Spectrosc. USSR* **1982**, *52*, 121.

4.48 Aristov, A. V.; Shevandin, V. S. *Opt. Spectrosc. (USSR)*, **1980**, *48*, 266.

4.49 Wilson, E. B.; Decius, J. C.; Cross, P. C. *Molecular Vibrations*; McGraw-Hill: New York, 1955.

4.50 Steen, H. B. *J. Chem. Phys.* **1974**, *61(10)*, 3997.

Chapter 5

Conclusions

The experimental work described within this dissertation has demonstrated that population modulation spectroscopy is not completely general as a technique to identify chromophores which arise from the same electronic ground state. The limitation [independent chromophores] encountered with rhodamine 6G is not universal, and for many molecules population modulation by pump laser radiation may well affect the intensity of probe wavelength absorptions originating in the molecular ground state. A thorough investigation of compounds which do not possess independent or geometrically isolated chromophores, and for which the ground state population can be modulated, would provide additional information regarding the potentiality of the method to identify chromophores which arise from the same ground state and the feasibility of extending population modulation spectroscopy to suitable multicomponent solutions.

Future investigations into the analytical applications of population modulation spectroscopy would be facilitated by the capability to tune both the pump and probe wavelengths across the entire visible spectrum. [The

use of two Nd:YAG/dye laser systems would provide the wavelength flexibility sufficient for such studies.] If a continuum source with an array detection system were employed to probe the induced spectral changes as a function of pump wavelength, spectral data could be acquired across the entire visible spectrum much more rapidly than if a probe laser beam is used to scan the spectrum. Investigations of the fundamental irradiance-dependent behavior of various compounds would be facilitated by using a transient recorder to monitor both the the time-dependence and peak transmissions of the pump and probe beams.

An approach to the problem of identification of coupled chromophores similar to the picosecond pump/probe spectroscopy which has been described by Langley, *et al.* (5.1,5.2), Beamen *et al.* (5.3) and Lytle *et al.* (5.4) merits consideration. The excellent signal-to-noise ratio which results from the fast modulation of the pump beam coupled with phase-sensitive probe beam detection should facilitate the detection of small changes in the probe beam transmission as the ground state population is modulated by the pump beam. The ability to detect small perturbations in the ground state population would allow the population modulation studies to be performed at lower incident irradiances than those used in the experiments described in this dissertation; beams of lower energy

content (e.g., dye laser beams) could then be used as pump beams. More importantly, the identification of coupled chromophores which have cross-sections for absorption from the pumped excited state at the probe beam wavelengths would be facilitated by the ability to very sensitively detect the induced changes in the probe beam transmittance; sensitive detection of probe beam transmittance changes is imperative if the ground and excited state absorption cross-sections at the probe beam wavelength of interest are similar. Since the magnitude of the change induced in the probe beam transmission is dependent on the fraction of the ground state molecules which are promoted to the excited state, as well as on the absorption cross-section, it is necessary to be able to detect small transmission changes in the event that the absorption cross-section is small at the probe wavelength.

Clearly, a thorough investigation of the ability to identify coupled chromophores in suitable compounds is required prior to assessing whether population modulation spectroscopy can be used for this purpose. Extension of the technique to selected multicomponent solutions will depend not only on the capability to identify coupled chromophores in solutions where the ground state spectra of the compounds of interest overlap, but also on the ability to identify the chromophores despite the

possibility that the excited state spectra which are induced as a function of pump wavelength may also overlap.

Rhodamine 6G was selected as a model system for the population modulation studies because its absorption characteristics well matched the laser wavelengths and peak powers available. Rhodamine 6G proved to be an imperfect choice because of the special properties of its chromophoric groups. Nonetheless, the measurements described in this dissertation have provided a great deal of information regarding the spectroscopy of rhodamine 6G on the nanosecond timescale.

REFERENCES

5.1 Langley, A. J.; Beaman, R. A.; Baran, J.; Davies, A. N.; Jones, W. J. *Opt. Lett.* 1985, *10(7)*, 327.

5.2 Langley, A. J.; Beaman, R. A.; Davies, A. N.; Joens, W. J.; Baran, J. *Chem. Phys.* 1986, *101*, 117.

5.3 Beaman, R. A.; Davies, A. N.; Langley, A. J.; Jones, W. J.; Baran, J. *Chem. Phys.* 1986, *101*, 127.

5.4 Lytle, F. E.; Parrish, R. M.; Barnes, W. T. *Appl. Spectrosc.* 1985, *39(3)*, 444.

APPENDICES

APPENDIX A

Intelligent multichannel data-acquisition system for pulsed laser applications

L. M. Jones, G. E. Leroi, C. A. Myerholtz, and C. G. Enke

Department of Chemistry, Michigan State University, East Lansing, Michigan 48824

(Received 12 August 1983; accepted for publication 20 October 1983)

A microcomputer-controlled data-acquisition system which is readily adapted to a wide variety of pulsed laser applications is described. Signals are sampled by commercially available gated integrators. Multichannel operation allows data to be normalized to a reference beam intensity, a necessity due to the pulse-to-pulse fluctuations of many pulsed lasers. Data are acquired and stored independently for each pulse. The advantages of postacquisition processing versus pulse-to-pulse averaging are demonstrated by an example of measurements on a nonlinear system.

PACS numbers: 06.50.Dc, 42.60.Kg

INTRODUCTION

The flexibility, tunability, and power of pulsed laser systems have led to a wide variety of spectroscopic applications in both static and dynamic systems. The narrow pulse widths, low repetition rates, and pulse-to-pulse intensity fluctuations characteristic of many pulsed lasers, present special challenges for signal processing.[1] The signal-to-noise enhancement devices that have been traditionally used, such as boxcar integrators and lock-in amplifiers, do not always satisfy the requirements demanded by a particular experiment.

A gated, integrating, microcomputer-controlled data-acquisition system, readily adapted to a wide variety of pulsed laser applications, has been designed and used with a pulsed Nd:YAG laser in our laboratory. The major components of the system are modular, commercially available, and relatively inexpensive.

Multichannel operation allows the measurement of several signals simultaneously. Data values can thus be easily normalized to a reference intensity. Data are acquired and stored for each pulse on every channel to allow any technique of postacquisition data processing to be used. The pulse-to-pulse data averaging of most direct signal processors is shown to result in loss of precision and information in nonlinear optical systems. Integrator gate positioning is controlled and optimized by the microcomputer because the temporal position of the laser pulse relative to the trigger pulse generated by the laser system is a function of the laser power setting.

FORTH, a threaded, high-level programming language, is the basis of the software written for this system. The software package allows the user to design an experiment, write the necessary software, perform the experiment and, if necessary, modify data-acquisition and manipulation parameters with minimal effort.

I. HARDWARE

A block diagram of the data-acquisition system is shown in Fig. 1. Detected signals are integrated and held by gated integrator modules (Model 4130, Evans Associates, Berkeley, CA). The digitized values of the integrator outputs obtained for each laser pulse are stored for any specified number of sequential laser pulses.

Gate and reset pulses for the integrators and an event trigger for the computer are generated for each laser pulse by a digital delay card. Multiple digital delay cards allow different gating delays for each integrator. A schematic diagram of the digital delay card and a timing diagram for the critical signals are shown in Figs. 2 and 3, respectively. The laser-generated trigger pulse is converted to a TTL pulse using an LM311 comparator with hysteresis; the trigger pulse is variable from $+800$ to -100 ns relative to the laser pulse and is set at $+800$ ns for triggering the digital delay card. Programmable logic delay lines (Model Nos. PTTLDL-20-5 and PTTLDL-20-2, Engineered Components Company, San Luis Obispo, CA) are used for the generation of timing pulses where the delay time is critical. The low temperature coefficient and, therefore, high stability of these modules makes them a better choice than monostable multivibrators.[2] The comparator output is the input to the first programmable logic delay line (U1). The output pulse delay of this module is variable from 20 to 1295 ns in 5-ns steps and is controlled and optimized by the microcomputer. The delayed pulse is inverted by flip–flop U5-1 and clocks section two of the 74S74 dual D flip–flop (U5), driving the GATE pulse for the integrators, $2\bar{Q}$, LO. The RESET pulse for the integrators is the Q output from the 74121 monostable multivibrator (U4). The exact width of this pulse is not critical. The $2Q$ output from the 74S74 triggers the monostable and drives the RESET pulse HI. Integration occurs when GATE is LO and RESET is simultaneously HI. The pulse from delay line U1 also goes to RST 7.5 on the microcomputer and to the input of delay line U2. The delayed pulse from delay line U2 is software programmable from 20 to 520 ns in 2-ns steps and controls the integrator gate width. The output pulse of this second delay line clears flip–flop U5-2, driving GATE HI. The integrated signal is held after GATE goes HI for as long as RESET remains HI. This is typically 0.8 ms which permits amplifier settling time and is long enough for the acquisition and storage of data from four simultaneously integrated signals. The magnitude of the droop which occurs over this period of time is less than the uncertainty in the measurements.

The integrator modules have a minimum gate width of 30 ns. Typical gate widths are 150 ns in our applications.

 0034-6748/84/020204-06$01.30

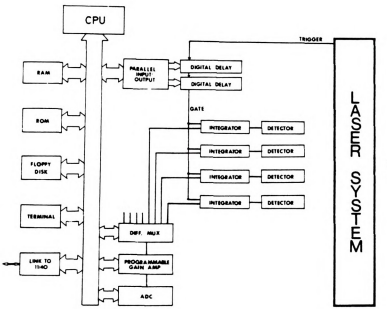

FIG. 1. Block diagram of the data-acquisition system.

This is much wider than optimal for integrating a 7-ns laser pulse; however, the temporal jitter between the laser pulse and the laser-generated trigger necessitates the wider gate. This method of triggering the data-acquisition system was chosen due to the impracticality of the length of the optical delay lines which would be required in order to use the laser pulse itself as a trigger. In the future, a multipass cell will be used to provide the required optical delays, and the laser pulse will trigger the system. The broad gate width has not caused difficulties because the extra noise that is integrated with the signal is essentially constant at a given laser power setting with fixed gate widths, and it can be nulled by applying currents equal in magnitude, but of opposite polarity, to the summing junctions of the integrators. This option is provided for on the integrator modules.

Each channel is multiplexed through an eight-channel differential multiplexer (Part No. MVD-807, Datel-Intersil Inc., Mansfield, MA) to a programmable gain amplifier (Part No. 3606, Burr–Brown Research Corp., Tucson, AZ), a sample-and-hold circuit (Part No. AD583, Analog Devices, Norwood, MA) and an analog-to-digital converter (Part No. AD574, Analog Devices). The amplifier has eleven software-programmable gains from 1 to 1024 v/v, thus accommodating signals of varying magnitude without loss of

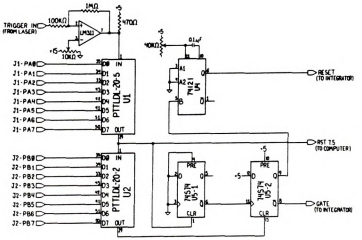

FIG. 2. Schematic diagram of the digital delay card. Multiple cards allow different gating delays for each integrator.

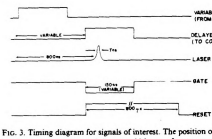

FIG. 3. Timing diagram for signals of interest. The position of the delayed trigger to the computer and the gate width are software programmable.

resolution in the analog-to-digital converter.

Photodiodes with less than 1 ns rise time (Part No. 5082-4220, Hewlett–Packard Components, Palo Alto, CA) and photomultiplier tubes (Model R928, Hamamatsu Corp., Middlesex, NJ) have been used as detectors. The active area of the photodiodes is small, which makes alignment more difficult, but the fast rise time facilitates pulse-shape analysis during an experiment. The use of larger and, therefore, slower photodiodes is often desirable for ease of alignment and is quite acceptable since the output current is integrated.[2]

The dynamic range of the system was determined both with and without the photodiode detectors. A gate width of 150 ns and a 100-pF capacitor were used. Current was supplied at an integrator input from a constant current source in order to determine the dynamic range of the detection system without the photodiode detectors. The response of the system is linear for input currents from 2.0 μA to 1.5 mA (equivalent to detector charges of 3×10^{-13} to 2.25×10^{-10} C). The dynamic range of the system (not including the photodiode detectors) is thus nearly three orders of magnitude. The relative standard deviation is larger for the smaller input currents and ranges from 7.0% at 2.0 μA to 2% at 8.0 μA. For input currents from 10 μA to 1.5 mA the relative standard deviation decreases from 1.0% to 0.2%. The entire range of gain on the programmable gain amplifier was used for this study. The amplifier linearity at and between all gains is excellent, as specified by Burr–Brown.

The dynamic range of the system including the photodiodes was determined by measuring the change in the normalized ratio of the outputs from two channels as the laser intensity incident on one of the photodiodes was attenuated from 100% to 0.2% with Schott glass neutral density filters. The ratio varied linearly with the transmission of the neutral density filters over this range. The dynamic range of the detection system with the photodiode detectors is, therefore, at least 500. The relative standard deviation of the ratioed measurements obtained with this system is typically 1%.

II. MICROCOMPUTER HARDWARE

The microcomputer system was assembled from components developed in our laboratory as parts of a general laboratory instrumentation system.[3] In this system each function (CPU, memory, ADC, etc.) is designed as a separate module. Modules are connected together by mounting several of them on a "motherboard", and these motherboards are in turn plugged into a common backplane. The system can thus be expanded to the size needed. The system assembled for this application consists of three motherboards. The first two form a general-purpose microcomputer, while the third provides the special interfaces needed in this application.

The first motherboard contains an 8085 CPU (Intel Inc., Santa Clara, CA) two serial I/O ports, and a memory board that contains 10 Kbytes of read-only memory (ROM) and 6 Kbytes of random access memory (RAM). The ROM is programmed with the basic FORTH system.[4] One serial port is used to communicate with the CRT terminal which controls the system and the second serial port is connected to a PDP 11/40 minicomputer.

Mounted on the second motherboard are 16 Kbytes of RAM, a floppy disk controller, a third serial I/O port, and a battery-powered real-time clock. The floppy disk controller is interfaced to two 8-in. floppy disk drives. Typically, one drive is used to hold the program disk while the other is used for data storage. The serial port is connected to a dot matrix printer. The date and time of data acquisition are logged via the real-time clock.

The third motherboard contains all of the interfaces specific to this application. This includes the eight-channel differential multiplexer (MUX), the programmable gain amplifier (PGA), the 12-bit analog-to-digital converter (ADC), and two parallel interface modules. The MUX, PGA, and ADC form the analog portion of the data-acquisition system. Acquisition of a data point proceeds as follows: the computer selects a channel to monitor with the MUX and a gain factor between 1 and 1024 for the PGA and then triggers the ADC. The ADC has a 35-μs conversion time and, allowing for the MUX and PGA settling time, conversion of a data point can be performed in about 190 μs. The parallel interface modules, each consisting of an Intel 8255 PIO chip, are used to control the programmable logic delay lines. Each module provides 3 bytes of parallel I/O; 2 bytes are used per digital delay card.

III. SOFTWARE

FORTH is a unique extensible language which is ideally suited to small microcomputer systems. It is interactive, compact, and fast.[3-4] A FORTH program, or "word", consists of a series of other previously defined words. Each word performs a function such as addition, the acquisition of a single data point, or the display of acquired data. Programs are easily written, even by the novice user, by merely concatenating existing words.

TABLE I. Frequency used commands.

GO	Acquires and stores specified number of data points.
SORT	Sorts data by incident laser intensity and stores sorted data.
RATIOS	Calculates and stores the ratio of the signal-to-reference intensities.
STATISTICS	Calculates the average and standard deviation for each channel and ratio, and the % relative standard deviation for each channel and ratio.
SHOW	Displays the data, ratios, and statistical information.

All the code for this data-acquisition system is written in FORTH, with the exception of the time-critical data-acquisition routine which is written in assembly language. Table I summarizes the functions of some FORTH words which have been implemented. A description of the pertinent software capabilities of the system is given below.

The data-acquisition routine controls the multiplexing, amplification, analog-to-digital conversion, and storage of the integrated data from each laser pulse. This series of events is initiated by a hardware interrupt, RST 7.5. The number of pulses which are acquired is a user-defined variable and determines the length of each run. The digitized data from one run are stored in RAM and can be immediately displayed on the terminal and/or stored on floppy disk.

The width and temporal position of the integrator gates are under computer control. The gate width is a variable and it is specified by the user. Optimization of the temporal position of the gate is achieved by moving the gate in 5-ns steps and sampling a series of laser pulses at each position. The gate position is set where the average of the digital values acquired is at a maximum.

The amplifier gain can be set independently for each signal channel. The gains are optimized by sampling a number of pulses at each gain on every channel. The gains are set such that the amplified signals use as much of the full scale of the analog-to-digital converter as possible without overranging. The best possible resolution can thus be achieved on each channel even if the magnitudes of the integrated signals are quite different.

Ratioing the signal and reference channels, sorting the data according to incident laser intensity, correcting for different gains, and calculating statistical information are accomplished for each run by the microcomputer. These data manipulations can be performed immediately after the data are acquired or after they have been stored and retrieved from floppy disk. The immediate display of normalized data and informative statistics is an invaluable aid in experimental setup and execution. When more extensive manipulation or plotting is required, data are transferred to a minicomputor.[9]

IV. APPLICATIONS

An application which clearly demonstrates the power of the data-acquisiton system is the optical saturation of an electronic transition in solutions of rhodamine 6G. The saturation of electronic transitions in solution is well known and the use of saturable absorbers for the passive Q-switching and mode-locking of lasers is well established.[10-13] A pulsed Nd:YAG laser (Model DCR-1A, Quanta-Ray, Mountain View, CA) with a 10-Hz repetition rate was used in the saturation studies reported here. The second harmonic (532 nm) was used to pump the $S_0 \rightarrow S_1$ transition of rhodamine 6G in methanol; the absorption maximum of this band is at 527 nm. The transmission behavior of rhodamine 6G was investigated at 532 nm as a function of the incident laser power.

The experimental setup is illustrated in Fig. 4. The incident laser beam is split, thereby providing a reference beam to monitor the incident intensity, I_0; the remainder of the beam passes through the sample cell. The transmitted beam I is also split and its intensity is monitored by a photodiode. (Microscope slides were used as beam splitters.) The intensity of the light incident on the photodiodes is further attenuated by Schott glass neutral density filters and is diffused using opal glass. The sample cell contains two flow-through quartz cuvettes with 1-cm path lengths for the sample and solvent.

Data were collected for 150 sequential laser pulses at each value of the nominal average laser power. A volume-absorbing disk calorimeter (Model 38-0101, Scientech, Inc., Boulder, CO) was used for the power measurements. The transmission of the rhodamine 6G solutions is $[(I/I_0)R\ 6G/(I/I_0)\text{MeOH}]$, and the transmission is calculated for each of the laser pulses monitored. The average value of (I/I_0)MeOH was used in calculating the transmission values since the transmission of methanol is independent of incident laser power. This is verified by the constant value of the ratio. the relative standard deviations for the normalized solvent transmission values are 1% or less at each power.

Transmittance versus peak power curves for three concentrations of rhodamine 6G are shown in Fig. 5. Transmis-

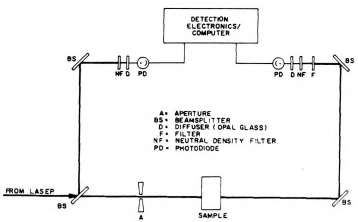

FIG. 4. Experimental setup for rhodamine 6G saturation studies.

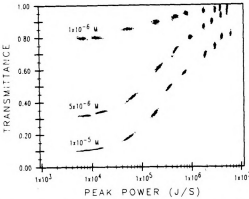

FIG. 5. Transmittance vs peak power curves for three concentrations of rhodamine 6G in methanol. Each cluster of points consists of 150 normalized data points around the nominal average power which is read from the power meter.

sion values are plotted for each laser pulse monitored, and a cluster of points is obtained for each nominal average laser power. At the lowest incident power, 0.5-mW average, the transmission values measured are the same as those that were obtained with a Cary 17D spectrophotometer and the transmission is constant within the pulse-to-pulse fluctuations. The transmission of rhodamine 6G increases with increasing incident laser power and asymptotically approaches a maximum value. The increased transmission results from the significant ground-state depopulation which occurs as the incident laser power is increased. Complete saturation is achieved when the ground and excited-state populations are equal; at this point, assuming no other absorbances, the transmission is unity, i.e., the net absorbance is zero. The transmission values obtained for the rhodamine 6G solutions reach a maximum which is somewhat below

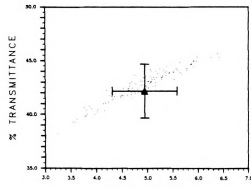

FIG. 6. Percent transmittance of 5×10^{-5}-M rhodamine 6G vs power. The average nominal power is 5 mW. Shown are 150 individual data points and the calculated average percent transmittance with standard deviations. The average value does not accurately represent the nonlinear transmission behavior of this solution.

unity, and this can be attributed to excited state absorption.[14]

The advantage of individual data point collection versus signal averaging is demonstrated in Fig. 6. Percent transmission versus power is shown at a nominal average power of 5 mW for the 5×10^{-5} M rhodamine 6G solution. In addition to the individual data points obtained for each pulse, the average percent transmission for the 150 pulses is designated (by the triangle) at the average power. The averages were calculated from the individual data points and the error bars represent one standard deviation.

Dramatically shown by the individual data points is the power dependence of the transmission as a function of the pulse-to-pulse fluctuations in incident power. This detailed information would be lost if only the averaged transmission and power values were obtained. Moreover, the precision of the data would be seriously underestimated by the signal-to-noise ratio of the averaged measurements. Among the advantages of this data-acquisition system is the ability to collect data for every pulse and then to choose the appropriate method of postprocessing, rather than forcing the data into a final form (i.e., an average). The amount and type of information available from the data can be optimized for each application.

This data-acquisition system has also been used in single- and dual-wavelength pump-probe experiments where photodiodes were employed as detectors. Four signal channels were monitored in the dual-wavelength experiments. Saturation of fluorescence[14] and two-photon fluorescence[15] are other applications in which this system has been used, in these instances with photomultiplier tubes as detectors.

V. DISCUSSION

The ability to acquire, store, and normalize data for each pulse is essential if the measured response of a chemical system is a function of the incident intensity in pulsed laser applications. Averaging the responses of such a system cannot accurately and fully represent the processes at hand, especially if the pulse-to-pulse intensity fluctuates significantly. Nonlinear processes, in particular, are extremely sensitive to these fluctuations. The performance and versatility of the data-acquisition system described in this paper make it more generally useful than those traditional methods of signal processing which depend upon pulse-to-pulse averaging.

ACKNOWLEDGMENTS

The authors would like to express their appreciation to Dr. T. V. Atkinson for writing the data-manipulation routines used on the PDP11/40 and to B. H. Newcome for his help and advice. This work was supported in part by grants from the National Science Foundation and the Office of Naval Reseach.

[1]G. P. Ritz, D. J. Wallan, and M. D. Morris, Appl. Spectrosc. 32, 493 (1973).
[2]C. A. Langhoff, W. H. Nugent, and M. Novak, Anal. Chem. 54, 1001 (1982).

[3]B. H. Newcome and C. G. Enke, Rev. Sci. Instrum. (accepted for publication).
[4]FORTH, Inc., 2309 Pacific Coast Highway, Hermosa Beach, CA 90254, U. S.A.
[5]J. James, BYTE **5**, 100 (1980).
[6]R. E. Dessy and M. K. Starling, Am. Lab. **12**, 21 (1980).
[7]S. M. Hicks, Electronics **56**, 114 (1979).
[8]R. E. Dessy, Anal. Chem. **55**, 650 (1983).
[9]P. A. Hoffman and C. G. Enke, Comput. Chem. **7**, 47 (1983).
[10]M. Hercher, W. Chiu, and D. L. Stockman, IEEE J. Quantum Electron. **QE-4**, 951 (1968).
[11]C. R. Giuliano and L. D. Hess, IEEE J. Quantum Electron. **QE-3**, 358 (1967).
[12]C. H. Skeen and C. M. York, Appl. Opt. **5**, 1463 (1966).
[13]A. J. DeMaria, D. A. Stetser, and H. Heynan, Appl. Phys. Lett. **8**, 174 (1966).
[14]L. M. Jones, Ph. D. thesis, Michigan State University, 1984.
[15]Y. C. Chung, J. Suzuka, and G. E. Leroi, paper MG12, Thirty-eighth Symposium on Molecular Spectroscopy, Columbus, OH, June 1983 (abstracts available from the Dept. of Physics, Ohio State Univ.).

APPENDIX B

APPENDIX B

CIRCUIT AND CONNECTOR DOCUMENTATION

Schematic diagrams of the data acquisition system circuits that are not shown in Appendix A are provided in this appendix. The edge connector for the digital delay card is also documented. Details regarding the microcomputer system may be found in reference B.1.

The schematic diagram for the 8-channel differential multiplexer (Part No. MVD-807, Datel-Intersil, Inc., Mansfield, MA) card is shown in Figure B.1. Channel selection is accomplished by the values written to latch U2. The output of the multiplexer may be input to a non-differential device by utilizing instument amplifier U3. U3 was not used in this application because the programmable gain amplifier that was employed required differential inputs.

Figure B.2 is a schematic diagram of the programmable gain amplifier (Part No. Burr-Brown Research Corp., Tuscon, AZ) card. The gain of the amplifier is determined by the values written to latch U1. Table B.1 lists the gains obtained for each digital value written to the

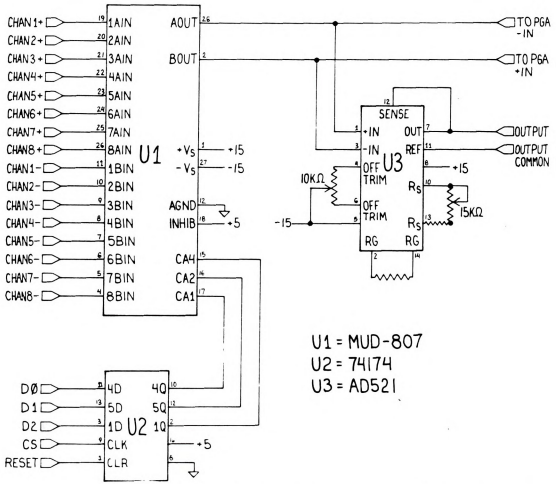

Figure B.1 Schematic diagram of 8-channel differential multiplexer card.

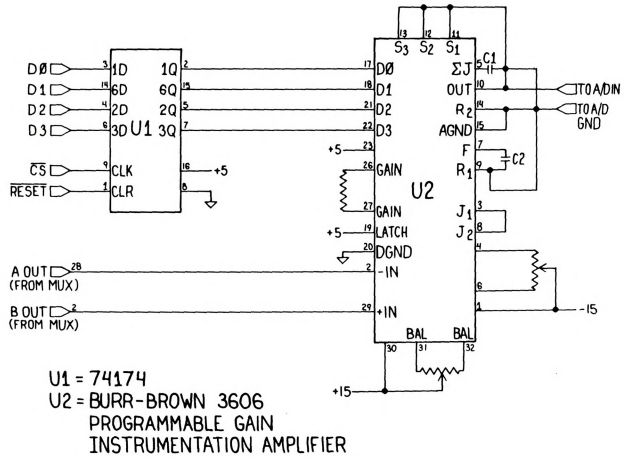

Figure B.2 Schematic diagram of programmable gain amplifier card.

Table B.1 Amplifier Gain Control

Digital Value	Gain
0	1
1	2
2	4
3	4
4	4
5	8
6	16
7	16
8	32
9	64
10	128
11	128
12	256
13	512
14	1024
15	1024

latch. The inverting amplifier input is differential and the signal of interest is directed to the negative input in this application due to the negative polarity of the output ofthe integrator cards (Model 4130 Evans Associates, Berkeley,CA).

The digital delay card connector is shown in Figure B.3. The "variable trigger in" is the laser-generated trigger pulse which is connected via a BNC connector to the box which houses the four integrator and two digital delay cards. The "computer trigger" is a TTL output generated by the delay card that is used to initiate the analog-to-digital conversion. The gating and reset pulses are directed to the connectors for the integrator cards. (Further details regarding this connector are well documented in the manufacturer's data sheet.) The integrator cards are simultaneously gated by using one digital delay card to generate the pulses required by the integrators. Alternately, one or more of the integrators can by gated independently of the other(s) by utilizing the second digital delay card to generate the gate and reset pulses at another delay time relative to the laser generated trigger pulse.

B.1 Newcome, B. H., Enke, C. G. Rev. Sci. Instrurm. 55 (12), 2017 (1984).

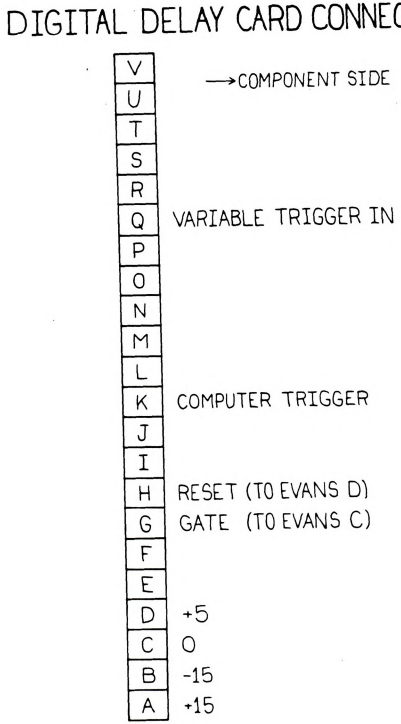

Figure B.3 Diagram of digital delay card connector.

APPENDIX C

APPENDIX C

SYSTEM SOFTWARE

The FORTH code written and utilized specifically for the experimental studies is described and listed by block in this appendix. The functional descriptions precede the software listings and are provided in the order that the code occurs in the listings. The assembly code that comprises the data acquisition routine is also listed and described. Information regarding the system software, polyFORTH, is available from FORTH, Inc. (Hermosa Beach, CA).

Block 17 contains data space and variable definitions. A matrix of 6 columns (channels) and 150 rows (data points per channel) is defined. Four columns are used for data channels 0 - 3. The two remaining columns contain the ratioed values of channels 1 and 0 and channels 3 and 2. Arrays which contain statistical information (i.e., averages, standard deviations and percent errors) for each column are established. The FORTH words that define the statistical calculations are found in Block 18.

Addresses for the analog-to-digital converter, the 8-channel differential multiplexer and programmable gain amplifier are established in Block 19. The assembly code performs data acquisition in the following manner. A trigger pulse from the laser starts the analog-to-digital converter. The analog signals from the integrators are latched at the multiplexer and converted in sequence. This routine includes the gain information that is written to the programmable gain amplifier for each channel.

Block 20 contains the FORTH words that calculate the ratios of channels 1 to 0 and channels 3 to 2 and that subsequently store these ratios in channels 4 and 5, respectively. The word STATISTICS defines the manner in which the aforementioned statistical calculations are performed. GO initiates data acquisition and the mathematical calculations.

Block 21 establishes the protocol for translating the user-specified gain for each data channel to the programmable gain amplifier. [For further information, refer to the data sheet for the amplifier (Part No. 3606 Burr-Brown Research Corp., Tucson, AZ.).]

The formatting information in Blocks 22 and 23 defines the manner in which header and statistical information is displayed. CRAZY-COUNT defines the order in which data are read from the columns of the data matrix. SHOW displays the formatted information on the CRT.

Words that perform a simple bubble sort of the data acquired on channel 0 (the reference channel) are found in Block 24. Abbreviations for the acquisition, display and sorting words are also defined.

Block 27 contains code which corrects the magnitude of the acquired data points for the gains applied by the programmable gain amplifier. The normalization factor applied to the data of each channel must result in numbers between 0 and 4096 due to the mathematical range limitations of the system. TWIDDLE acquires and displays 15,000 data points facilitating fine tuning of the optical components. RZAXXO reformats a flexible FORTH disc.

Block 100 serves to define the parameters associated with the two digital delay cards. The gate delay time, referenced to the laser-generated trigger pulse, and the width of the gate are specified independently. The desired gate widths and delays are specified in units of nanoseconds.

Automatic optimization of the temporal gate position, referenced to the laser generated trigger pulse, is accomplished via the code in Block 101. FINDEM samples and stores the average value of the integrated reference signals (channel 0) at all of the available delay times. A maximum average signal is obtained at the delay time for which the gate position is optimized. Integrator gating is then set to occur at the optimal delay time.

```
Block Number:  17
0   ( LASER ROUTINES       CARL MYERHOLTZ     10/3/82 )
1      ( DATA SPACE DEFINITIONS )
2
3   VARIABLE #POINTS      10 #POINTS !
4   VARIABLE RUN#
5   VARIABLE LABLE    68 ALLOT    LABLE 70 BLANK
6   VARIABLE ISAVE
7
8   6 ARRAY AVERAGES
9   6 ARRAY STD-DEVS
10  6 ARRAY %ERRORS
11
12  5 CARRAY GAINS      ' GAINS 5 ERASE
13
14  6 150 MATRIX DATA
15
```

```
Block Number:  18
0   ( SQRT, AVERAGE, AND SDEV ROUTINES )
1
2   : SQRT  ABS >R  I 2/
3      BEGIN  DUP DUP I SWAP / + 1+ 2/ DUP ROT  = END
4      R>  DROP  ;
5
6   : AVERAGE  >R  0 0 ROT DUP I 2* + SWAP
7      DO I @ M+ 2 +LOOP  R> M/ ;
8
9   : SUMS  >R 2* OVER + SWAP 0. 2SWAP
10     DO I @ J - ABS DUP U* D+ 2 +LOOP  R> DROP ;
11
12  : SDEV  DUP ROT ROT 2DUP AVERAGE SUMS ROT 1- M/ SQRT ;
13
14
15
```

```
Block Number:  19
0   ( LASER ROUTINES      CARL MYERHOLTZ     10/7/82 )
1      ( ADC ROUTINES )      HEX
2   FFC0 CONSTANT ADC-CS  FFD0 CONSTANT MUX-CS  FFD8 CONSTNAT PGA-CS
3
4   CODE ACQUIRE   C L MOV   B H MOV   ISAVE SHLD   D POP
5      ' GAINS B LXI   B LDAX   PGA-CS STA   B INX   D A MOV
6      08  # A MOV   SIM   MUX-CS STA D INR HLT  EI
7      BEGIN   ADC-CS STA   B LDAX   PGA-CS STA   B INX   D A MOV
8      MUX-CS STA   D INR   20 # A MOV   BEGIN   A DCR   0= END
9      ADC-CS LDA   A H MOV   ADC-CS 1+ LDA   A L MOV   H PUSH
10     E DCR   0= END   ISAVE LHLD   L C MOV   H B MOV   NEXT JMP
11
12  CODE (GET) H POP   ' GAINS D LXI   XCHG   D DAD   XCHG   D LDAX
13     PGA-CS STA   L A MOV   MUX-CS STA   HLT   ADC-CS STA
14     10 # A MOV   BEGIN  A DCR  0= END   ADC-CS LDA   A H MOV
15     ADC-CS 1+ LDA   A L MOV   H PUSH NEXT   JMP   DECIMAL
```

```
Block Number:  20
0   ( LASER ROUTINES      CARL MYERHOLTZ    10/3/82 )
1      ( DATA ACQUISITION )
2   : 16/  2/ 2/ 2/ 2/  4095 AND ;
3
4   : GET  (GET)  16/ ;
5
6   : RATIOS   #POINTS @ 0 DO
7      1000  1 I DATA @  0 I DATA @ */  4 I DATA !
8      1000  3 I DATA @  2 I DATA @ */  5 I DATA !  LOOP ;
9
10  : STATISTICS  6 0 DO  I 0 DATA  #POINTS @  2DUP
11     AVERAGE DUP  I AVERAGES !  ROT ROT SDEV  DUP
12     I STD-DEVS !  1000 ROT */  I %ERRORS !  LOOP ;
13
14  : GO  #POINTS @ 0 DO  4 ACQUIRE  0 3 DO  16/  I J DATA !
15     -1 +LOOP   LOOP  OFFSETS  RATIOS  STATISTICS  1 RUN# +! ;
```

```
Block Number:  21
0   ( LASER ROUTINES      CARL MYERHOLTZ    10/7/82 )
1      ( GAIN CONTROL )
2
3   CREATE GTABLE  1 , 2 , 4 , 0 , 0 , 8 , 0 , 16 , 32 , 64 , 0 ,
4      128 , 256 , 512 , 0 , 1024 ,
5
6   : >GAIN  2* GTABLE + @ ;
7
8   : >PGA 16 0 DO DUP GTABLE I 2* + @= IF DROP I LEAVE THEN LOOP ;
9
10  : RANGE  SWAP  >PGA  SWAP  GAINS  C!  ;
11
12
13
14
15
```

```
Block Number:  22
0   ( LASER ROUTINES      CARL MYERHOLTZ    10/3/82 )
1      ( DATA DISPLAY )
2
3   : N.1 0 SWAP <# # 46 HOLD #S #> DUP  5 SWAP - SPACES TYPE ;
4   : N.3 0 SWAP <# # # # 46 HOLD #S #> DUP  5 SWAP - SPACES TYPE ;
5
6   : .FORMAT   ( N6,N5...N2,N1)  5 U.R 2 SPACES  5 U.R 2 SPACES
7      N.3 2 SPACES  5 U.R 2 SPACES  5 U.R 2 SPACES  N.3  CR  ;
8
9   : .GAIN  GAINS C@  >GAIN  5 U.R  2 SPACES ;
10
11  CREATE CRAZY-COUNT  5 C, 3 C, 2 C, 4 C, 1 C, 0 C,
12
13  : K  I'  [']  CRAZY-COUNT +  C@ ;
14
15  : TITLE   92 TEXT  PAD LABLE 70 MOVE  0 RUN# ! ;
```

```
Block Number:  23
0   ( LASER ROUTINES      CARL MYERHOLTZ   10/3/82 )
1     ( DATA DISPLAY CONT. )
2
3   : STATS  CR  8 SPACES ." GAIN" 6 SPACES  0 .GAIN  1 .GAIN
4     7 SPACES  2 .GAIN  3 .GAIN  CR   8 SPACES  ." AVERAGE   "
5     6 0 DO  K AVERAGES @  LOOP   .FORMAT
6     8 SPACES ." STD.DEV.   "  6 0 DO  K STD-DEVS @  LOOP .FORMAT
7     8 SPACES ." %RELSD     "  0 5 DO  K %ERRORS @  N.1  2 SPACES
8     -1 +LOOP  CR ;
9
10  : HEADING  ."         POINTS  CHAN.0 CHAN.1 RATIO  CHAN.2 CHAN
11  .3 RATIO" CR  ;
12
13  : SHOW  ( PAGE) CR  LABLE 70 TYPE  ." RUN# "  RUN# @ .  CR CR
14    HEADING  #POINTS @ 0 DO   10 SPACES  I 4 U.R  4 SPACES
15    6 0 DO  K J DATA @  LOOP  .FORMAT  LOOP  STATS ;
```

```
Block Number:  24
0   ( LASER ROUTINES      CARL MYERHOLTZ   10/3/82 )
1     ( SORT ROUTINE )
2
3   : EXCHANGE  >R >R  0 5 DO  I J DATA @  -1 +LOOP
4     I I'  6 0 DO  2DUP  I SWAP DATA @  SWAP I SWAP DATA !  LOOP
5     2DROP  R> DROP  6 0 DO  I J DATA ! LOOP  R> DROP  ;
6
7   : SORT  #POINTS @ 1- 0 DO   #POINTS @   I DO
8     0 J DATA @  0 I DATA @  > IF  J I EXCHANGE  THEN LOOP LOOP ;
9
10  : G GO ;      : S SHOW ;      : SSS SHOW SORT SHOW ;
11
12
13
14
15
```

```
Block Number:  27
0   ( NORMALIZATION ROUTINE )
1
2
3
4
5   : (NORM)  #POINTS @ 0 DO DUP I DATA @ ROT DUP 2SWAP ROT 100 */
6    OVER I DATA ! LOOP DROP DROP ;
7
8   : NORM 3 (NORM) 2 (NORM) 1 (NORM) 0 (NORM) RATIOS STATISTICS ;
9
10
11
12
13
14  : TWIDDLE BEGIN G S 15000 0 DO LOOP ?TERMINAL END ;
15
```

```
Block Number:  31
0      ( MORE DATA STORAGE ROUTINES )
1
2    : DIR ( 1 DRIVE) 1+ SWAP ( ?EVEN) DO CR I 3 U.R 2 SPACES
3      I BLOCK 70 -TRAILING TYPE 2 +LOOP CR ;
4
5    : PSTATS 2 DUP DIR SWAP RDATA STATS RDATA STATS CR ;
6
7
8
9
10   VARIABLE STORE
11   : SDATA STORE @ WDATA 2 STORE +! ;
12
13
14   : RZAXXO 250 0 DO I BLOCK 1024 BLANK UPDATE  LOOP FLUSH ;
15
```

```
Block Number:  36
0    0 0 DATA CONSTANT DBUF
1    : WDATA DUP BLOCK LABLE OVER 70 MOVE
2     #POINTS @ OVER 80 + ! DBUF SWAP 124 + 900 MOVE UPDATE
3     DBUF 900 + SWAP 1+ BLOCK 900 MOVE UPDATE FLUSH ;
4
5    : RDATA DUP BLOCK DUP DUP LABLE 70 MOVE
6    80 + @ #POINTS ! 124 + DBUF 900 MOVE
7    1+ BLOCK DBUF 900 + 900 MOVE STATISTICS ;
8
9
10
11
12
13
14
15
```

```
100 LIST

     0 ( DELAY CARD STUFF )  HEX
     1
     2 F801 CONSTANT 1GATE      F800 CONSTANT 1TRIG
     3 F841 CONSTANT 2GATE      F840 CONSTANT 2TRIG
     4 80 F803 C!  80 F843 C!    ( INITIALIZE PORTS )    DECIMAL
     5
     6 : 1WIDTH  20 - 2/ 1GATE C! ;
     7 : 2WIDTH  20 - 2/ 2GATE C! ;
     8 : 1DELAY  20 - 5 / 1TRIG C! ;
     9 : 2DELAY  20 - 5 / 2TRIG C! ;
    10
    11 : WIDTHS  DUP 1WIDTH 2WIDTH ;
    12 : DELAYS  DUP 1DELAY 2DELAY ;
    13
    14
    15
```

```
Block Number:  101
0   ( FIND MAX )
1
2   VARIABLE DMAX
3
4   : FINDEM  #POINTS @  10 #POINTS !  0
5     1295 800 DO  I 1DELAY  GO DUP 0 AVERAGES @  < IF  DROP
6      0 AVERAGES @  I DMAX !  THEN  20 +LOOP  DROP  DMAX @
7      1DELAY  #POINTS ! ;
8
9
10
11
12
13
14
15
```